PERFORMANCE EVALUATION OF ADVANCED DC-DC CONVERTERS FOR BLDC MOTOR DRIVEN STANDALONE SOLAR WATER PUMPING SYSTEM

A DISSERTATION

SUBMITTED IN PARTIAL FULFILLMENT OF THE REQUIREMENTSFOR THE AWARD OF THE DEGREE
OF

MASTER OF TECHNOLOGY

IN

POWER SYSTEM

SUBMITTED BY:

SHANTANU

(2K20/PSY/18)

UNDER THE SUPERVISION OF

Dr. MAYANK KUMAR

DEPARTMENT OF ELECTRICAL ENGINEERING

DELHI TECHNOLOGICAL UNIVERSITY

(Formerly Delhi College of Engineering)

Bawana Road, Delhi-110042

JUNE,2022

DEPARTMENT OF ELECTRICAL ENGINEERING

DELHI TECHNOLOGICAL UNIVERSITY

(Formerly Delhi College of Engineering)

Bawana Road, Delhi-110042

CANDIDATE'S DECLARATION

I hereby declare that the work which is presented in the Major Project – II entitled "Performance Evaluation of Advance DC-DC Converters for BLDC Motor Driven Standalone Solar Water Pumping System" in fulfilment of the requirement for the award of the Degree of Master of Technology in Power System and submitted to the Department of Electrical Engineering, Delhi Technological University, Delhi is an authentic record of my own, carried out during a period from January to May 2022, under the supervision of Dr. Mayank Kumar.

This work has not previously formed the basis for the award of any Degree, Diploma, and Associateship, Fellowship or another similar title or recognition.

Place: New Delhi
Date: 31/05/2022

SHANTANU
2K20/PSY/18

DEPARTMENT OF ELECTRICAL ENGINEERING

DELHI TECHNOLOGICAL UNIVERSITY

(Formerly Delhi College of Engineering)

Bawana Road, Delhi-110042

CERTIFICATE

This is to certify that the Project Dissertation, submitted along with the project entitled "Performance Evaluation of Advance DC-DC Converters for BLDC Motor Driven Standalone Solar Water Pumping System" has been carried out by Shantanu (Roll No. 2K20/PSY/18) under my guidance and supervision, in partial fulfilment of the requirement for the award of the degree of Master of Technology in Power System from Delhi Technological University, during the academic year 2021 - 2022. To the best of my knowledge this work has not been submitted in part or full for any Degree or Diploma to this University or elsewhere. I, further certify that the publication and indexing information given by the student is correct.

Place: Delhi

Date: 31/05/2022

Dr. Mayank Kumar

SUPERVISOR

DEPARTMENT OF ELECTRICAL ENGINEERING

DELHI TECHNOLOGICAL UNIVERSITY

(Formerly Delhi College of Engineering)

Bawana Road, Delhi-110042

ACKNOWLEDGEMENT

First and foremost, I express my deep sense of gratitude to Dr. Mayank Kumar, Project Supervisor and Professor, Department of Electrical Engineering (EED), DTU for his constant guidance, support, motivation and encouragement throughout the period of this work. His readiness for consultation at all times, concern, tremendous effort and assistance has been invaluable. He showed me the path to achieve my targets by explaining all the tasks to be done and explained to me the importance of this project as well as its industrial relevance. He was always ready to help me and clear my doubts regarding any hurdles in this project. Without his constant support and motivation, this project would not have been successful.

I am thankful to Prof. Uma Nangia, Head of Department and Electrical Engineering Department faculties in DTU for their kind help, encouragement and for providing necessary information regarding the project and also for their support in completing the project. I want to thank all the staff of the Project and Research Lab, Electrical Engineering Department (EED), DTU for their full cooperation.

Finally, yet importantly, I would like to express my heartfelt thanks to my beloved parents for their blessings and moral support, my friends/classmates for their help and wishes for the successful completion of my dissertation in time.

Place: Delhi

Date: 31/05/2022

SHANTANU

2K20/PSY/18

M. Tech (Power System Engineering)

Department of Electrical Engineering

Delhi Technological University

ABSTRACT

The increment in advanced technology for pumping applications has been possible due to very swift development in power semiconductor devices. At the same time the reliable and stable operation of whole system is affected due to presence of harmonic distortions being produced by power converters which then results in additional losses. The DC-DC converters are known for converting DC voltage level of output with respect to input via control of duty cycle of principal switches present in the circuits. The necessity of these converters is subject to supplying a constant output voltage, without being affected by input voltage disturbances.

The two parts of designing Standalone Solar Water Pumping System (SSWPS) comprises of the passive components selection and the optimized composition of control system. This project presents the complete comparative analysis by considering the overall procedure for implementation of optimum design and control of SSWPS, which primarily comprises of a Permanent Magnet Brush-Less DC (PMBLDC) motor coupled to pump, a configuration of Voltage Source Inverter (VSI), a high gain Advanced DC-DC Converter (ADDC) and a Solar Photo-Voltaic (SPV) array. The idea of designing passive components is such that the operation of inductor of ADDC, even at lower sun radiation, should remain in Continuous Conduction Mode (CCM). Whereas, in designing of control system the optimization of system parameters is done so that cognitive control of ADDC's switching via Incremental Conductance-Maximum Power Point Tracking (INC-MPPT) algorithm for drawing the paramount obtainable power from SPV array can be made possible. Also, this algorithm offers a reduced current starting (i.e., soft starting) to the PMBLDC motor, deployed for driving a centrifugal water pump coupled to its shaft, which restrain motor from the damaging consequence of high starting current. In order to avoid the VSI switching losses due to high frequency switching a proper electronic commutation circuitry for PMBLDC motor is employed.

In order to achieve the desired performance of BLDC motor, there is an immense requirement of proper speed controller and an input supply having low ripple value. Thus, by integrating PI controller with an ADDC, an attempt has been made to implement a better speed control system for the BLDC motor drive. The specifications of the controller have been fine-tuned to optimize motor performance. Also, the relative performance evaluation of three different ADDCs such as Luo converter, Single-Ended Primary-Inductance Converter (SEPIC) and ZETA converter have been calculated and analysed by using the respective converter mathematical analysis and summarized in tabulation form. Considering PMBLDC motor drive as load, the transient and steady state analysis of all the designed ADDCs has been carried out in terms of voltage, current and power. In addition, the performance parameters values such as ripple voltage, switching losses and efficiency of the proposed three different converters were compared with each other in open as well as closed loop control system environment. The suitability of the intended system under dynamic conditions is demonstrated by the simulation results using MATLAB/Simulink software.

TABLE OF CONTENTS

LIST OF FIGURES

LIST OF TABLES

LIST OF ABBREVIATIONS

SPV	Solar Photo Voltaic
FDI	Foreign Direct Investment
MNRE	Ministry of New and Renewable Energy
RTS	Roof-Top Solar
LCOE	Levelized Cost of Energy
BLDC	Brush Less Direct Current motors
PMBLDC	Permanent Magnet Brush Less Direct Current motors
PMSM	Permanent Magnet Synchronous Machine
VSI	Voltage Source Inverter
RES	Renewable Energy Sources
SSWPS	Standalone Solar Water Pumping System
MPPT	Maximum Power Point Tracking
INC	Incremental Conductance
P&O	Perturb and Observe
ADDC	Advanced Dc-Dc Converter
SEPIC	Single Ended Primary Inductance Converter
CCM	Continuous Conduction Mode
EMI	Electro-Magnetic Interference
PSI	Power System Integrator
ZSI	Z-Source Inverter
PSO	Particle Swarm Optimization
PI	Proportional and Integral controller
FL, FLC	Fuzzy Logic, Fuzzy Logic Controller
CSC	Canonical Switching Cell
ANFIS	Adaptive Neuro-Fuzzy Inference
FPA	Flower Pollination Algorithm
MPP	Maximum Power Point
BLAC	Brush-Less Alternating Current motor
EMF	Electro-Motive Force
VCR	Video Cassette Recorder
CD	Compact Disc
PWM	Pulse Width Modulation

ZCS	Zero Current Switching
ZVS	Zero Voltage Switching
ZT	Zero Transition
SR	Synchronous Rectifier
IC	Integrated Circuit
MER	Multi-Elements Resonant converter
BCM	Boundary Conduction Mode
MOSFET	Metal-Oxide Semiconductor Field Effect Transistor
IGBT	Insulated Gate Bipolar Transistor

LIST OF SYMBOLS

V_{dc}	DC link voltage across capacitor, DC bus voltage
C_{dc}	DC link capacitor
V_{PV}	SPV array input voltage
I_{PV}	SPV array input current
I_H	Hall current
V_H	Hall voltage
R_H	Hall constant
V_{an} , V_{bn} , V_{cn}	Phase a, b and c voltages of BLDC motor
i_{an} , i_{bn} , i_{cn}	Phase a, b and c currents of BLDC motor
e_{an} , e_{bn} , e_{cn}	Phase a, b and c back-EMF of BLDC motor
T_e	Electromagnetic torque
ω_m	Mechanical angular velocity
ω_r	Electrical angular velocity
N_r	Rotor speed
K_t	Torque coefficient
K_e	Line back-EMF coefficient
r_a	Line resistance of winding
V_{ref}	Reference voltage
$\epsilon(t)$	Error signal
$V_C(t)$	PI controller output
K_i	Integral gain constant
K_p	Proportional gain constant
V_{OC}	Open circuit voltage
I_{SC}	Short circuit current
P_{MPP}	Power at maximum power point
I_{MPP}	Current at maximum power point
V_{MPP}	Voltage at maximum power point
V_{LO}	Output voltage of Luo converter
i_{LO}	Output current of Luo converter
R_L	Load resistance of Luo Converter
V_{LP}	Input voltage of Luo converter
i_{LP}	Input current of Luo converter
S_L	Switch of Luo converter

L_{L1}, L_{L2}	Inductors of Luo converter
C_{L1}, C_{L2}	Capacitors of Luo converter
i_{LL1}, i_{LL2}	Inductive currents of Luo converter
V_{CL1}, V_{CL2}	Capacitive voltage of Luo converter
D_L	Diode of Luo converter
I_{DL}	Diode current of Luo converter
V_{SO}	Output voltage of SEPIC converter
i_{SO}	Output current of SEPIC converter
R_S	Load resistance of SEPIC Converter
V_{SP}	Input voltage of SEPIC converter
i_{SP}	Input current of SEPIC converter
S_S	Switch of SEPIC converter
L_{S1}, L_{S2}	Inductors of SEPIC converter
C_{S1}, C_{S2}	Capacitors of SEPIC converter
i_{LS1}, i_{LS2}	Inductive currents of SEPIC converter
V_{CS1}, V_{CS2}	Capacitive voltage of SEPIC converter
D_S	Diode of SEPIC converter
I_{DS}	Diode current of SEPIC converter
V_{ZO}	Output voltage of Zeta converter
i_{ZO}	Output current of Zeta converter
R_Z	Load resistance of Zeta Converter
V_{ZP}	Input voltage of Zeta converter
i_{ZP}	Input current of Zeta converter
S_Z	Switch of Zeta converter
L_{Z1}, L_{Z2}	Inductors of Zeta converter
C_{Z1}, C_{Z2}	Capacitors of Zeta converter
i_{LZ1}, i_{LZ2}	Inductive currents of Zeta converter
V_{CZ1}, V_{CZ2}	Capacitive voltage of Zeta converter
D_Z	Diode of Zeta converter
I_{DZ}	Diode current of Zeta converter
f_S	Switching frequency
P_{nom}	Nominal inverter capacity
P_{inv}	Power rating of inverter
R_S	Per phase resistance of BLDC motor
L_S	Per phase inductance of BLDC motor

CHAPTER -1

INTRODUCTION

With expanding global energy needs, skyrocketing fossil fuel costs, finite deposits of our basic energy sources, the risk of nuclear disasters, and an uncertain international political scenario, interest in renewable energy sources has exploded in past few decades. Solar energy is considered the most feasible source of energy among all existing renewable energy sources, and it has shown the fastest growth over the years, resulting in lower PV module prices as production capacity expands at a rapid rate [1]. The efficient harvesting of solar photovoltaic (SPV) energy may easily meet the world's current energy requirements. This is especially true now that a new global challenge has emerged: the planet's overheating as a result of rising greenhouse gas concentrations in our atmosphere, such as carbon dioxide (CO_2) and methane [2].

Even if solar energy became the most cost-effective alternative energy source, power generation is the most expensive per-watt expense in a solar system [3]. This is because solar energy harvesting and the quantity of power generated are nonlinear and are affected by variations in ambient temperature, solar irradiance, system mismatch, and a variety of other variables [2, 4]. These variables change during the day, which can have a significant impact on the efficiency and output power of PV modules. Because PV modules are inherently inefficient, the theoretical maximum efficiency of crystalline silicon, which accounts for 90.0% of the worldwide market, is only 33.7% [5, 6]. Any variation in efficiency can dramatically reduce the quantity of energy generated. As a result of these characteristics, much emphasis has been placed on the development of power electronics converters that deduce the maximum power from the PV module, thereby enhancing the efficiency of the power processing stage, increasing power yield, and lowering the overall cost of the system that interfaces with the grid [2].

Solar based systems have emerged as a feasible alternative for domestic usage, agricultural applications like irrigation, industrial usage, and space aircraft in India, which has abundant sunshine but limited fossil-fuel supplies. In a country where agriculture sector dominates over other sectors, solar-powered pumping systems are gradually becoming a dependable, environmentally beneficial, and economical option for farmers' irrigation needs for long usage, reducing the need of traditional diesel and electric pumps [7]. The use of solar-powered pumps instead of fossil-fuel pumps helps to save the environment by lowering CO_2 emissions. Due to the limited availability of electricity through the grid in rural and isolated places, standalone PV-fed water pumping systems are becoming a viable option for meeting energy needs. This dissertation will explore the benefits and downsides of employing the PV system, as well as the emerging technology of DC-DC converters that allow the PV system to function independently, extracting the maximum power from PV modules and utilising the module to its full potential [8].

1.1 CURRENT REAL-WORLD SCENARIO OF PROPOSED WORK

India's renewable energy business is the world's fourth most appealing renewable energy market. As of 2020, India ranked fourth in wind power, fifth in solar power, and fourth in renewable power installed capacity. India's installed renewable energy capacity was 152.36 GW as of January 2022, and is going to reach the ambitious target of 175 GW till the end of year 2022 [3]. The advantages of working with solar power are:

- **Immense growth potential:** India's traditional energy supplies are insufficient to meet the country's energy demands, which are driven by a large population and a quickly growing economy. India, on the other hand, can take advantage of solar energy's enormous potential because it receives sunlight for the majority of the year.
- **Robust demand:** Electricity consumption in India is expected to rise from 4,926 TWh in 2012 to 15,280 TWh in 2040 as the economy grows. The real estate and transportation sectors will account for the majority of demand.
- **Competitive advantage:** In India, solar and wind power generation is expected to be cost-competitive with thermal power generation by 2025-2030.
- **Ambitious targets:** Prime minister Narendra Modi promised to raise India's renewable energy generation capacity to 500 GW and fulfil 50 percent of India's energy needs through renewables by 2030 at the COP 26 summit in Glasgow, in November 2021.
- **Increasing investment:** India's non-conventional energy sector has grown quite attractive to investors, with foreign direct investment (FDI) inflows totalling US$11.21 billion between April 2000 and December 2021. Since 2014, around Rs 5.2 lakh crore (US$ 70 billion) has been invested in India's renewable energy sector. The EY Renewable Energy Country Attractive Index 2021 rated India at third rank
- **Policy support:** The Ministry of New and Renewable Energy (MNRE) launched Rooftop Solar (RTS) Programme Phase-II in July 2021 to promote RTS across the country, particularly in rural areas, with the goal of installing 4,000 MW of RTS capacity in the residential sector by 2022 with a subsidy.

One of the Ministry's oldest programmes, the Off-Grid Solar PV Applications Program, aims to provide solar PV-based applications in locations where grid power is either unavailable or unreliable. The scheme provides solar home lights, solar street lighting, solar power plants, solar pumps, solar lanterns, and solar study lamps, among other applications. The following is the application-wise status of the installations under the Off-grid and Decentralised Solar PV Applications Program, till may 2022 [3]:

- Solar Lamps/Lanterns: 65,17,180 units.
- Solar Pumps: 2,37,120 units.
- Solar Street Lights: 6,71,832 units.
- Solar Home Lighting Systems: 17,15,639 units.
- Solar Power Plants: 212 MW capacity.

Solar pumps are a crucial part of the solar off-grid initiative since they enable sustainable irrigation in rural or isolated parts of the country. Solar photovoltaic water pumping systems may readily satisfy the irrigation needs of small and marginal farmers' landholdings. As a result, solar pumps are being built to replace the current diesel irrigation pump. MNRE launched the programme for the first time in 1992. Around 11,600 solar pumps were deployed in the nation between 1992 and 2014. The government set aside Rs. 400 crores in 2014-15 to build one lakh solar pumps for irrigation and drinking water across the country. Approximately 2.37 lakh solar pumps have been installed as part of the solar pump initiative to date. The Scheme provides up to 30% of the benchmark cost of solar pumps. Up to March 31, 2017, stand-alone solar pumps were part of the Off-grid and Decentralized Solar PV Applications Scheme. The government has announced the pradhan mantri kisan urja suraksha evam utthan mahabhiyan (PM-KUSUM) initiative, which focus onto build new standalone solar pumps in off-grid locations as well as solarize existing grid-connected agricultural pumps. Farmers will have a reliable supply for irrigation, which will boost their revenue as well as their general economic standing and well-being [3].

In the alternative energy sector, the solar industry is the fastest expanding portion. The global expansion of photovoltaics has followed an exponential trajectory for more than two decades and will continue to climb. Annual installations are expected to rise from 40.0 GW to 135.0 GW by 2020, with worldwide total capacity approaching 700.0 GW. Rapidly increasing consumer demands, environmental awareness, new national and state subsidisation/mandates, and new government R&D initiatives are all driving forces behind this growth [4]. There has been a lot of study towards lowering the cost of PV modules and discovering technologies to make PV systems smarter and more efficient in order to reduce the levelized cost of energy (LCOE) to grid parity. Integrating power electronics converters directly into the system is one approach to do this. Solar energy has already attained grid parity with conventional energy sources in more than 30 nations [5], and with power electronics incorporated into the system, this number will continue to rise.

Electric drives are crucial in the modernization and growth of human communities. Motors consume more than 40% of the energy consumed in drive systems. As a result, motors play an important part in applications that need electric drives, such as solar-powered water pumping. DC motors were originally utilised for water pumping. Because of the disadvantages of DC motors, such as low efficiency and frequent maintenance owing to the presence of brushes and commutators, AC Induction motors are used for water pumping applications. Induction motors, on the other hand, were inefficient for water pumping due to their intricate control and overheating under low voltages, especially in low and medium power applications. For water pumping, synchronous motors, whose rotor is made up of high power density permanent magnets, turns out to be better alternative for DC and induction motors. Sinusoidal wave permanent magnet motors (permanent magnet synchronous motors, PMSMs) and trapezoidal wave permanent magnet motors (BLDC motors) are two types of synchronous motors. BLDC motors are suited for PV-fed solar water pumping

applications because of their high efficiency, low maintenance requirements, high dependability and strong dynamic performance [9]. A voltage source inverter (VSI) is used to feed PV-generated electrical power to the motor.

1.2 SCOPE OF WORK

The modern arena is proceeding towards cutting edge renewable technologies which are highly advanced, developed, cost effective and reliable with respect to conventional times. The fear of energy crisis due to shortage of non-renewable energy sources like coal, petroleum etc are pushing the demand and production of renewable energy thereby reducing its cost to a greater extent [2]. The renewable energy also intends to provide power in areas having lack of suitable conventional power grid. Solar and wind energy systems, which are among the numerous available renewable energy sources (RES) such as biomass, solar, wind, mini-hydro, and tidal power, rely on modern power electronics converters and control equipment since they generate DC power that must be converted to AC power.

The Standalone Solar Water Pumping System (SSWPS) which is an excellent application of solar energy resource for water pumping in industries, fields for irrigation purpose or household usage. Mainly, three topologies are used in PV fed solar water pumping systems. The first one is single stage PV system which consists of a PV array directly connected to DC-DC converter fed DC motor, the second one is single stage PV system which comprise of a PV array directly connected to inverter fed AC motor (directly fed) and the third one is double stage PV system where a dc-dc converter is used as an intermediate converter between PV array and Inverter fed BLDC or PMSM motor, as shown in Figure 1.1 and 1.2. The reason of selecting the third stage for our research dissertation using BLDC motor is explained further in chapter 3 and chapter 4.

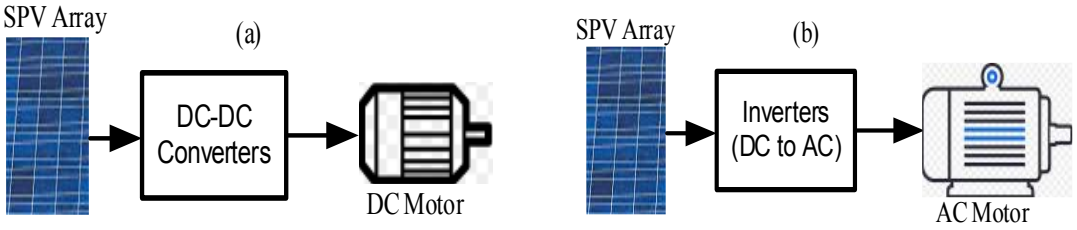

Figure 1.1 Block Diagram of single stage (a) DC motor-driven pumping system (b) AC motor-driven pumping system.

Figure 1.2 shows a multi-stage standalone solar PV water pumping system with power electronic control, which includes a SPV array, DC-DC converter, a DC-AC VSI for BLDC motor control, and a centrifugal water pump. Except for some particular reliability criteria, the water is held in tanks and works as a storage system, effectively eliminating the need for a battery [10]. PV arrays are created by connecting PV modules in a series–parallel configuration to meet the required voltage, and the PV output power changes based on solar insolation variation. As a result, the PV Array should be operated at its peak performance, commonly known as maximum power point (MPPT). Various MPPT Algorithms can be used in conjunction with DC-DC converters or inverters to run at a voltage that will lead to maximum power [11]. In solar PV-based

water pumping systems, basic DC-DC converters such as boost, buck-boost, Cuk, and certain advanced DC-DC converters such as Luo, SEPIC, and Zeta converters are employed. The DC-DC converter's output is fed into a three-phase VSI, which powers the BLDC motor. Solar water pumping pumps should be chosen depending on daily water requirements and pumping head. The most prominent used pumps for water pumping are centrifugal pumps.

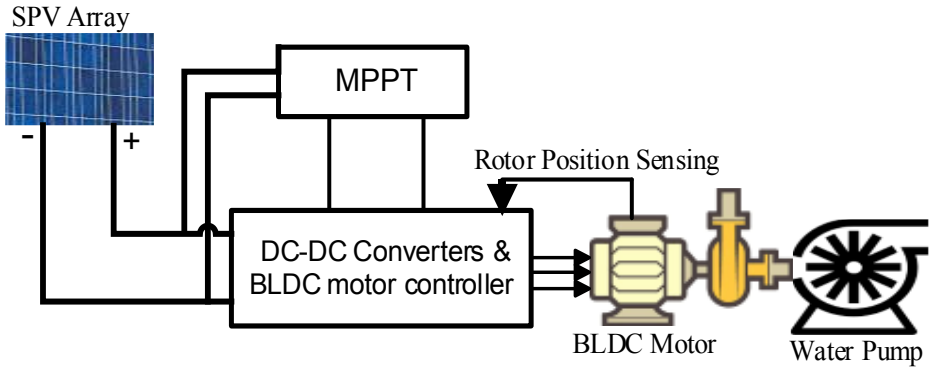

Figure 1.2 Block Diagram of Multi-Stage BLDC motor-driven pumping scheme.

The increment in advanced technology for pumping applications has been possible due to very swift development in power semiconductor devices. At the same time, stable and reliable operation of whole system is affected due to presence of harmonic distortions being produced by power converters which then results in additional losses and antagonistic inference. The necessity of the DC-DC power converters is subject to supplying a constant output voltage by changing the duty cycle of principal switches, without being affected by input voltage disturbances [2]. The two parts of designing SSWPS comprises of the passive components selection and the optimized composition of control system algorithm for the cognitive control of ADDC's switching, for drawing the paramount obtainable power from SPV array and to abstain from the switching losses in VSI due to high frequency switching by employing a proper electronic commutation [3].

The first comparative analysis using open loop system is done by considering the overall procedure for implementation of optimum design and control of SSWPS, which primarily comprises of a PMBLDC motor coupled to pump, an arrangement of voltage source inverter (VSI), a high gain advanced DC-DC converter (ADDC) and a SPV array, as shown in Figure 1.3. The intended system of water pumping is modelled and designed in a way so that the overall performance, even under the dynamically changing atmospheric conditions, is not affected. The idea of designing passive components is such that the operation of inductor of ADDC, even at lower sun radiation, should remain in continuous conduction mode (CCM) [4-6]. The proposed system comprising of ADDCs and BLDC motor have the ability to operate in a manner adequate for the dynamically changing atmospheric conditions. It consists of SPV array, ADDC being controlled by a pulse generator via INC-MPPT algorithm, a BLDC motor drive (having VSI embedded electronic commutation using hall signals) coupled to a centrifugal pump for irrigation application [7].

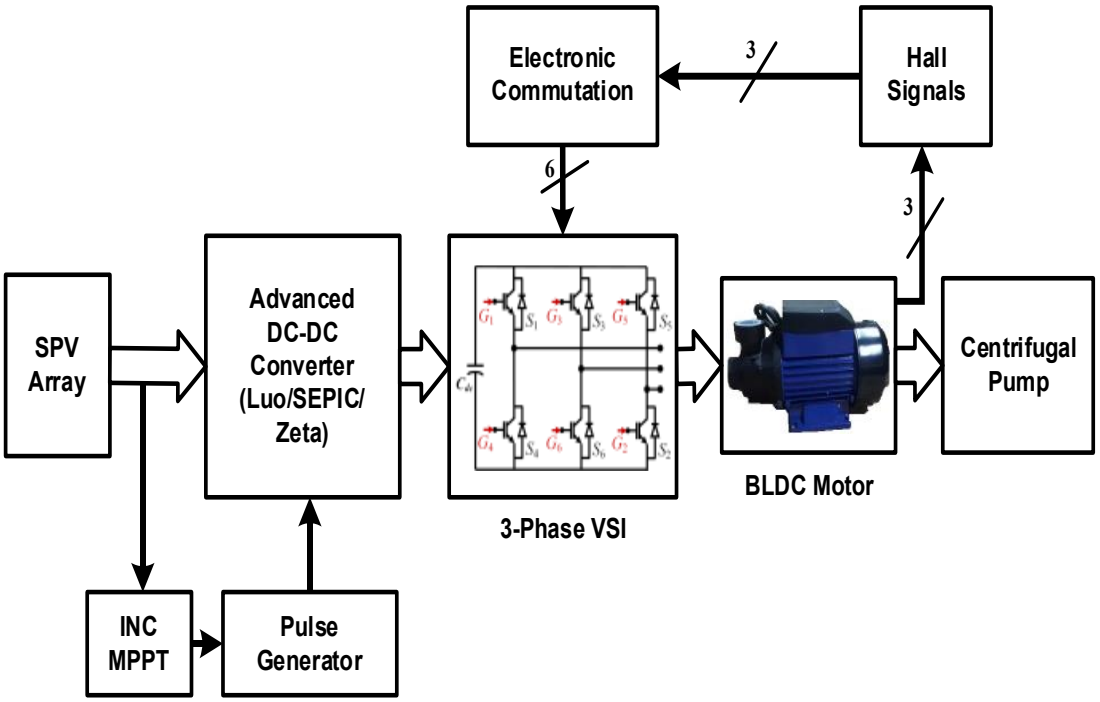

Figure 1.3 Open-Loop Block Diagram of SSWPS.

The hall signals via hall sensors measure the rotor position, in order to properly commutate the motor correctly. Also, the variation in solar irradiance level is taken care of by optimum design of SPV array. The results in the variation of three different ADDCs performance parameters in open-loop, i.e., without speed control, is examined using simulation in MATLAB/Simulink software.

The BLDC motors are popular because of its high efficiency, high reliability, low inertia, maintenance free operation, swift response, high torque density and smaller size for similar work. But due to the way it's been constructed, its applications possess high non-linearities which results in higher current and torque ripples. So, we use a closed-loop control namely speed control using different controllers.

In the second comparative analysis a closed-loop speed control system is considered using PI controller because it has excellent compliance over load torque variation as it annuls disturbance effects as load torque changes and have higher steady state accuracy. The output of the proportional controller is directly proportional to the error. If the error is zero, the controller's output is zero, and the system slows down with damping. There is also an overshoot. The integral controller shortens the rise time, enhances the settling time, and, most importantly, removes the steady state error. In several industries, PI controllers are one of the most often used controllers. The essential requirement for using these controllers is to tune their parameters in order to achieve the desired result.

The input supply voltage to the motor has numerous harmonics components due to the use of high frequency switching of power devices, power electronic commutation, flaws in the stator, and the auxiliary control system. High frequency components in the voltage input may produce substantial electro-magnetic interference (EMI) during

operation, and the pulsating current input caused by electronic commutation would cause torque ripple. To eliminate the harmonics, present in the input voltage of the motor and the pulsating variation of line current of the motor, an efficient controller is necessary. Brushless DC motors with a low torque ripple coefficient are frequently required by the industrial control systems. Cogging torque ripple and commutations torque ripple are two common causes of torque ripples in brushless motors. Cogging torque ripple is caused by the interlinkage of teeth and slots with permanent magnets, and it is usually reduced by using a more coherent motor structure, such as notching in teeth, skewing stator teeth or rotor magnet poles, finding the best pole arc to pole pitch ratio, and shifting magnet poles pair. Commutation torque ripple is caused by winding inductances, which limit the current rising speed of the in-going phase and cause current to sink during the commutation interval. In order to eliminate commutation torque ripple, we need to keep the conducting current constant by sensing phase currents alone. So, by employing a voltage controller and a current controller, we may improve BLDC motor drive system performance and eliminate torque ripples [10].

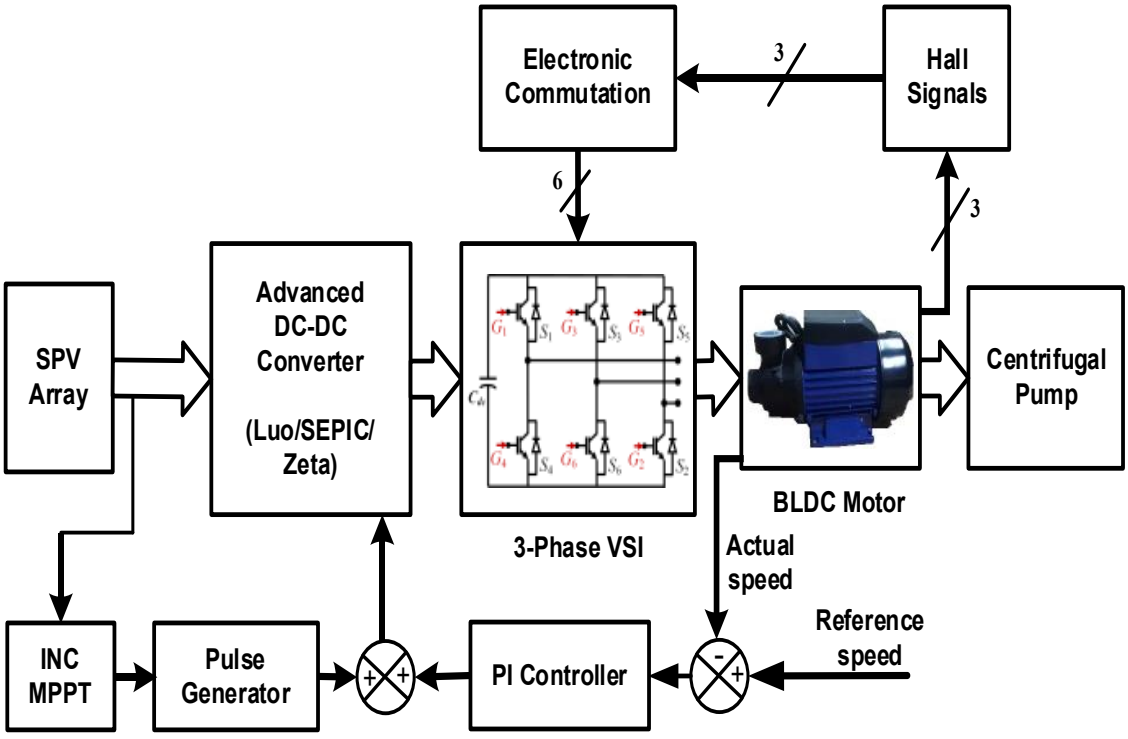

Figure 1.4. Block Diagram of speed controller integrated SSWPS.

The Figure 1.4 depicts the proposed system's operation stages. The BLDC motor is coupled to centrifugal pump and is being fed from SPV array via ADDC's and three phase voltage source inverter (VSI). The switches of VSI are being commutated electronically by sensing the rotor position using hall sensors using hall signals. Now for keeping the dc link voltage of capacitor (C_{dc}) constant, the switch of ADDC's is being controlled using the summation of signals generated by the PI controller and pulse generator. The input to PI controller consists of the difference between the measured rotor speed and rated rotor speed as reference speed. The input to the pulse generator is provided by analysing the voltage (V_{PV}) and current (I_{PV}) from SPV array using INC-

MPPT algorithm. The results in the variation of three different ADDCs performance parameters in closed-loop, i.e., with speed control, is examined using simulation in MATLAB/Simulink software.

Finally, a conclusion is derived using the results obtained through the comparison of performance parameters of nine different the modes of the three ADDC's considering each of the open-loop and closed-loop control system using simulation in MATLAB/Simulink software.

1.3 OBJECTIVE OF RESEARCH AND SPECIFIC CONTRIBUTION

The following objectives are to be achieved with respect to the research carried out on calculating the performance of advanced dc-dc converters for BLDC motor driven standalone solar water pumping system.

1. The standalone solar water pumping system should be cost effective for the consumers in long run which is achieved by eliminating the use of unreliable components, decreasing the losses, increasing the efficiency of the overall system.
2. The BLDC should start in a soft starting mode avoiding high inrush current, which is achieved by employing proper electronic commutation.
3. The switching losses in voltage source inverter should be minimized which is achieved by switching any two switches of the three phase VSI at a time in 120^0 conduction mode.
4. To avoid the effect of input voltage disturbances on the output of the advanced DC-DC converter which is achieved by properly designing the components of advanced DC-DC converter and employing an INC-MPPT algorithm.
5. To achieve better dynamic response characteristics which is achieved by using a closed loop speed control using PI controller

1.4 THESIS ORGANIZATION

This thesis contains six chapters describing the design, integration methods, modeling and control approach of a standalone solar water pumping system and is organized as follows:

Chapter 2- Presents a complete analysis of the literature review on standalone solar PV-fed water pumping systems utilizing BLDC motor. The study findings of solar photovoltaic water pumping systems employing BLDC motor drives with and without dc-dc converters are the emphasis of this chapter.

Chapter 3- Describes principal of working of permanent magnet BLDC motor, its construction, its comparison with the available alternative in the market, different types of control techniques used for BLDC control (like Hall Effect sensor based electronic commutation and speed control using PI controllers), mathematical modeling of BLDC machine and its speed-torque relationship.

Chapter 4- Explains the subsequent sections having design of passive components, in order to operate the given system in continuous conduction mode (CCM). It includes the selection and design of SPV array and related MPPT controlling algorithm, introduces classification of DC-DC converters as well explains the principal of working and performance parameter calculation procedure of advanced DC-DC converters and briefs about voltage source inverters (VSIs).

Chapter 5- Provides the optimal design and selection of pump and BLDC motor as well as open-loop and closed-loop control approaches using suitable controller for ADDC's switching and commutation of PMBLDC deployed for driving a pilot-tube centrifugal water pump coupled to its shaft.

Chapter 6- Discuss the comparative conclusion and further work to be carried out.

CHAPTER 2

LITERATURE REVIEW

In 1996, W Lawrance et al. built a water pumping system for field pumping applications like stock watering and irrigation, using a BLDC motor and helical rotor pump. As a dc-dc converter, a buck converter was employed. Individual component models, such as the PV array, MPPT, BLDC motor, and helical rotor pump, were created with PSI/e, a block-oriented software programme that allows for the production of complicated electro-mechanical system models. The MPPT methodology employed was the open circuit voltage method [12]. The system was simulated during a 12-hour daily cycle and the results were compared to experimental data. The simulated model and the system's test results were found to be highly correlated.

In 1996, Bhim Singh et al suggested a high-efficiency as well as low-cost PV-powered BLDC motor drive for water pumping. Without any extra dc-dc converters, the system employed a sensorless control technique. To evaluate the dynamic characteristics of the PMBLDC motor drive system, a mathematical system model was built and a basic low-cost microcontroller was employed [13]. The suggested model was found to operate adequately at various power levels when the simulated results were compared to experimental data.

In 2010, S.H. Hosseini et al. presented the performance of a BLDC motor operating a water pumping system using PV input. To obtain most of the power from the PV array and supply to the BLDC motor, the suggested system used a Z-source inverter (ZSI). Fuzzy logic controlled incremental conductance MPPT algorithm was created to eliminate operating point instability. The speed controller was regulated using particle swarm optimization (PSO) to obtain the reference speed for the BLDC motor and hence gain excellent dynamic response characteristics. PSCAD/EMTDC connected to MATLAB software was used to simulate the performance of the proposed system under various operating parameters of the SPV array [14]. Low torque ripple was obtained through inverter's voltage regulation, according to simulation findings. The suggested system also has a minimal number of power switches, a cheap cost, and a high efficiency.

In 2012, Terki et al. investigated the performance of a brushless dc motor controlled by a hysteresis current loop in PV-fed water pumping systems. Standard PI and fuzzy logic (FL) speed controllers were utilised [15]. To improve the efficiency of the PV generators, a maximum power tracker was incorporated. Control of the system employing the two kinds of controllers was evaluated under no load and during loading conditions, as well as overall system performance. For both controllers, the simulation revealed that the speed converges to the reference value rapidly without overshoot and with null steady state error, but the FL controller provides substantially superior dynamic features for difficult and nonlinear control systems.

In 2013, Mahdi Ouada et al. [16] proposed an intelligent control scheme that used fuzzy logic control with an MPPT controller for a PV standalone water pumping

system, to increase the energy conversion efficiency, with a BLDC motor. As an intermediate converter, a DC–DC boost converter was employed. The hysteresis current control technique was used to create the PWM signals for the VSI. The system was simulated in the Matlab Simulink environment, and the proposed method's efficiency was demonstrated.

In 2013, M.H. Taghvaee et al analyzed non-isolated DC–DC boost, buck, buck–boost, Cuk, and SEPIC converters in order to develop a solution that best fits the Maximum Power Point application. The review was divided into four categories: converter topology, application, operating region and topologies' pros and cons [17]. A comparison among these converters was also performed. The buck-boost converter had the greatest efficiency rate of 96.2% when compared to other converters. The buck–boost DC–DC converter was found to be the ideal type of converter for PV systems, as it was able to assure optimum MPPT performance for any solar irradiation, load circumstances and cell temperature while also improving the system's performance.

In 2014, R.Kumar et al. analyzed and designed a canonical switching cell (CSC) converter as an auxiliary DC-DC converter for a PV-fed BLDC motor drive for a water pumping system. Unlike buck and boost converters, there is absence of MPPT operating range the CSC converter. The maximum power was tracked using the incremental conductance MPPT method. VSI's electronic commutation with fundamental frequency switching was applied, resulting in a dynamic DC output voltage and lower switching losses [18]. The suggested water pumping system's detailed performance for different modes of operation was simulated, and the results revealed that the system achieved steady state values for the assigned irradiances, as well as soft starting of the BLDC motor.

In 2014, R. Kumar et al. developed a LUO converter-based BLDC motor-driven water pumping system that uses SPV as an input voltage source. A negative output elementary LUO converter was chosen because it offers features such as continuous conduction mode of operation, limitless MPPT operating zone, and reduced output current ripple [19]. The system's performance under varying environmental circumstances was investigated. According to the simulation results, the BLDC motor-pump parameters reached their rated values in steady state, and the motor always reached a speed more than 1100 rpm, even at the least solar insolation.

In 2015, Le An et al, for a standalone PV-battery-powered pump system, developed a single-switch non-isolated dc-dc converter. The intermediate dc-dc converter was created by combining a buck converter and a buck-boost converter, resulting in increased conversion efficiency. MPPT and output voltage regulation were achieved using duty cycle modulation and variable switching frequency control to operate the pump at a constant flow rate. The dc-link capacitor's voltage stress problem in traditional single-stage converters was solved by using a battery, which gives a more stable dc-link voltage than a conventional converter [20]. A prototype of the suggested PV battery-powered water pump was created as an experiment. In the presence and absence of MPPT control, the transient state and steady state responses, as well as the

responsiveness under partial shade circumstances, were recorded. The advantages of the suggested system were demonstrated by the findings. When comparing the conversion efficiencies of the proposed converter to a traditional two-stage converter under various loading conditions, the suggested converter achieved a maximum efficiency of 92%.

In 2015, Kumar et al, in a PV-fed BLDC motor-driven water pump, used a dc-dc boost converter as an auxiliary converter. A boost converter was employed to optimise the power of the solar PV array while also reducing the BLDC motor's starting inrush current. The desirable qualities of boost converters, such as increased conversion efficiency, high switch utilisation, minimal stress on semiconductor devices, and a small number of reactive components, prompted its utilisation for SPV array water pumps. The MPPT algorithm employed was incremental conductance. Electronic commutation was used to run the VSI. Because the BLDC motor's speed was governed by the variable DC link voltage, no separate sensors for speed control were needed [21]. The system's performance parameters were assessed under various circumstances. The motor reached its rated speed of 3000 rpm at 1000 W/m^2 insolation, resulting in full capacity water pumping, and the designed water pumping system performed well even at 20% solar irradiation.

In 2015, Bhim Singh et al examined the behaviour of a SEPIC converter in a BLDC motor-driven SPV array-fed water pumping system. The SEPIC converter which is a buck-boost converter, has the advantages of non-inverting polarity output voltage, low input current ripple and a simple gate-drive circuit [22]. The SPV array was operated at its optimal operating point using the incremental conductance MPPT algorithm, which also accomplished soft starting of the BLDC motor. The VSI switching sequence was created by the BLDC motor's electrical commutation. The suggested system's performance was measured under various environmental conditions. Under each solar insolation level, the BLDC motor reached a speed greater than 1100 rpm, the minimum speed necessary to pump the water, indicating that the system performs excellently under a variety of operating conditions.

In 2016, Kumar et al. implemented and tested a buck-boost converter for use as an intermediary DC-DC converter in between SPV array and VSI for application of water pumping. A centrifugal kind of water pump was driven by a BLDC motor. The buck-boost converter has a high conversion efficiency, employs the incremental conductance MPPT algorithm to maximise SPV array efficiency, and softly starts BLDC motors. The electrical commutation of the BLDC motor generated the switching sequence for the VSI. The envisioned system's behaviour was examined using a hardware prototype at different irradiances ranging from $200W/m^2$ to $1000W/m^2$ [23]. According to both hardware and simulated findings, the MPP was successfully tracked and the throughput was unaffected even under varying weather conditions. Furthermore, the analysis indicated that the BLDC motor always runs at a speed greater than 1100 rpm, which is the lowest speed essential to pump water at a solar insolation level of $200W/m^2$. The envisioned technology has various advantages over traditional buck and boost converter techniques.

In 2016, Bhim Singh et al suggested a layout of a zeta converter, employed to solar PV array fed BLDC motor-driven water pump, used to retrieve the maximum available power from the SPV array. The Zeta converter has a number of benefits over traditional buck, boost, buck–boost, and Cuk converters, such as continuous ripple–free output current, an unbounded MPPT region, and non–inverting output voltage. The zeta converter was operated using an incremental conductance MPPT algorithm, ensuring that the SPV array always functions at its MPP and the BLDC motor starts softly. Because the suggested control algorithm does not need sensors, it is a simple and cost-effective system. The VSI's fundamental frequency switching prevents power losses caused by high frequency. The variable dc link voltage of VSI [24] was used to govern the speed of a BLDC motor. The suggested system was conceived, modeled, and tested while taking into account stochastic and instantaneous fluctuations in solar irradiation. Weather conditions had little effect on the performance of the BLDC motor-pump, according to simulations. A better tracking efficiency was reported when the performance of the created prototype was evaluated for solar irradiation levels ranging from 400 to 1000 W/m^2.

In 2016, R. Kumar et al, suggested a water pumping system using a DC–DC Landsman converter, based on an SPV array driven BLDC motor. The Landsmann converter [25], which is based on buck-boost converter, was employed to optimize the power output of the SPV array and to enable safe and soft starting of the BLDC motor by using the incremental conductance MPPT technique. For speed control, no further circuitry was required. The suggested system's starting, dynamic, and steady-state responses were all simulated. The incremental conductance MPPT approach demonstrated that MPP was tracked accurately with little fluctuation around the peak power point at 1000 W/m^2. Also, the findings shows that even at a low solar irradiation level of 200 W/m^2, the motor achieves the minimum speed necessary to pump the water. The suggested system's viability for water pumping was further demonstrated by hardware tests. The total efficiency of the suggested system was calculated using experimental data for various irradiances. At rated load and 1000 W/m^2 insolation, the proposed system has an efficiency of 83.3%, with a minimum efficiency of 74.4% at insolation 200 W/m^2.

In 2017, R. Kumar et al. proposed a single-stage energy conversion system for water pumping applications using a PV-fed BLDC motor drive. The BLDC motor pump was fed directly from the SPV array through a VSI. When compared to an induction motor-driven system, the suggested system with the abolition of phase current sensors and DC-DC converters provided a high efficiency power conversion [26]. Control of the solar PV array operating point through INC-MPPT technique, electronic commutation of BLDC motor, switching signal generation for VSI, and monitoring the speed of the BLDC through the optimum power of the solar PV array were the four major parts of the single-stage system's control. Even under dynamic situations, the motor maintained its smooth performance. Experiments on a prototype under varied operating circumstances further confirmed the system's satisfactory operation. A comparison was done between the existing single stage system and the suggested single stage system.

The efficiency of the two systems was calculated at different irradiance levels and under similar operating conditions. Irrespective of the operating conditions, the suggested system appeared to be more efficient than its traditional ones, demonstrating the single stage system's superiority in every regard.

In 2017, Ulliboina Suribabu et al presented BLDC motor-driven water pumping system based on solar PV array using a Landsman converter as an intermediary dc-dc converter. For speed control, a fuzzy logic controller (FLC) was employed. The INC-MPPT algorithm was used to control the Landsman converter, which served as an interface between both the VSI and the SPV array, in order to extract the maximum available power from the SPV array. The VSI feeds the BLDC motor pump and also enables soft starting through electronic commutation. For speed control, no extra phase current sensors or accompanying circuits were required [27]. Simulated results were used to examine the various performance characteristics of the proposed water pumping system. Even though there were abrupt atmospheric disturbances, the functioning and performance remained satisfactory.

In 2017, R. Kumar et al proposed a BLDC motor drive for water pumping fed by SPV array using Cuk converter as intermediate dc-dc converter. For tracking MPP, the MPPT algorithm utilised is incremental conductance. The VSI feeds the BLDC motor that operates the pump load. Utilising hall effect position signals, electronic commutation was used to create switching pulses. When compared to other non-isolated dc-dc converters, the Cuk converter had benefits such as decreased current ripples, continuous input and output currents, reduced switching losses, soft motor starting, high efficiency, and so on. Simulated results using matlab/simulink were used to determine the effectiveness of the proposed scheme under various weather conditions. A performance comparison with a traditional DC–DC boost converter proved the advantages of the presented topology.[28]. Experimental data were used to assess the efficiency of both conventional and recommended systems at varied insolation levels and under similar operating circumstances. The Cuk Converter was shown to be more efficient than its traditional version regardless of the operating circumstances. To demonstrate commercial viability, a cost study of the recommended scheme with a PV fed induction motor water pumping system, a single-stage PV-ZSI fed BLDC motor and a single-stage oriented water pumping system was done. The Cuk converter-based system was found to be relatively cost-effective.

In 2017, for a solar PV array fed water pumping system, S. Sarada et al proposed a fuzzy logic-based BLDC Motor Drive. The DC-DC converter used was a cascaded pair of DC-DC boost and buck converters that met the MPPT and soft starting requirements of the BLDC motor. It has features such as high efficiency, better switch utilisation, least stress on power electronics switches and non-inverting output voltage. The recommended converter's control was divided into three categories: Buck converter voltage control, incremental conductance MPPT control algorithm and BLDC motor electronic commutation [29]. The system's performance was examined, and it was realised that the motor's speed never drops below 1100 rpm, even at very low

irradiances. The efficiency at 200 W/m^2 was 78.3% whereas at 1000 W/m^2 maximum efficiency of 86.8% was obtained from the experimental results.

In 2017, Aboul Zahaba et al. demonstrated a standalone PV water pumping system that supplied a water pump powered by a BLDC motor and stored energy in lead acid batteries. A single PV module, dc-dc boost converter, a MPPT, an energy storage system with charging controller, BLDC motor control and a BLDC motor running a positive displacement pump, are all part of the proposed system. Three control units contribute in the control strategy [30]. The first unit is used to regulate the speed of a BLDC motor via hysteresis current control. The MPPT is the second control unit, and it was here that the P&O-based MPPT algorithm and the fuzzy logic-based method were investigated. The third controller manages the battery charging and discharging system, which employs intermittent charging regulation method. The system was simulated using the two MPPT techniques using the same motor control (hysteresis current control). From the simulation results it was found out that Fuzzy Logic Control was faster and has lower oscillation around the maximum power point than the perturb & observe (P&O) algorithm.

In 2018, Neeraj Priyadarshi et al. showed a Luo converter-based BLDC-driven PV pumping system with MPPT control using the hybrid adaptive neuro-fuzzy inference system or adaptive network-based fuzzy inference system (ANFIS) flower pollination optimization algorithm (FPA). The Luo converter features a greater voltage transfer gain, higher power density, and a smoother output waveform with the least amount of ripple content and improved transformation efficiency. The hybrid ANFIS-FPA is easy to implement, has a fast convergence rate with tuned parameters, and is easier to code [31]. It is used to provide the needed pulse for the Luo converter's power semiconductor switch. The VSI BLDC motor is controlled by an electronic commutation mechanism. Experimentally the dSPACE controller was used to test the behaviour of BLDC-driven PV pumping with a Luo converter. The system's performance was evaluated at both steady state (1000W/m^2) and variable irradiance levels (300W/m^2 to 1000W/m^2). The ANFIS-FPA based MPPT delivers effective tuning with an excellent performance index, and hence the system functions efficiently under all operating situations, according to the experimental results.

In 2018, S. Sashidhar et al designed a single-stage sensor-less control using ferrite permanent magnet BLDC motor drive which can be submerged in a deep bore well. By employing only six switches, the control scheme was able to conduct both MPPT and phase commutation utilising a single-stage three-phase VSI. The system's efficiency and reliability were improved by eliminating the requirement for a specialised dc-dc converter for MPP operation and hall sensors. The MPPT process was accomplished using the P&O method. The Matlab/Simulink platform was used to simulate the sensor less pre-positioning, start-up, and transition to operating mode of the submersible BLDC motor drive. It was discovered that the PV voltage remained constant amidst the step variation in insolation, demonstrating the MPPT's efficacy. [32]. The system's prototype was built, and the BLDC motor and inverter efficiencies at rated power were found to be 87% and 92%, respectively. A cost comparison was made

between a two-stage induction motor design and the suggested one, revealing that the proposed technology was significantly less expensive.

According to the findings of the literature research, direct fed PV water pumping systems are less efficient than dc-dc converter fed water pumping systems.

CHAPTER 3

OVERVIEW OF BLDC MODELLING, DESIGN AND CONTROL

Brushless DC motors – or BLDC motors in short – are an indispensable part of modern drive technology. Other names are also EC (electronically commutated) motor or synchronous motor. They have for many years been standard for actuating drives or also for electrical power generation. However, the use of miniature motors up to the kilowatt range was reserved for a long time for brushed (DC) motors. At the beginning of the technology of power electronics, DC was much easier to control. But as considered in more detail later, brushless motors need multi-phase, mostly three phase AC. It was at that time very complex to produce that in the different frequencies and voltages required. So, their use was only worthwhile for larger power classes. But today's microprocessor technology combined with efficient transistors of the smallest size allowed since the beginning of the 21st Century that ever-smaller brushless motors have been competitive in price compared to DC motors. As will be shown, they are par excellent to DC motors in various ways, either because of the low wear or the high efficiency. Anyone who has ever replaced a DC drive with a brushless drive will therefore never look back on the other technology.

This is particularly true for model construction. In the last years of the 20th Century almost all small electric motors were brushed. Here, the change to brushless drives took place within a few years. The many benefits of this technology ensured that they became not only the standard drives for boat and car models, but even for flight models. This is particularly interesting because there they need to compete with combustion engines. For a long time, these seemed to be undisputed in terms of power density.

3.1 CLASSIFICATION OF MOTORS

According to the kind of power source employed, electric motors may be divided into two categories, as illustrated in Figure 3.1: direct current (DC) motors and alternating current (AC) motors. Because its design is similar to that of a permanent magnet synchronous motor (AC motor) yet its electrical properties are similar to those of a DC motor, thus the brushless DC (BLDC) motor is difficult to classify as either of the motors.

Because of its ease of torque control and outstanding drive performance, DC motors have long been a popular choice for speed and position control applications among developed motors. Induction motors, on the other hand, have been widely employed for general purpose constant speed applications due to their inexpensive cost and robust design. Induction motors absorb around 80% of the power consumed by motors. There have been several advancements in motor drive technology to go along with the developments in motor design. The introduction of power electronic converters based on power semiconductor devices in the 1960s made it possible to design motors

with specialised operation characteristics for certain system applications. Furthermore, the engineers were able to apply advanced control techniques to motors by employing microcontrollers with increased performance digital signal processing technologies, considerably improving the performance of motor-driven systems.

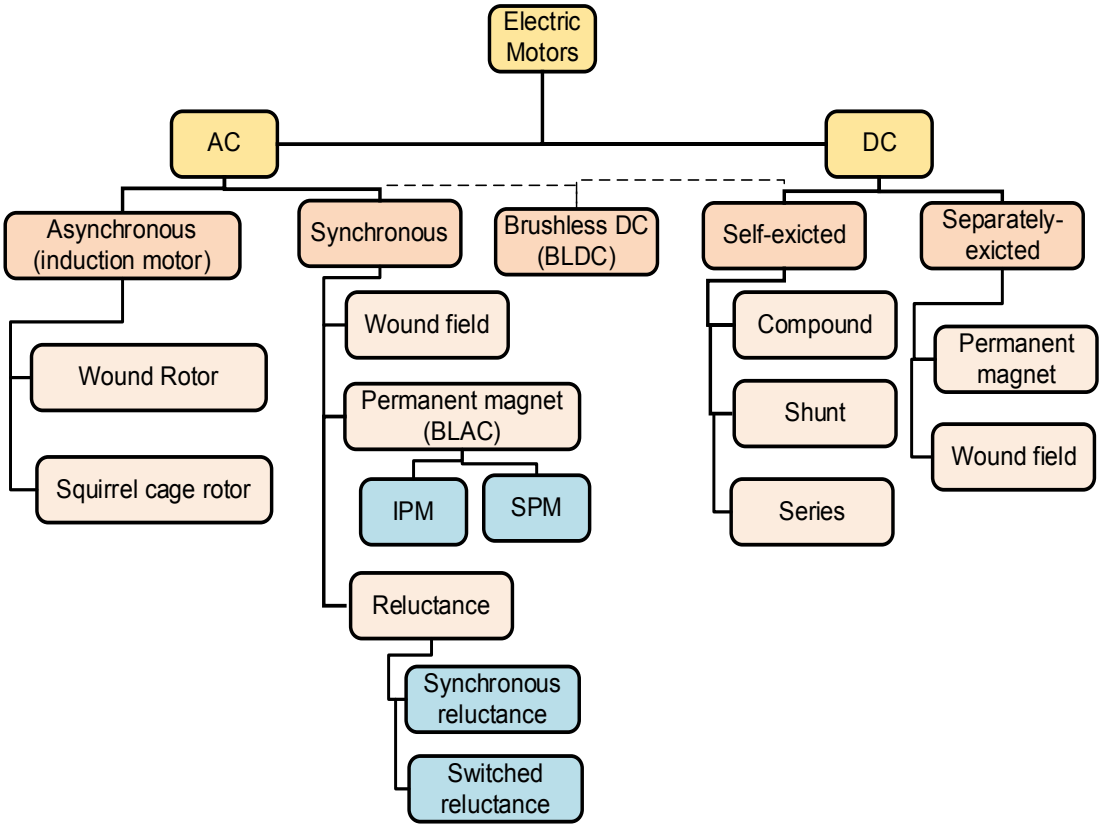

Figure 3.1 Classification of electric motors.

3.2 COMPARISON OF BLDC WITH ITS ALTERNATIVE

3.2.1 Comparison between brushed DC and BLDC motors

In a traditional (brushed) DC motor, brushes are responsible for making mechanical contact with a series of electrical connections on the rotor known as the commutator [33]. Between the DC electrical supply and the armature coil windings, an electric circuit is formed. The stationary brushes make contact with various portions of the commutator while the rotation of armature takes place. The rotating commutator and brush arrangement work together to create a set of electrical switches that enable electric current to pass through the armature coils nearest to the field, which can be either an electromagnet or a permanent magnet [33].

In a brushed DC motor, the DC current passing through the coil windings of the rotor generates an electromagnet with the poles as seen in the Figure 3.2. To make the rotor spin, these rotor magnetic poles interact with the poles of the stationary permanent magnet, called the stator.

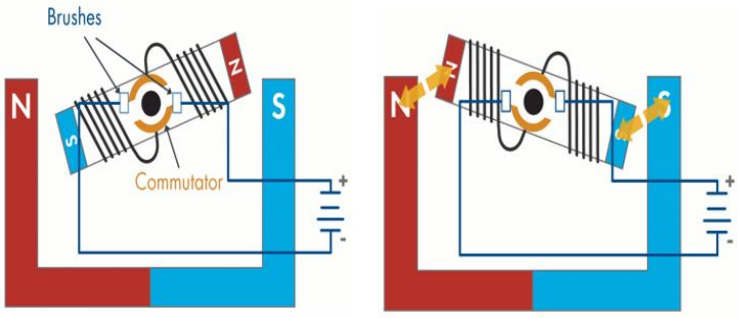

Figure 3.2 Brushed DC motor working.

To keep the motor spinning, the rotor poles must be flipped every half turn by reversing the polarity of the current inside the coil windings. Commutation is the process of changing this polarity of a current. Commutation in a brushed DC motor happens mechanically: when the rotor rotates, electrical contacts called brushes form a circuit to the opposite side of the commutator on the rotor. Brushes wear down over time as a result of this direct contact, prohibiting the motor from running.

When compared to alternating current (AC) motors, DC motors have been frequently employed for speed or position control applications due to their control simplicity. Direct current (DC) motors, on the other hand, require mechanical commutation devices, such as brushes and commutators, to change the direction of current in conductors and provide an average torque for continuous rotation, as illustrated in Figure 3.2. As a result, mechanical commutation produces electromagnetic and acoustic noise, and brushes and commutators must be maintained on a regular basis owing to wear and flashover. As a result, their use in many motor drive applications that demand continuous operation and increased system dependability has been limited.

Brushless direct current (BLDC) motors were invented in 1962 to solve the problem with DC motors [33]. This motor has electrical properties comparable to a DC motor, but it is more reliable due to the electronic commutation that replaces mechanical commutation. BLDC motors employ sensors and drive circuitry to accomplish electronic commutation. Magnet's position on the rotor is detected by the sensors. The drive circuits use the detected magnet position to stimulate a specified winding for continuous rotation.

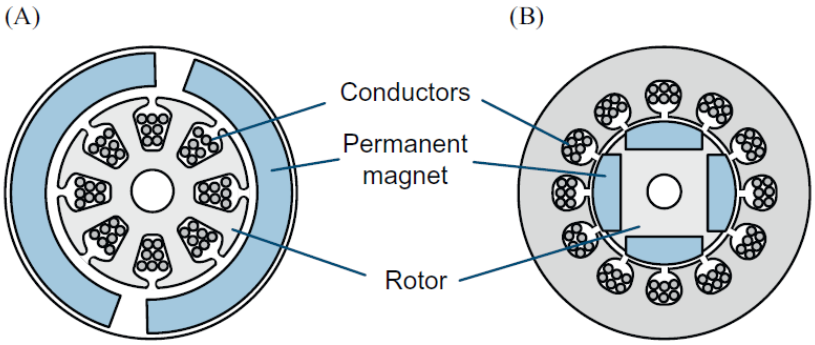

Figure 3.3 Construction of (A) DC motor and (B) BLDC motor.

Since the role of brushes and commutators is replaced by semiconductor switches that operate based on the rotor position, BLDC motors do not have the critical weakness of DC motors. The configuration of a BLDC motor differs from that of a DC motor as a result of this replacement, but it is comparable to that of a permanent magnet synchronous motor (PMSM). The BLDC motor has a layout in which the windings are on the stator side and the magnets are on the rotor side, as illustrated in Figure 3.3(B). So, this seems to be an inverted arrangement of a DC motor (A). Its design, on the other hand, is similar to that of a PMSM.

The current running in the windings of a BLDC motor, like the current flowing in the armature windings of a DC motor, has a quasi-square waveform. The advantages of BLDC motors in this setup versus DC motors are as follows. BLDC motors feature a low inertia rotor compared to DC motors that have a hefty rotor with numerous wires. As a result, BLDC motors can respond quickly to changes in speed. Furthermore, stator-side windings can quickly dissipate heat, enabling BLDC motors to achieve higher peak torque capabilities than DC motors whose maximum current is constrained to avoid magnet demagnetization. Moreover, due of nonmechanical commutation components, BLDC motors may run at a greater speed. Some of the additional advantages of BLDC motors are high torque-to-inertia ratio, high efficiency, high-speed operation capabilities, high power density, simple driving mechanism, and are relatively inexpensive. As a result, they are currently widely employed in a variety of medium and small motor drive applications, such as household appliances, industrial, office items, and light automobiles, as a cost-effective alternative.

3.2.2 Comparison between PMSM and BLDC motors

BLDC motors are sometimes mistaken with PMSMs due to their structural resemblance. BLDC motors are often differentiated from PMSMs by the form of their back-electromotive force (back-EMF). As demonstrated in Figure 3.4(A), a BLDC motor is designed to produce a trapezoidal back-EMF waveform. As a result, along the air gap, the amplitude of the magnetic flux density created by the rotor magnets remains constant. Magnets with parallel magnetization can be used to achieve this. A constant torque may be created when a BLDC motor with a trapezoidal back-EMF waveform is supplied with a rectangular stator current. A PMSM, on the contrary, is an AC motor with a sinusoidal back-EMF waveform, so its current should have a sinusoidal waveform for continuous torque production, as illustrated in Figure 3.4(B). The magnetic flux density created by the rotor magnets must be spread sinusoidally along the air gap to produce a sinusoidal back-EMF waveform [34].

In contrast to BLDC motors, a PMSM is commonly referred to as a BLAC motor. A BLDC motor with a trapezoidal back-EMF waveform has a 15% greater power density than a PMSM [35]. This is because, while having the same peak value, the trapezoidal waveform has a greater fundamental component than the sinusoidal waveform. There are significant differences between BLDC motors and PMSMs, aside from the back-EMF waveform. The comparison between the BLDC motors and PMSMs is summarized in Table 3.1.

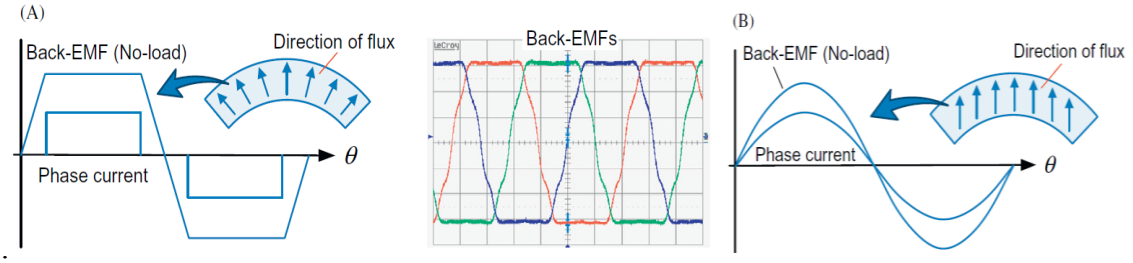

Figure 3.4 Waveforms pertaining back-EMFs of (A) BLDC motor and (B) PMSM.

Concentrated stator windings are used in BLDC motors, and quasi-square current waveform passes through them. A PMSM, on the other hand, typically employs distributed stator windings through which the sinusoidal current waveform flows. Recently, even PMSMs are increasingly using concentrated windings due to their short end windings and simple construction, which makes them suited for automated manufacture.

The driving systems for these two motors are clearly different. The phase current passes in only two out of the three-phase windings at a time in a three-phase BLDC motor at the time of its excitation of, hence each inverter switch functions for a 120^0 conduction period of a fundamental operational cycle. However, in a three-phase PMSM, the phase currents flow in all the three-phase windings at the same time, ensuring that each inverter switch always runs for a conduction period of 180^0 of a fundamental operational cycle. In comparison to the PMSM drive, which needs a complicated vector control approach, the BLDC motor drive is simple and economical. However, during the phase commutation of altering an active switch, BLDC motors have a considerable torque ripple, which can be eliminated using proper design aspects.

Table 3.1 Comparison of BLDC motors and PMSMs.

Parameters	**BLDC motor**	**PMSM**
Back-EMF waveform	Trapezoidal	Sinusoidal
Stator current waveform	Quasi-square	Sinusoidal
Stator winding type	Concentrated	Distributed
Drive methodology	Simple (using low-cost Hall effect sensors)	Complex (using high-resolution position sensor such as an encoder or a resolver)
Driving circuit (conduction interval)	Inverter (120^0 conduction)	Three-phase inverter (180^0 conduction)
System cost	Low cost	High cost
Torque ripple	Significant torque ripple	Nearly constant torque

3.3 BLDC MOTOR CONSTRUCTION

According to the number of windings present on stator BLDC motors are classified into single-phase, two-phase, three-phase, and/or multi-phase. Because of its simple driving circuit, simple structure and inexpensive nature, single-phase BLDC motors are frequently utilised for appliances and small machinery. In contrast, the rotation of such motors occurs in only such motors can only rotate in one direction. Additionally, because they have a detent point when no starting torque exists, they require a motor design with an auxiliary element for start-up. The starting torque is generally a reluctance torque, which results in substantial cogging torque. Small power applications below 10W, such as fans and blowers, benefit from single-phase BLDC motors since they have a low starting torque. Because of its enhanced power density and fault-tolerance capability, multi-phase BLDC motors above four-phase are mostly used in aerospace and military applications that need great dependability. The most common are three-phase BLDC motors than single phase [33].

In terms of magnetic flux direction, there are two types of BLDC motors: radial-flux type, which has the flux from the rotor magnet crossing the air gap in a radial direction, and axial-flux type, which has the flux crossing the air gap in an axial direction, as illustrated in Figure 3.5. Conventionally, radial-flux motors were solely used. As illustrated in Figure 3.5(A) and (B), this motor could either be an inner rotor or an outer rotor type. The inner rotor design, which is the most popular, has a greater heat dissipation capacity, a better torque-to-inertia ratio, and smaller rotor inertia. Servo drives that require a rapid dynamic reaction are a popular application.

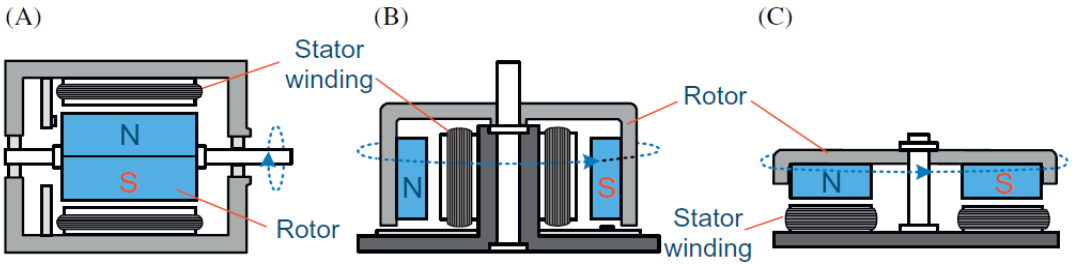

Figure 3.5 BLDC motor construction (A) Radial-flux (inner rotor), (B) Radial-flux (outer rotor), and (C) Axial-flux.

This type of motor produces minimal vibration and acoustic noise since the rotor is usually cylindrical in shape with a shaft upon which the bearings are mounted. The rotor inertia of outer rotor motors, as illustrated in Figure 3.5(B), is quite large because the rotor magnets move around the stator windings placed in the iron core of the motor. As a result, this motor is well suited to systems that require constant speed operation. High-speed operation is aided by the magnets mounted within the yoke. Even if lower energy product magnets are employed, the outer rotor motor may use more magnetic material than that of the inner rotor device, allowing it to produce greater flux. This sort of motor is now widely employed in a variety of applications, including, cooling fans, computer disc drives and washing machines [34].

A disc rotor containing magnets whose flux is in an axial direction rotates towards the stator, in the axial-flux motors depicted in Figure 3.5(C). Permanent magnets are affixed to the rotor's surface. Small motors with this design topology frequently utilize coreless stator windings installed on a nonmagnetic substrate or slot-less stator windings put on an iron core without slots. Because the cogging torque associated with conventional iron core motors can be eradicated due to minimal fluctuations in reluctance, the fundamental advantage of such a technology is that it has very low ripple torque and acoustic noise. Constant-speed operation is possible due to the presence of its high rotor inertia. Nevertheless, the available flux is considerably low due to the increased effective air gap. VCR and CD player drivers are common example. This axial-flux motor features a smaller body with a shorter axial length, making it ideal for situations where the motor's axial length is a limiting design parameter or the motor is directly linked to the driven load. In-wheel motors for electric vehicles and elevator motors are examples of such uses [33].

3.4 BLDC motor drive

The BLDC motor's main driving principle is to vary the phase windings, which should be excited according to the position of the permanent magnet on the rotor in order to provide a continuous torque. Information about the rotor magnet position is required to accomplish this operation. Hall effect sensors are often used for position sensing.

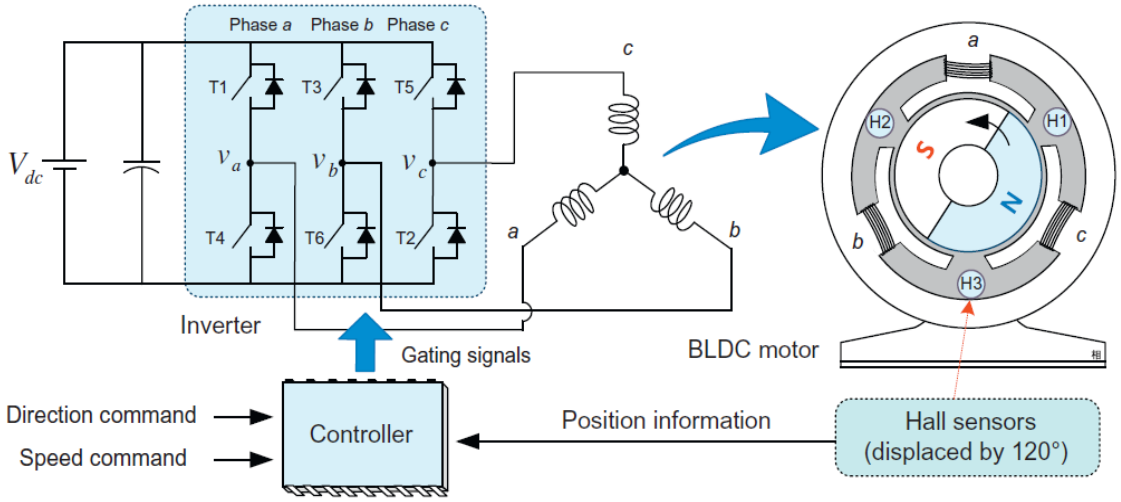

Figure 3.6 Drive system for BLDC motors.

Figure 3.6 depicts a two-pole three-phase Y-connected brushless DC motor drive system. On the stator, three Hall effect sensors are separated by 120 electrical degrees to monitor the magnetic field flux created by the rotor magnets. We can distinguish the rotor position separated into six sectors using three output signals from hall effect sensors. As a result, a simple drive (also known as a six-step commutation drive) for completing one electrical cycle is made up of six distinct stages.

3.4.1 Hall Effect sensors

The Hall effect sensor is a device that uses the hall effect phenomenon on semiconductor material to detect magnetic fields. When a current I_H passes through a plate of semiconductor material (called a hall element with a hall constant 'R_H') having a width 'd' and a magnetic field density 'B' passes through the plate, the hall effect generates a voltage V_H in response to the magnetic field and is given by

$$V_H = \frac{R_H}{d} I_H B \ (V) \tag{3.1}$$

The polarity and position of a magnetic field may be determined by calculating the hall voltage V_H. Permanent magnet motors, such as BLDC motors and PMSMs, employ hall sensors to determine the rotor position. The amplitude and direction of the current that creates the magnetic field may be determined by monitoring the hall sensor's output voltage.

Some of the benefits of a hall effect design are listed below:

- Hall effect sensors have a faster response time to changes in the magnetic field, which means they can commutate a BLDC motor more efficiently.
- They provide constant torque due to their accuracy.
- They can provide temperature stability and high sensitivity using a technique called chopper stabilization [5], [9].

The cost of a sensored methodology is significantly higher owing to the increased hardware and wiring.

3.4.2 Electronic commutation of PMBLDC motor

The PMBLDC motor is regulated by a voltage source inverter (VSI), which is controlled by the PMBLDC motor's electrical circuitry. Current commutation is provided by an electronic commutation for BLDC motors, which uses a decoder to provide current commutation flowing through the primary windings. Various hall-effect signals were used to generate switching pulses [19], [21], [22], [24]. At regular intervals of roughly 60^0, the required combination of three hall-effect signals is created for each unique rotor position. Table 3.2 lists the six switching pulses that correspond to rotor position. Due to the fact that only two switches may conduct at the same time in 120^0 conduction mode VSI operation, conduction losses may be minimized. In the recommended system, a BLDC motor with an integrated encoder is employed, and the decoder combinations are shown in Table 3.2.

Table 3.2 Truth table of switching states for electronic commutation of BLDC motor.

Rotor Position	**Hall Signals**			**Switching States**					
(Degrees)	**H_1**	**H_2**	**H_3**	**S_1**	**S_2**	**S_3**	**S_4**	**S_5**	**S_6**
NA	0	0	0	0	0	0	0	0	0
0	0	0	1	0	0	0	1	1	0

60-120	0	1	0	0	1	0	0	0	0
120-180	0	1	1	0	1	1	0	1	0
180-240	1	0	0	1	0	0	0	0	1
240-300	1	0	1	1	0	0	1	0	0
300-360	1	1	0	0	0	1	0	0	1
NA	1	1	1	0	0	0	0	0	0

3.4.3 Modeling of BLDC motors

We'll look at the mathematical equations for a three-phase BLDC motor in this part [35]. A BLDC motor's model is comparable to that of a PMSM due to structural similarities.

3.4.3.1 Voltage equations

BLDC motors control themselves directly using three-phase abc values whereas AC motors control themselves via the d-q axis reference frame. For sinusoidal values, the d-q transformation is required. The d-q transformation on a BLDC motor is useless since currents, flux, and back-EMFs are non-sinusoidal variables.

The mathematical equations of a BLDC Motor for phase voltages are given as follows:

$$V_{an} = R_s i_{an} + (L_s - M)\left(\frac{di_{an}}{dt}\right) + e_{an} \tag{3.2}$$

$$V_{bn} = R_s i_{bn} + (L_s - M)\left(\frac{di_{bn}}{dt}\right) + e_{bn} \tag{3.3}$$

$$V_{cn} = R_s i_{cn} + (L_s - M)\left(\frac{di_{cn}}{dt}\right) + e_{cn} \tag{3.4}$$

where V_{an}, V_{bn}, V_{cn} and i_{an}, i_{bn}, i_{cn} are phase voltages and phase currents of phase a, b and c respectively, as shown is Figure 3.6. R_s is stator resistance, L_s is stator winding inductance, M is the mutual inductances between stator windings and e_{an}, e_{bn}, e_{cn} are back-EMF due to magnetic flux. It's worth noting that the self-inductances and mutual-inductances are all the same for symmetrical three-phase windings.

3.4.3.2 Torque equations

Generally, the output torque (T_e) of a three-phase motor is calculated using the output power (P_e) and the mechanical angular velocity (ω_m) as

$$P_e = e_{an} i_{an} + e_{bn} i_{bn} + e_{cn} i_{cn} \tag{3.5}$$

$$T_e = \frac{P_e}{\omega_m} = \frac{e_{an} i_{an} + e_{bn} i_{bn} + e_{cn} i_{cn}}{\omega_m} \tag{3.6}$$

where, the mechanical angular velocity $\omega_m=\omega r/P$, ω_r is the electrical angular velocity and P is the number of poles. We can see from Equation (3.6) that the phase current must be in phase with the back-EMF in order to generate the maximum torque.

The currents flowing in the two-phase windings of a BLDC motor are of same magnitude but flows in the opposite direction except during the commutation interval. Because the phase current and back-EMF are in phase, the torque Equation (3.6) may be simply written as the product of the phase current and back-EMF magnitudes like as

$$T_e = \frac{P_e}{\omega_m} = \frac{e_{an}i_{an}+e_{bn}i_{bn}+e_{cn}i_{cn}}{\omega_m} = \frac{2EI}{\omega_m} \quad (3.7)$$

The output electromagnetic torque equation (3.7) becomes a constant value if I and E are constant. Even if the BLDC motor is fed with constant stator currents, there is torque ripple if the back-EMF is not a perfect trapezoidal waveform.

3.4.3.3 BLDC motor speed-torque characteristic

The relationship between speed (N_r) and electromagnetic torque (T_e) with constant DC bus voltage (V_{dc}), is also denoted as mechanical characteristics of BLDC motor. The relationship between speed (N_r), electromagnetic torque (T_e) and DC bus voltage V_{dc} is given by equation

$$T_e = \frac{K_T(30V_{dc}-\pi K_e N_r)}{30r_a} \quad (3.8)$$

such that

$$N_r = \frac{\left(\frac{30}{\pi}\right)(K_T V_{dc}-r_a T_e)}{K_e K_T} \quad (3.9)$$

where K_T is the torque coefficient, r_a is the line resistance winding and K_e is the coefficient of line back-EMF. From Equation (3.8), which is a linear equation, mechanical characteristics curves can be obtained with different V_{dc}, as shown in Figure 3.7, where $V_{dc1} > V_{dc2} > V_{dc3} > V_{dc4}$.

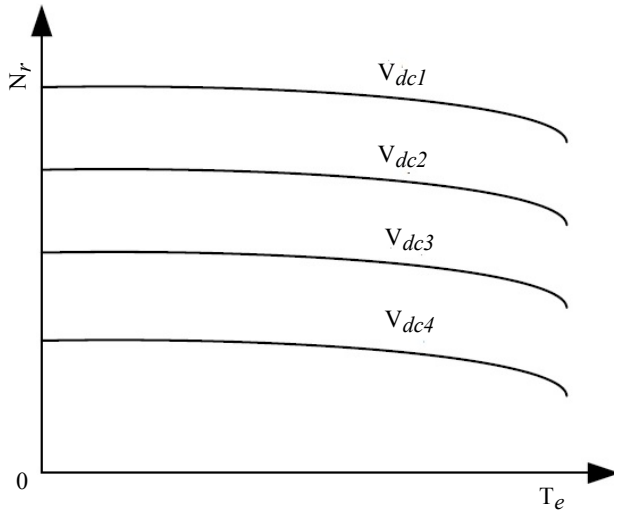

Figure 3.7 Speed-Torque (Mechanical) characteristics BLDC motor.

In reality, the curve of mechanical properties is only regarded to be essentially linear due to effect of variable loss and the armature reaction. The speed of the motor

reduces as the electromagnetic torque increases, as illustrated in Figure 3.7, with a certain DC bus voltage V_{dc}. Furthermore, when V_{dc} rises, the curve will move upward. Because BLDC motors employs power electronic switches having nonlinear saturation characteristics for commutation, the voltage drop of the power switch increases swiftly as the armature current increases when the motor is approaching standstill. As a result, near the termination of the mechanical characteristics curve, there will be a considerable downward shift, as illustrated in Figure. 3.7 [36].

The mechanical parameters of a BLDC motor are comparable to those of a separately excited DC motor, as previously mentioned. Changing the DC bus voltage can change the mechanical properties' no-load point. As a result, PWM modulation is commonly used to regulate the speed of a BLDC motor.

3.4.4 Speed control of BLDC motor using PI controller

Low ripple input supply and an appropriate speed controller are required to achieve optimum motor performance. The most prominent controller in a speed loop feedback control system is a proportional-integral (PI) controller, which is broadly utilized in industries due to its capacity and the ability in operating linear processes. The performance indicators of the speed controller is the drive system's step response for a certain reference speed. It is intended that the system's step response achieves a rapid settling response with no overshoot. As a result, the PI controller is adaptable to changes in load torque and enables steady-state precision. As compared to other prominent controller available, i.e., fuzzy logic controller (FLC), the PI controller primarily maintains steady-state accuracy and eliminates perturbation effects when there is any change in load torque, whereas the former responds when reference input variations are sufficiently large, particularly during start-up [16]. Also, PI controller has more undershoot and is able to keep up with the reference speed with a longer settling period while the FLC has less undershoot as it has a continuous speed inaccuracy which causes the actual rotor speed to be lower than the reference speed (Vref).

The simulink toolbox of the matlab software was used to create the speed controller model. The speed controller block's primary job is to give a reference torque, which is thereafter converted to reference current and sent to the reference generator. To generate the reference torque, the output of speed controller is constrained to an appropriate value in compliance with the motor rating. The following equation defines the PI controller's output in time domain:

$$V_C(t) = K_P \epsilon(t) + K_i \int_0^t \epsilon(t)dt \tag{3.10}$$

where $\epsilon(t)$ is the instantaneous error signal which is integrated from time 0 to t , K_i is the integral gain, K_P is the proportional gain and $V_C(t)$ is the output of the PI controller.

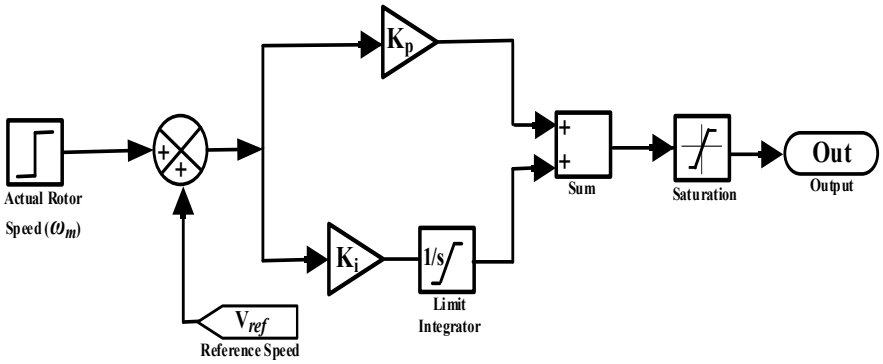

Figure 3.8 Block diagram schematic of PI Controller.

The key benefit of including the integral component in the proportional controller is that it eliminates the controller variable's steady state inaccuracy. However, if there is no change in the direction of the error, the integral controller saturates after certain period. This problem can be avoided by adding a limiter to the integral component of the controller prior to actually connecting it to the proportional controller's output. The speed error Є(t) is fed into the PI controller, and the PI controller's output is fed into the reference current block, as illustrated in Figure 3.8. The system will become unstable if the proportional factor is too large. If it is too modest, the system will take much time to reach the predetermined point. As a result, the gain of the PI controller or proportional factor is tuned to keep the speed stable. P-controller and I-controller benefits are merged in the PI-controller. The proportional action makes the system less sensitive to system parameter fluctuations and enhances the loop gain whereas the integral action removes or minimises the steady state error.

CHAPTER 4

STANDALONE SOLAR WATER PUMPING SYSTEM

In places where there is no connection to a utility grid, standalone PV systems are employed. In rural places, traditional power systems rely on manually regulated diesel generators that run constantly or for a few hours. Diesel generators that are used at low load levels for an extended period of time have higher maintenance costs and a shorter life. Renewable energy sources, such as solar panels, can be added to distant location power networks to replace diesel and other fossil-fuel-powered generators, resulting in cost-effective and efficient 24-hour electricity. To fulfil energy demand during periods of low solar irradiation and at night, a standalone PV energy system requires storage. So, for this the water can be stored in a tank replacing the need of batteries and thus reducing the cost. The subsequent section discusses the components necessary for the standalone solar water pumping system like SPV array operated using MPPT, DC-DC converters for controlling the solar power and the VSI used to operate BLDC drive coupled to centrifugal pump.

4.1 SOLAR PHOTO-VOLTAIC ARRAY

In many isolated and rural locations, photovoltaic technology is utilised to generate electricity using hand pumps or diesel-powered pumps in areas where power lines do not reach. It aids in the improvement of living conditions in rural regions in developing nations, particularly in the fields of health care, education, and agriculture. Such technology has been widely employed and connected into the power grid in industrialized nations. To maximise the noontime and day energy output, photovoltaic arrays are normally installed in a permanent location and slanted toward the south. To catch the maximum energy for the season or year, the fixed panel's orientation should be properly chosen.

4.1.1 Characteristics of solar photovoltaic arrays

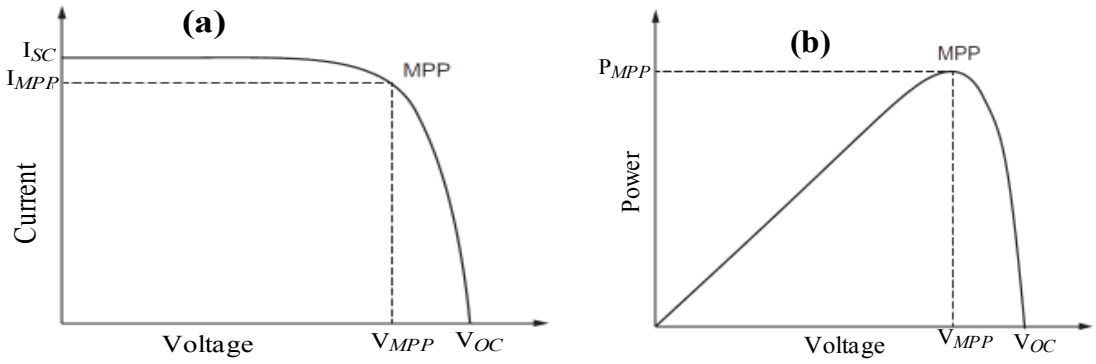

Figure 4.1 Typical PV module curves: (a) maximum power point (MPP) I-V characteristic of a solar cell and (b) maximum power point (MPP) P-V characteristic of a solar cell.

As illustrated in Figure 4.1, photovoltaic arrays have an optimal operating point termed the maximum power point (MPP). It's worth noting that power rises as voltage

rises, reaching a peak value, and then falls as resistance rises, causing current to drop off. According to the maximum power transfer principle, for a certain temperature and insolation, this is the point at which the load is matched to the solar panel's resistance. When demonstrated in Figure 4.2, the I-V curve changes as temperature and insolation levels fluctuate, and the MPP varies appropriately.

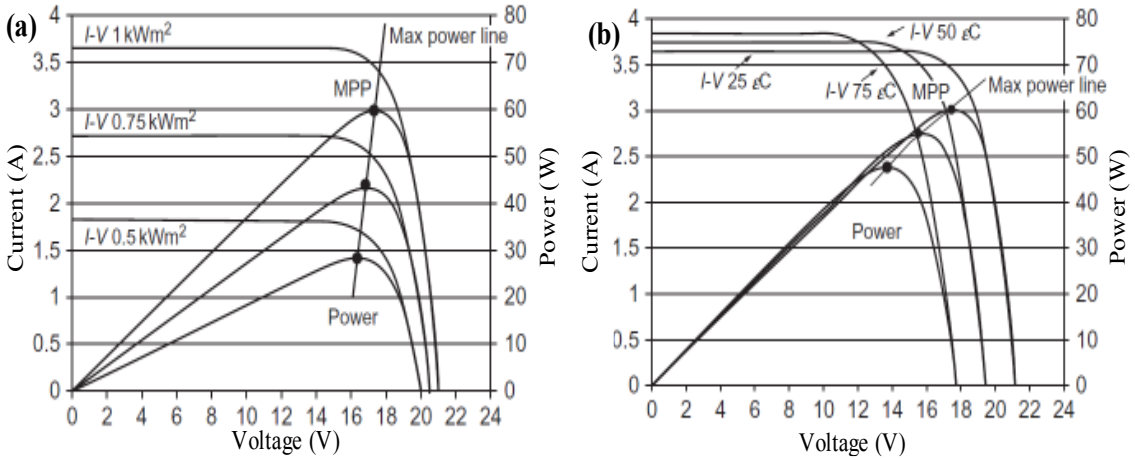

Figure 4.2 SPV module characteristics: (a) Insolation of PV panel and (b) Temperature.

As the isolation level increases, the open-circuit voltage climbs logarithmically, whereas the short-circuit current increases linearly. Furthermore, increasing the temperature of the cell lowers the open-circuit voltage and somewhat raises the short-circuit current, lowering the cell's efficiency [11].

PV panels are set to face the sun at an angle that corresponds to the country's latitude and are commonly put on the roof or near an open space. Seasonal adjustment of the module's orientation toward the sun is done manually if feasible. Due to the relatively high cost of solar power technology, it is critical to use panels at their optimum output. However, to gather as much solar energy as possible, a sun tracking mechanism that causes the module's surface to track the sun throughout the day is more convenient and efficient. Tracking can be done on one or both axes, with double axis tracking providing a larger power output. Depending on the seasonal climate and geographic location, the energy production can be improved by around 20%–30%. Although some argument claims that a fixed system is less expensive and requires little maintenance, several tracking technologies for controlling the orientation of PV panels have shown to be more efficient than fixed systems in terms of converted electricity.

The operating voltage or current should be regulated by a maximum power point tracker (MPPT) that meets the following parameters to receive maximum power from the PV panel at the present temperature and insolation conditions:

- Regardless of atmospheric fluctuations, operate the PV system near to the MPP.
- Have a low capital investment and a high conversion efficiency.
- Provide an output interface that is compliant with the charging requirements of the battery.

4.1.2 MPPT controlling Algorithms

In the next sections, we'll go through a few of the recommended MPPT algorithms.

4.1.2.1 Perturb and Observe (P&O) MPPT technique

The perturb and observe (P&O) approach is characterised by a basic feedback mechanism and a small number of measured parameters. It works by perturbing (i.e., increasing or decreasing) the duty cycle while managing the array current, as illustrated in Figure 4.3, and comparing the PV output power to the preceding perturbation cycle. It determines the movement of the operating point by measuring the derivative of power Δp and the derivative of voltage Δv. If the perturbation causes the array power to rise (or decrease), the next perturbation is produced in the same (or opposite) direction.

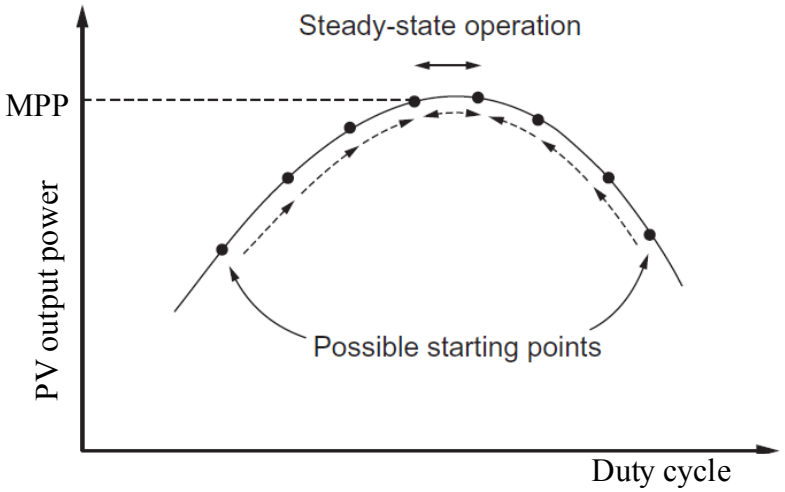

Figure 4.3 P&O MPPT technique.

This cost-effective technology is characterised by continually tracking and harvesting the most power from PV in a very efficient manner. However, due to its moderate tracking speed, such a system may fail under quickly changing atmospheric circumstances.

4.1.2.1 Incremental Conductance (INC) MPPT technique

As illustrated in Figure 4.4, the incremental conductance method (INC) procedure is based on the fact that the derivative of power with respect to voltage (dp/dv) disappears at the MPP since it is the curve's maximum point.

The INC method finds the MPP by comparing di/dv with -I/V until the incremental conductance equals the source conductance at the voltage operating point. The method calculates incremental changes as $dI=I-I_b$ and $dV=V-V_b$ by measuring the current values of the I and V and then using the equivalent stored values (I_b and V_b) measured during the prior cycle. The control reference signal V_{ref} will be changed based on the results received in order to shift the array voltage closer to the MPP value. Because no control action is required at the MPP, di/dv = -I/V, the adjustment stage will be skipped, and the algorithm will update the stored parameters at the completion of the cycle.

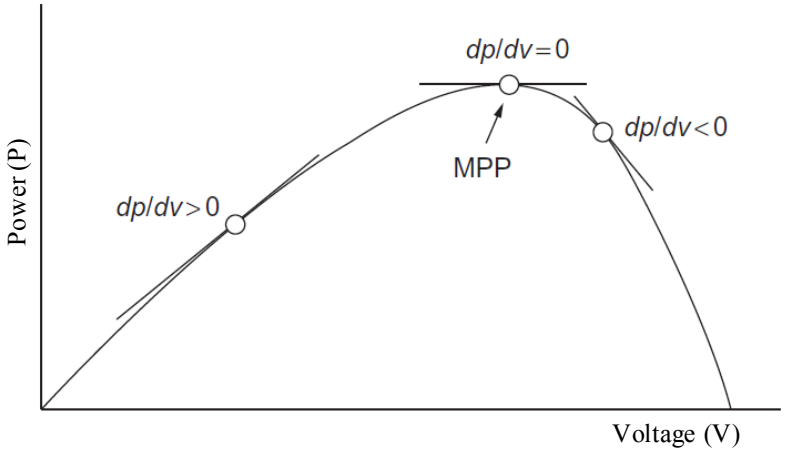

Figure 4.4 The slope 'conductance' of the P-V curve viz. INC MPPT technique.

The method identifies whether a control operation was performed when the array was running at the previous cycle MPP (dV=0) in order to identify any changes in weather conditions. INC demands exact estimations of both instantaneous and increasing conductance since the increment size approach is required to assess how quickly the system is responding.

4.1.3 Ratings and parameters consideration

The selection of SPV array of maximum power capacity (P_{mpp} (in kW)), under "Standard Test Conditions (STC: 1000W/m², 25°C, AM 1.5; refer appendix 1)", should be slightly more than demanded by the centrifugal motor-pump and its parameters are designed accordingly.

The SPV array's current at MPP, I_{mpp} is hence estimated as,

$$I_{mpp} = P_{mpp}/V_{mpp} \quad \text{(in Amperes)} \tag{4.1}$$

The required module's number to be connected in series is given by,

$$N_S = V_{mpp}/V_m \tag{4.2}$$

The required module's number to be connected in parallel is given by,

$$N_P = I_{mpp}/I_m \tag{4.3}$$

As illustrated in Figure 4.1, a solar cell may be operated at any position along its typical current-voltage curve. The open-circuit voltage (V_{OC}) and short-circuit current (I_{SC}) are two critical points on this curve. The maximum voltage at zero current is the open-circuit voltage, whereas the maximum current at zero voltage is the short-circuit current. V_{OC} is generally 0.6–0.7 V for a silicon solar cell under STC, while I_{SC} is typically 20–40 mA per square centimetre of cell surface. I_{SC} is proportional to the light level, whereas V_{OC} is proportional to the logarithm of the illumination level, to a fair approximation.

A plot of power (P) against voltage (V) for SPV array (refer Figure 4.4) reveals that the solar cell generates maximum power at a single point on the I-V curve. It is called as maximum power point (V_{mpp} and I_{mpp}). Steps are frequently made during

manufacturing to maximise power output; the three primary cell characteristics are open-circuit voltage (V_{OC}), short-circuit current (I_{SC}), and fill factor (FF)- a term describing how "square" the I-V curve is given by

$$FF = (V_{mpp} * I_{mpp}) / (V_{OC} * I_{SC}) \quad (4.4)$$

4.2 DC-DC CONVERTERS

The DC-DC converters are primarily used to convert a DC voltage at one level to another level by merely varying the duty cycle of the employed power semiconductor switches. It is further discussed in the subsequent sections.

4.2.1 Classification of DC-DC converters

In the last six decades, more than 800 prototypes of DC-DC converters have been built. All present DC-DC converters were created to fulfil the needs of certain applications. Buck, boost, and buck-boost converters, as well as zero-current-switching (ZCS) and zero-voltage-switching (ZVS) converters, are commonly termed for their functions.

According to their properties and development history, DC-DC converters are divided into six generations. This categorization has gained widespread recognition since it categorises all current DC-DC converters as well as new prototypes. It is now simple to categorise and distribute DC-DC converters, as well as examine their individual technical qualities, owing to this classification.

4.2.1.1 First-generation DC-DC converters

The first-generation converters operate in a single-quadrant mode with a limited power range (up to around 100 W). Since their development lasts a long time, they briefly have five categories, as shown in Figure 4.5:

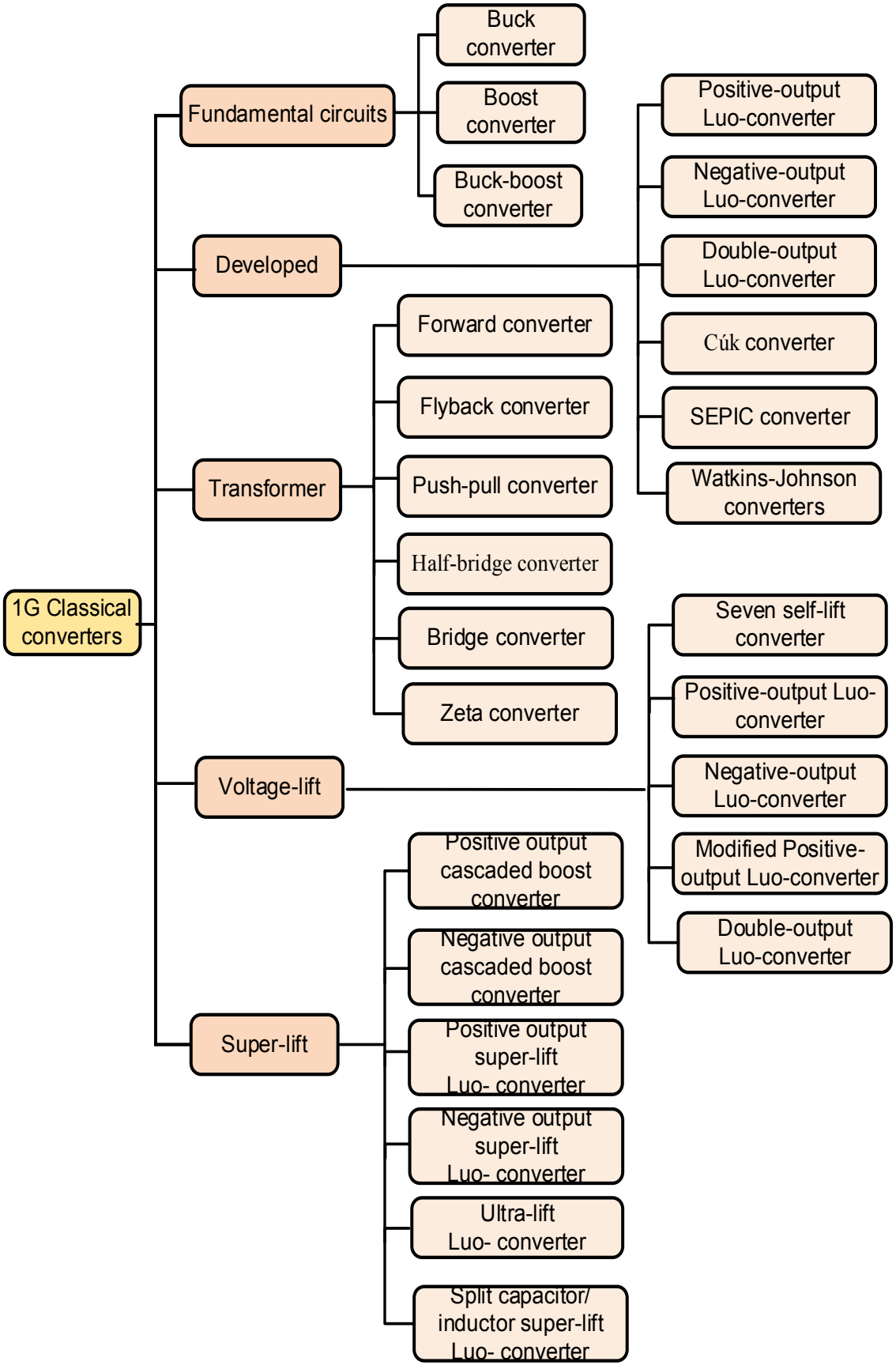

Figure 4.5 First-generation: Classical DC-DC converters.

4.2.1.2 Second-generation DC-DC converters

Multiple-quadrant operation converters are the second-generation converters. With a medium output power range, these converters operate in two-quadrant and four-quadrant modes (hundreds of watts or higher). The topologies may be divided into two groups: first, converters generated from multiple-quadrant choppers and/or first-generation converters, and second, transformer-based converters. In most cases, one-quadrant operation mandates the use of at least one switch. As a result, a two-quadrant operation converter must have at least two switches, whereas a four-quadrant operation converter must have at least four.

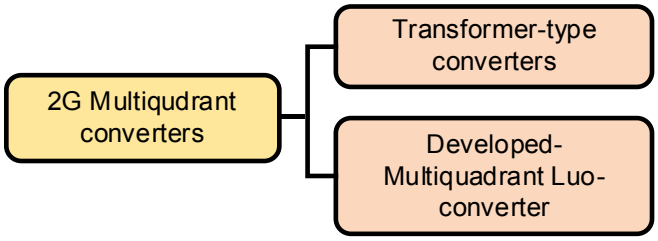

Figure 4.6 Second-generation: Multiquadrant DC-DC converters.

For a long time, multiple quadrant choppers were used in industrial applications. They can be utilised to implement multiple-quadrant DC motor operating. There are class-A converters (one-quadrant operation), class-B converters (two-quadrant operation), class-C converters, class-D converters, and class-E (four-quadrant operation) converters, as indicated by the chopper headings. Class-B converters come from B-type choppers, whereas class-E converters come from E-type choppers. The class-A converter operates in quadrant I, which corresponds to a DC motor drive's forward motoring function. The quadrant I and II function of the class-B converter corresponds to the forward-running driving and regenerative braking operations of a DC motor drive. The class-C converter may operate in quadrants I and VI. The class-D converter operates in quadrants III and VI, which corresponds to reverse motoring and regenerative braking on a DC motor drive. A four-quadrant operation is used by the class-E converter, which corresponds to the four-quadrant operation of a DC motor drive.

Many publications have looked into class-E converters for industrial applications in recent years. The first-generation converters may be used to create multi-quadrant operation converters. Multi-quadrant Luo converters, for example, are generated from positive-output (P/O) and positive-output (N/O) Luo converters. The transformer-type multi-quadrant converters use transformer polarity and a diode rectifier to rapidly alter the current direction. The forward converter, half-bridge converter, and bridge converter are the three basic forms of such converters.

4.2.1.3 Third-generation DC-DC converters

Switched-component converters, also known as switched inductors and switched capacitors, are third-generation converters comprised of inductors or capacitors. They have a great output power range and may operate in two or four quadrants (thousands of watts). They are compact because they are built entirely of inductors or capacitors. As a result, the power density and efficiency are both quite high.

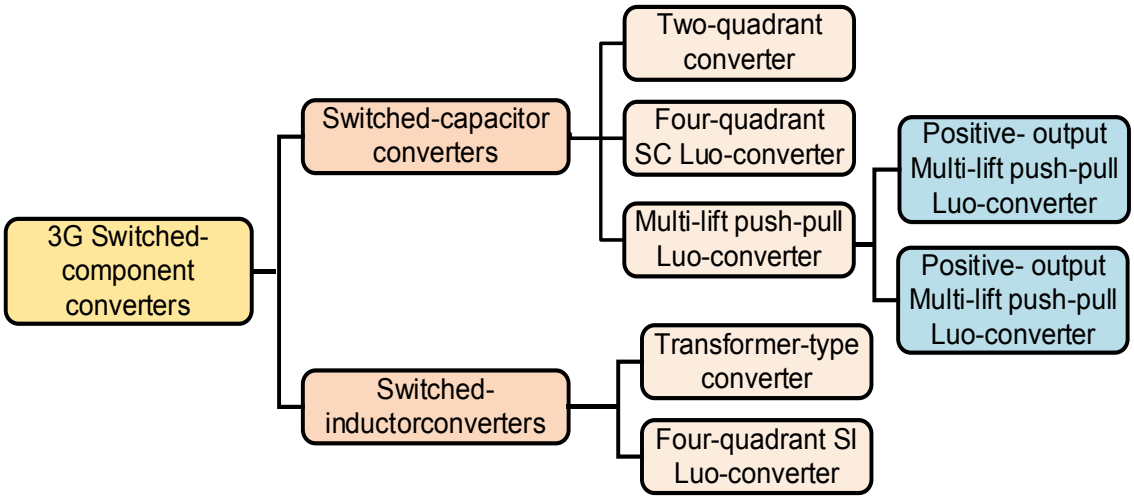

Figure 4.7 Third-generation: Switched component DC-DC converters.

4.2.1.4 Fourth-generation DC-DC converters

Soft-switching converters are the fourth-generation DC/DC converters. Soft-switching techniques are divided into four categories:

1. Converters with resonant switches
2. Load-resonant converters.
3. DC-link resonant converters
4. Integral-half-cycle converters with a high-frequency connection

Only the resonant-switch conversion approach has received attention so far. Most topologies operate in single-quadrant operation, and thus resonance approach may work independently of the load. Zero-current switching (ZCS), zero-voltage switching (ZVS), and zero-transition (ZT) converters are the three basic types. In fact, these converters may operate in two and four quadrants with a wide range of output power (thousands of watts).

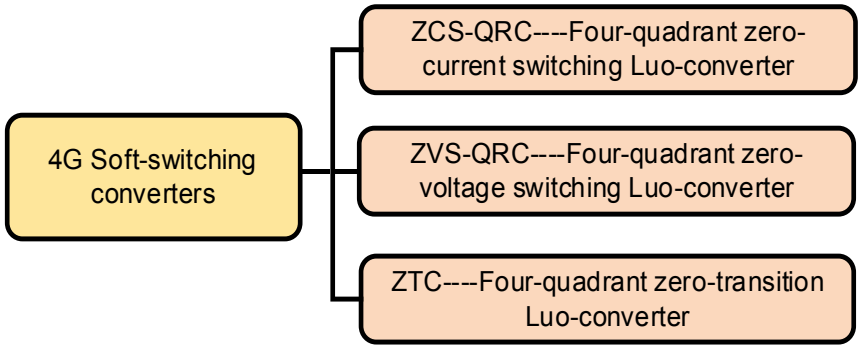

Figure 4.8 Fourth-generation: Soft-switching DC-DC converters.

When the amount of power delivered increases, the power losses increase dramatically. The switch-on and switch-off periods are when the most power losses occur. The key to improving power transfer efficiency is to decrease power losses across the switch. This problem was successfully handled using the soft-switching approach. Over resonance (complete resonance), optimal resonance (critical resonance),

and quasi-resonance are the three resonant states of ZCS and ZVS converters (sub-resonance). In a recurring period, only the quasi-resonance state contains two distinct zero-cross points.

4.2.1.5 Fifth-generation DC-DC converters

Synchronous rectifier (SR) DC/DC converters are the fifth-generation converters. The advancement of computing technology necessitated the use of this sort of converter. Power supplies with low output voltage and high current are widely employed in communications, computer equipment, and other industrial applications, as a result of the development of micropower consumption technology and high-density IC manufacturing.

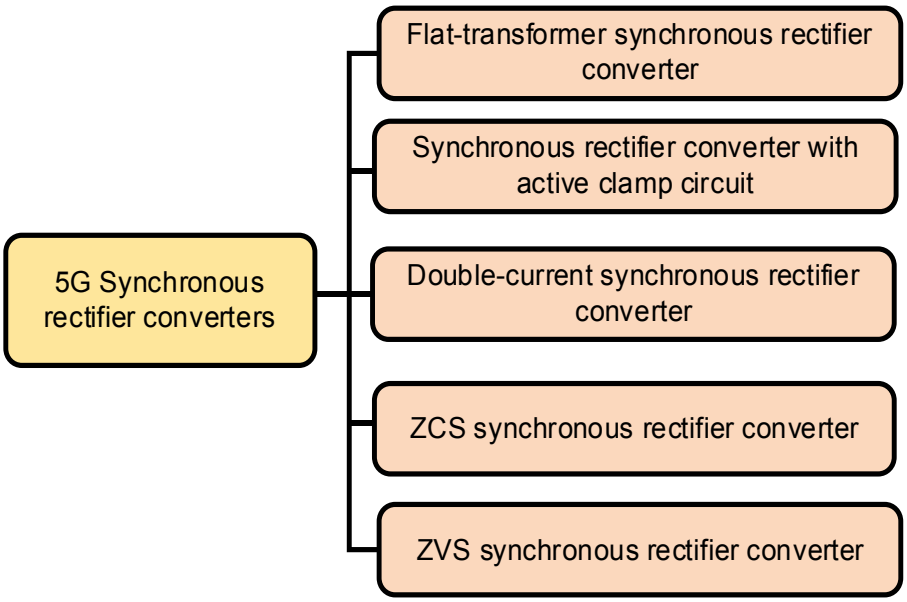

Figure 4.9 Fifth-generation: Synchronous rectifier DC-DC converters.

For a long time, Intel, which created the Zelog-type computers, ruled the international market. The 5 V power supply was utilised by Inter-80 computers. Large-scale integrated chip technology was soon developed in order to enhance memory capacity and operating speed. The gaps between the layers got shorter as the volume of IC production increased. The micropower consumption technology was also accomplished at the same time. As a result, new computers with Pentium I, II, III, and IV processors utilise a 3.3 V power supply. Computers in the future will have more memory and require lower power supply voltages, such as 2.5 V, 1.8 V, 1.5 V, and even 1.1 V. The typical diode rectifier bridge cannot achieve such low power supply voltages due to the high diode voltage loss. As a result of this necessity, new MOSFET designs have been created. They have a low conduction resistance of 6–8 mΩ and an extremely low forward voltage drop of 0.05-0.2 V. The forward converter is used to obtain the fundamental topology. In SR DC-DC converters, active-clamped circuits, flat transformers, double-current circuits, soft-switching techniques, and multiple-current methods can all be employed.

4.2.1.6 Sixth-generation DC-DC converters

Multielements resonant power (MER) converters are the sixth-generation converters. Many systems and equipment, such as uninterruptible power supplies and high frequency annealing apparatus, rely on current source resonant inverters.

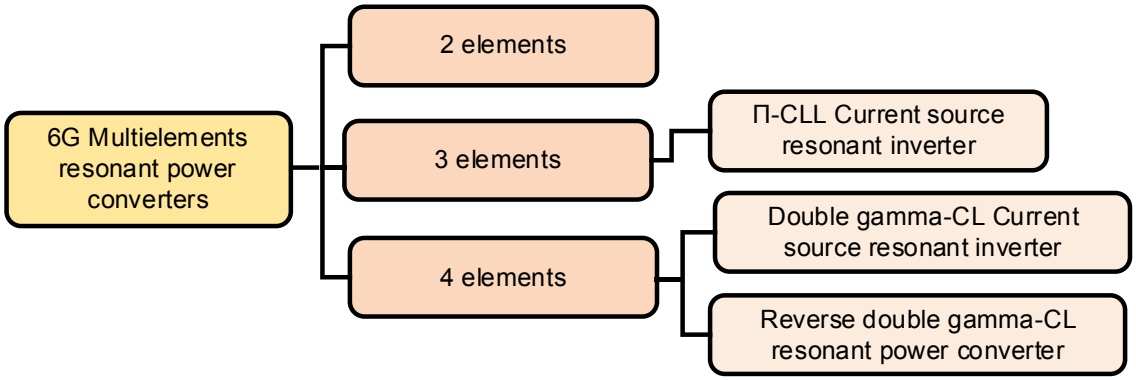

Figure 4.10 Sixth-generation: Multielements resonant power DC-DC converters.

4.2.2 Advanced DC-DC converters

To adjust the input voltage according to the application, numerous DC-DC converter topologies are used nowadays. Isolated DC-DC converters and non-isolated DC-DC converters are the two most common types of DC-DC converters. The input and output of an isolated DC-DC converter are separated by an electrical barrier utilising a high-frequency transformer. The isolated DC-DC converter's key benefit is that it safeguards the sensitive load. The converter's output may be set to either positive or negative polarity. It has a high level of noise interference resistance. The electrical barrier is absent in a non-isolated DC-DC converter. Non-isolated DC-DC converters are simpler to build and less expensive than isolated DC-DC converters. Advanced DC-DC converter topologies, such as Luo, SEPIC, and Zeta converters, are based on non-isolated DC-DC converters and are designed for greater efficiency, dependable control switching techniques, fault-tolerant setups, and largely renewable energy–related applications.

4.2.2.1 LUO converter

The super-lift approach is more powerful than the cuk and SEPIC converters; it has a high power density, is efficient, and can provide an output voltage in arithmetic progression. With massive voltage amplification and high voltage transfer gain, a positive-output super-lift Luo converter works in the first quadrant. However, the use of this sort of converter in industrial and home applications is currently under investigation [37–39].

Luo et al. [37] proposed a new super-lift technique with series capacitors and inductors that implements the output voltage rise in a higher geometric progression, and Kumar et al. [39] used a sliding mode control strategy to balance the correct load current sharing and load voltage regulation in a parallel positive-output elementary super-lift Luo converter.

The voltage transfer gain conversion of the Ultra-lift Luo converter is extremely high. Its voltage transfer gain is the sum of the gains of the voltage-lift and super-lift Luo converters. Because it may create high output voltage with a little fluctuation in duty ratio, the closed-loop controller design is complicated. In comparison to all other non-isolated DC-DC converters, it has a high efficiency [37].

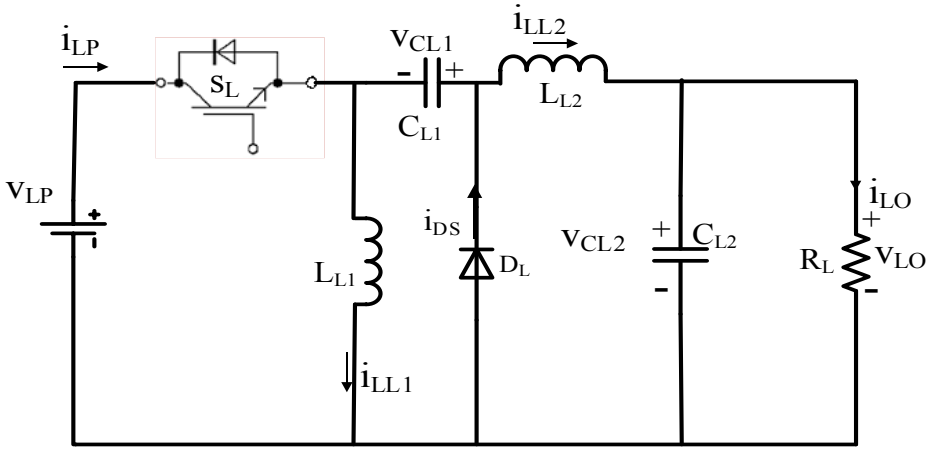

Figure 4.11 LUO converter circuit diagram.

The various mathematical expressions for the design of Luo converter circuit components and parameters are summarized in Table 4.1.

Table 4.1 Mathematical expressions for Luo converter.

Sr. No.	Parameters	Formula
1.	Voltage gain	$\frac{V_{LO}}{V_{LP}} = \frac{D}{1-D}$
2.	Peak-to-Peak inductor L_{L1} ripple current	$\Delta i_{LL1} = \frac{V_{LP} D}{f. L_{L1}}$
3.	Peak-to-Peak inductor L_{L2} ripple current	$\Delta i_{LL2} = \frac{V_{LP} D}{f.(1-D) L_{L2}}$
4.	Peak-to-Peak capacitor C_{L1} ripple voltage	$\Delta V_{CL1} = \frac{i_{LP} D(1-D)}{f.(2-D) C_{L1}}$
5.	Peak-to-Peak capacitor C_{L2} ripple voltage	$\Delta V_{CL2} = \frac{i_{LO} D}{f. C_{L2}}$
6.	RMS inductor L_{L1} current	$i_{LL1,rms} = \sqrt{\frac{i_{LP}^2}{2-D} + \frac{\Delta i_{LL1}^2}{4}}$
7.	RMS inductor L_{L2} current	$i_{LL2,rms} = \sqrt{\frac{i_{LO}^2}{1-D}}$
8.	RMS capacitor C_{L1} current	$i_{CL1,rms} = \sqrt{\left(\frac{i_{LP}^2}{2-D} + \frac{\Delta i_{LL1}^2}{4}\right)\left(\frac{(1-D)}{D}\right)}$
9.	RMS capacitor C_{L2} current	$i_{CL2,rms} = i_{LL1,rms} - i_{LO,rms}$

10.	RMS diode D_L current	$i_{DL,rms} = \sqrt{\left(\frac{i_{LP}^2}{2-D} + \frac{\Delta i_{LL1}^2}{4}\right)\left(\frac{(1-D)}{D}\right)} + \sqrt{\left(\frac{i_{LP}^2}{2-D} + \frac{\Delta i_{LL1}^2}{4}\right)}$
11.	RMS switch S_L current	$i_{SL,rms} = \sqrt{\left(\frac{i_{LP}^2}{2-D} + \frac{\Delta i_{LL1}^2}{4}\right)(1-D)}$
12.	Voltage stress on switch S_L	$V_{SL} = V_{LO}\frac{1}{1-D}$

4.2.2.2 SEPIC converter

SEPIC converter stands for single-ended primary inductance converter. In order to get a larger output voltage, the ON period should be longer than the OFF duration (due to longer charging of the inductor). Otherwise, the converter will not provide the desired result (due to the inability of the capacitor to charge its full capacity). Several factors should be taken into account when developing the converter. By combining a high-frequency transformer with a normal SEPIC converter, the amount of output voltage ripple is decreased. This configuration results are minimal switching stress, a continuous output current, and low output ripple. To extract DC power from an accessible AC line, AC–DC conversion is necessary. This conversion causes harmonics to be injected into the AC current waveform, resulting in a low power factor. Here, the SEPIC converter is used in boundary conduction mode (BCM) [40-45].

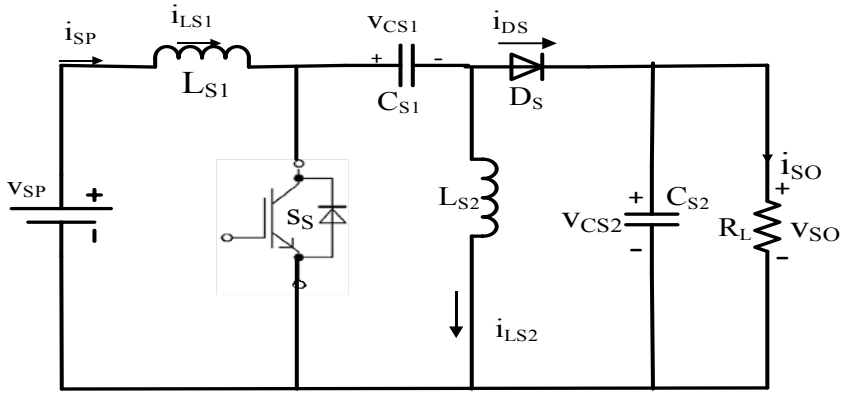

Figure 4.12 SEPIC converter circuit diagram.

Likewise, SEPIC converters are commonly used to manage flickering in DC voltage in solar power generation. To achieve maximum power, multiple control approaches such as PI control, fuzzy logic control, sliding mode control, and dP/dV feedback control are advocated [42]. The SEPIC converter provides sensorless control of a solar-fed BLDC motor, and thus suggested drive system might be a solution for solar-based transportation. Conduction and switching losses are important considerations in converter design, and they may be decreased by employing the soft switching approach, which is also used to reduce output current ripple. For a fuel cell

generating system, a hybrid architecture (combining SEPIC and flyback converters) is proposed [45].

The various mathematical expressions for the design of SEPIC converter circuit components and parameters are summarized in Table 4.2.

Table 4.2 Mathematical expressions for SEPIC converter.

Sr. No.	Parameters	Formula
1.	Voltage gain	$\frac{V_{SO}}{V_{SP}} = \frac{D}{1-D}$
2.	Peak-to-Peak inductor L_{S1} ripple current	$\Delta i_{LS1} = \frac{V_{SP} D}{f . L_{S1}}$
3.	Peak-to-Peak inductor L_{S2} ripple current	$\Delta i_{LS2} = \frac{V_{SP} D(1-D)}{(1-D) L_{S2}}$
4.	Peak-to-Peak capacitor C_{S1} ripple voltage	$\Delta V_{CS1} = \frac{i_{SP}(1-D)}{f . C_{L1}}$
5.	Peak-to-Peak capacitor C_{S2} ripple voltage	$\Delta V_{CS2} = \frac{(i_{SP} L_{S2} - V_{SO} D)(1-D)}{f . C_{S2} L_{S2}}$
6.	RMS inductor L_{S1} current	$i_{LS1,rms} = \sqrt{i_{SP}^2 D + \frac{\Delta i_{LS1}^2}{4}}$
7.	RMS inductor L_{S2} current	$i_{LS2,rms} = -\sqrt{i_{SP}^2 D(1-D)}$
8.	RMS capacitor C_{S1} current	$i_{CS1,rms} = \sqrt{i_{SP}^2 (1-D)} - i_{LS1,rms}$
9.	RMS capacitor C_{S2} current	$i_{CS2,rms} = \sqrt{i_{SP}^2 (1-D)} - i_{LO,rms}$
10.	RMS diode D_S current	$i_{DS,rms} = \sqrt{i_{SP}^2 (1-D)} - \sqrt{i_{SP}^2 D(1-D)}$
11.	RMS switch S_S current	$i_{SS,rms} = \sqrt{\left(i_{SP}^2 D + \frac{\Delta i_{LS1}^2}{4}\right)} + \sqrt{i_{SP}^2 (1-D)}$
12.	Voltage stress on switch S_S	$V_{SS} = V_{SO} \frac{1}{1-D}$

4.2.2.3 ZETA converter

From an input voltage that fluctuates above and below the output value, the ZETA converter architecture produces a positive output voltage. Figure 4.13 shows a simple circuit diagram of a ZETA converter, consisting of an AC coupling capacitor, C_{Z1}; an output capacitor, C_{Z2}; coupled inductors L_{Z1} and L_{Z2} an IGBT switch, S_Z; and a diode, D_Z.

It is necessary to study the circuit at DC while both switches are off and not switching in order to comprehend the voltages at the various circuit nodes. Capacitor

C_{Z1} will be in parallel with C_{Z2}, so C_{Z1} is charged to the output voltage, V_{ZO}, during steady-state CCM [46].

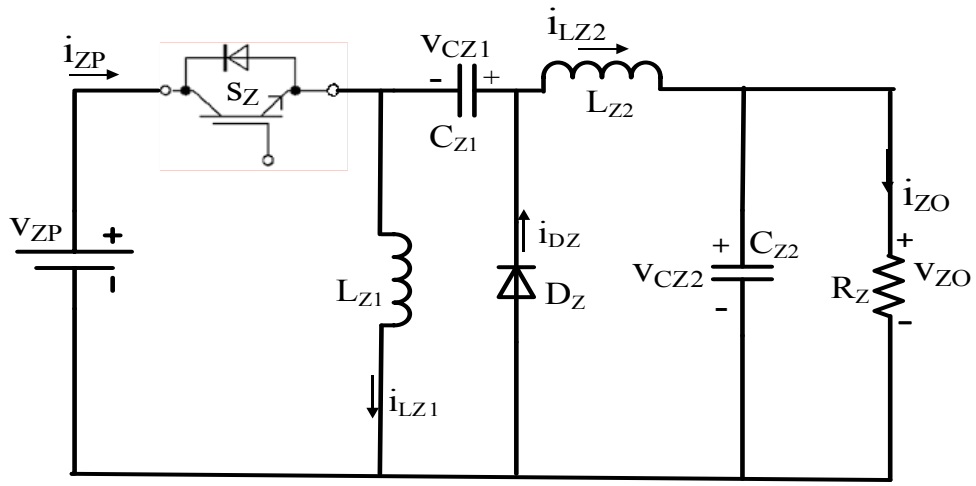

Figure 4.13 ZETA converter circuit diagram.

When S_Z is off, the voltage across L_{Z2} must be V_{ZO} since it is in parallel with C_{Z2}. Since C_{Z2} is charged to V_{ZO}, the voltage across S_Z when S_Z is off is $V_{ZP} + V_{ZO}$; therefore, the voltage across L_{Z1} is $-V_{ZO}$ relative to the drain of S_Z. When S_Z is on, capacitor C_{Z1}, charged to V_{ZO}, is connected in series with L_{Z2}; so, the voltage across L_{Z2} is $+V_{ZP}$, and diode D_Z sees $V_{ZP} + V_{ZO}$.

When S_Z is on, energy from the input supply is being stored in L_{Z1}, L_{Z2}, and C_{Z1}. L1b also provides I_{ZO}. When S_Z turns off, L_{Z1}'s current continues to flow from current provided by C_{Z1}, and L_{Z2} again provides I_{ZO} [47,48].

The various mathematical expressions for the design of ZETA converter circuit components and parameters are summarized in Table 4.3.

Table 4.3 Mathematical expressions for ZETA converter.

Sr. No.	Parameters	Formula
1.	Voltage gain	$\frac{V_{ZO}}{V_{ZP}} = \frac{D}{1-D}$
2.	Peak-to-Peak inductor L_{Z1} ripple current	$\Delta i_{LZ1} = \frac{V_{ZP} D}{f . L_{Z1}}$
3.	Peak-to-Peak inductor L_{Z2} ripple current	$\Delta i_{LZ2} = \frac{V_{ZP} D}{f . L_{Z2}}$
4.	Peak-to-Peak capacitor C_{Z1} ripple voltage	$\Delta V_{CZ1} = \frac{i_{ZP}(1-D)}{f . C_{Z1}}$
5.	Peak-to-Peak capacitor C_{Z2} ripple voltage	$\Delta V_{CZ2} = \frac{V_{ZO} D}{f^2 . L_{Z2} C_{Z2}}$

6.	RMS inductor L_{Z1} current	$i_{LZ1,rms} = \sqrt{i_{ZP}^2 D + \frac{\Delta i_{LZ1}^2}{4}}$
7.	RMS inductor L_{Z2} current	$i_{LZ2,rms} = \sqrt{\left(i_{ZP}^2 D + \frac{\Delta i_{LZ1}^2}{4}\right)(1-D)}$
8.	RMS capacitor C_{Z1} current	$i_{CZ1,rms} = \sqrt{i_{LP}^2 \left(\frac{D}{1-D}\right)}$
9.	RMS capacitor C_{Z2} current	$i_{CZ2,rms} = i_{ZO,rms}$
10.	RMS diode D_Z current	$i_{DZ,rms} = \sqrt{i_{LP}^2 (1-D)} + \sqrt{\left(i_{ZP}^2 D + \frac{\Delta i_{LZ1}^2}{4}\right)(1-D)}$
11.	RMS switch S_Z current	$i_{ZL,rms} = \sqrt{\left(i_{ZP}^2 D + \frac{\Delta i_{LZ1}^2}{4}\right)} + \sqrt{\left(i_{ZP}^2 (D - D^2) + \frac{\Delta i_{LZ1}^2}{4}(1-D)\right)}$
12.	Voltage stress on switch S_Z	$V_{ZL} = V_{ZO} \frac{1}{1-D}$

4.2.3 Performance parameters calculation

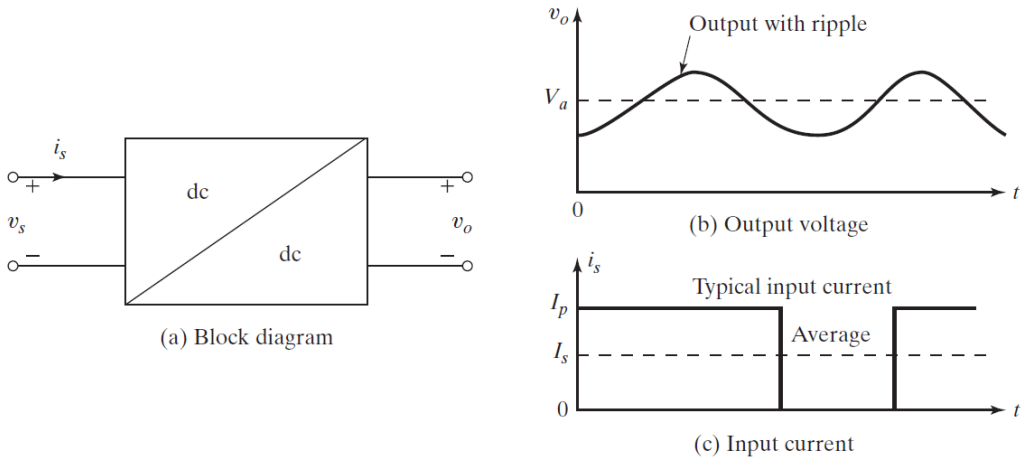

Figure 4.14 Input and output relationship of a dc–dc converter.

A DC-DC converter's input and output voltages are both dc. As illustrated in Figure 4.14(a), this sort of converter may create a constant or variable dc output voltage from a fixed or variable dc input voltage. The output voltage and input current should

ideally be pure dc, however as illustrated in Figures 4.14(b) and (c), the output voltage and input current of a realistic dc–dc converter contain harmonics or ripples. When the converter links the load to the supply source and the input current is discontinuous, the converter draws current from the dc source.

The power efficiency, which is the ratio of output power to input power, is determined by switching losses, which are further determined by the converter's switching frequency. To decrease the values and sizes of capacitances and inductances, the switching frequency f_S should be high. These contradictory criteria force the designer to make a compromise. Generally, f_S is higher than the audio frequency of 18 kHz. The formulae for the calculations of performance parameters for DC-DC converters are summarized in Table 4.3.

Table 4.4 Performance parameter's calculation formulae of DC-DC converter.

Sl. No.	**Parameters**	**Formula**	**Remarks**
1.	DC output power (P_{DC})	$P_{DC} = I_a V_a$	I_a = Average load current V_a= Average load voltage
2.	AC output power (P_{AC})	$P_{AC} = I_o V_o$	I_o = RMS load current V_o= RMS load voltage
3.	DC input power (P_{IN})	$P_{IN} = I_s V_s$	I_s=Average DC supply current V_s= Average DC supply voltage
4.	RMS ripple content of the output voltage (V_{RO})	$V_{RO} = \sqrt{V_o - V_a}$	--------
5.	RMS ripple content of the output current (I_{RO})	$I_{RO} = \sqrt{I_o - I_a}$	--------
6.	RMS ripple content of the input current (I_{RI})	$I_{RI} = \sqrt{I_i - I_s}$	I_i=RMS DC supply current I_s=Average DC supply current
7.	Ripple Factor of the Output Voltage (RF_{OV})	$RF_{OV} = V_{RO} / V_a$	--------
8.	Ripple Factor of the Output Current (RF_{OI})	$RF_{OI} = I_{RO} / I_a$	--------
9.	Ripple Factor of the Input Current (RF_{II})	$RF_{II} = I_{RI} / I_s$	--------

10.	Converter Efficiency (η_c)	$\eta_c = P_{DC} / P_{AC}$	It is not the power efficiency.
11.	Power Efficiency (η_p)	$\eta_p = P_{DC} / P_{IN}$	Depend on the switching losses, which in turn depend on the switching frequency of the converter.
12.	Conduction Losses (P_L)	$P_L = P_{IN} - P_{DC}$	Due to switching losses.

4.3 VOLTAGE SOURCE INVERTER (VSI)

Power is converted from DC to AC by inverters, and from AC to DC by rectifiers. Many inverters are bidirectional, meaning they can switch between inverting and rectifying modes. Alternating current is required to run 230 V (or 110 V), 50 Hz (or 60 Hz) appliances in many stand-alone PV setups. Depending on the power level, stand-alone inverters often run at 12 V, 24 V, 48 V, 96 V, 120 V, or 240 V DC. The following features should be included in an inverter for a stand-alone PV system:

- Sinusoidal output voltage.
- Voltage and frequency must be within permissible limits.
- Capable of handling a wide range of input voltages.
- Voltage control at the output.
- At light loads, it has a high efficiency.
- Reduced harmonic production by the inverter to prevent damage to electronic equipment like as televisions, extra losses, and appliance heating.
- Photovoltaic inverters must be able to tolerate short-term overloading in order to handle larger beginning currents from pumps, refrigerators, and other appliances.
- Proper over-/undervoltage and frequency protection, as well as short circuit protection.
- Surge capacity
- Idling and no-load losses are low.
- Disconnects due to low battery voltage.
- Low audio noise and radio frequency (RF) interference

The power stage of inverters uses a variety of semiconductor devices, including Metal-Oxide Semiconductor Field-Effect Transistors (MOSFETs) and Insulated-Gate Bipolar Transistors (IGBTs). MOSFETs are often employed in units up to 5 kVA and 96 V DC. At higher frequencies, they have the advantage of minimal switching losses. IGBTs are typically employed only above 96 V DC systems due to the on-state voltage drop of 2 V DC.

In stand-alone applications, voltage-source inverters are typically employed. They are available in single phase or three phase configurations. Square-wave, quasi-

square-wave, and pulse-width modulation are the three most prevalent switching mechanisms. Power tools, resistive heaters, and incandescent lights can all benefit from square-wave or modified square-wave inverters since they don't require a high-quality sine wave for dependable and efficient performance. Many domestic equipment, on the other hand, require low-distortion sinusoidal waveforms. For remote-area power systems, pure sine-wave inverters are preferred. For sinusoidal output from inverters, pulse-width modulated (PWM) switching is commonly utilised [46].

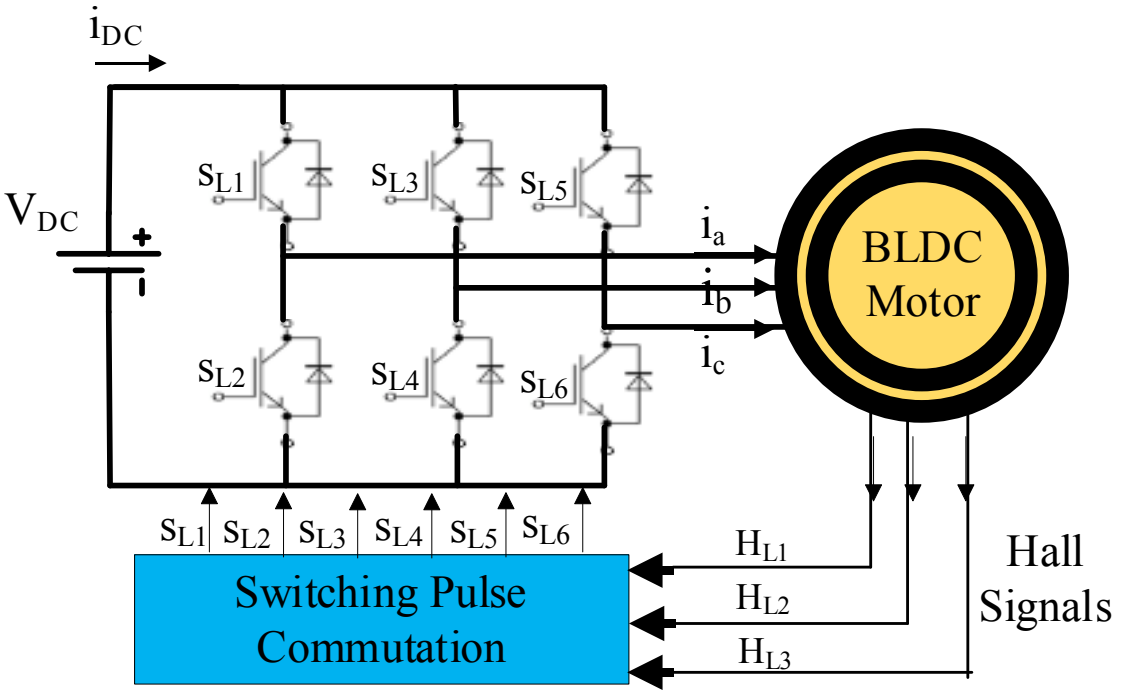

Figure 4.15 Three-phase VSI for BLDC motor.

The BLDC motor's three-phase VSI, as shown in the Figure 4.15, is switched at fundamental frequency via electronic commutation process and consequently, the high frequency switching loss associated with the VSI is significantly reduced. Thus, the efficiency of the operation of SSWPS is increased. VSI's are used in stand-alone systems with certain required features such as very less harmonic generation, proper withstand capability for short term overloading or higher starting currents, large input voltage variation handling capacity and so on. The frequency and output voltage can be easily controlled within the permissible limits.

Inverter efficiency for a typical inverter used in remotely located power systems is shown in Figure 4.16. It's vital to remember that system loads are often much lower than the nominal inverter capacity P_{nom}, resulting in low conversion efficiency for loads less than 10% of the rated inverter output power. If the total energy dissipated in the inverter is kept to a minimum, the overall system operation will be optimal. The high conversion efficiency of newly developed inverters for grid-connected PV systems at low power levels indicates that there is tremendous room for additional efficiency improvements.

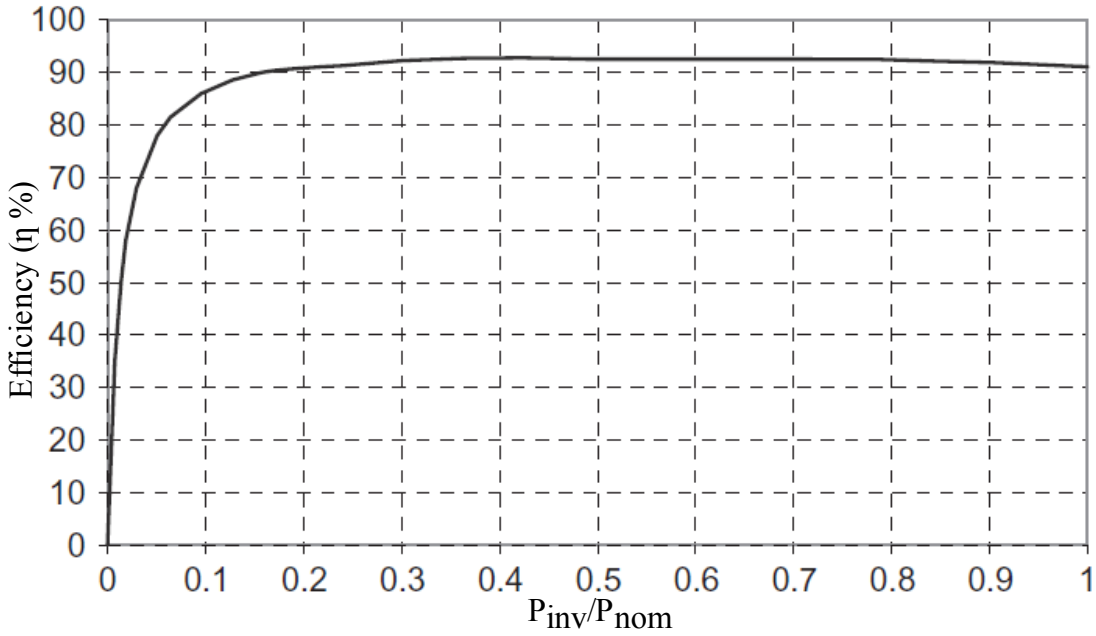

Fig. 4.16 Typical inverter efficiency curve.

CHAPTER 5

SOLAR PV FED BLDC MOTOR SYSTEM DESIGN

In order to reduce the stress on the power semiconductor switches of ADDC's and the various circuit components, the design of the intended system should be such that it should always operates in continuous conduction mode (CCM). The subsequent section deals with the disposition of the system regarding the selection and design of motor, inverters, SPV array and ADDCs.

5.1 PUMP SELECTION AND DESIGN

In many isolated and rural regions, water is supplied by manual pumps or diesel-powered pumps. Diesel pumps use fossil fuels, have a negative impact on the environment, are less dependable and often require more maintenance. Due to recent advancements in the fields of power electronic system technology and solar cell materials, the solar photovoltaic-powered water pumps have drawn a lot of interest of researcher, stakeholders and consumers.

5.1.1 Classification of pumps

It's worth looking at a few distinctive kinds of pumps so that we can establish a relation between their characteristic and the selected motor to which it will be coupled. Generally, the pumps are classified into two categories namely: 1) positive displacement pumps and 2) kinetic (also known as rotodynamic or dynamic) pumps, as shown in the Figure 5.1.

The fluid velocity within the kinetic (or dynamic) pump is raised by providing (kinetic) energy, leading to consecutive velocity drop resulting in pressure increments. However, the displacement pump is a device that adds energy periodically by applying force to one or more moving boundaries of any number of enclosed, fluid-containing volumes, leading to a direct increase in pressure to the level needed to transfer the fluid through vanes or ports into the discharge line.

Among the classifications shown in Figure 5.1, positive and centrifugal displacement pumps are the most prevalent types of pumps used in water pumping applications. Both of them may be divided further into two types: those coupled with surface-mounted motors and those coupled with motors that are immersed in the water (submersible pumps).

The water output of displacement pumps is directly proportional to the pump's speed, but it is practically independent of the head (H) of the pump. These are used to pump water from deep wells or bores using solar energy. They can be piston-type pumps with a cam-driven diaphragm or rotary screw-type pumps with a progressive cavity system. These pumps are suitable for constant torque applications because the pumping rate of these pumps is proportional to their speed.

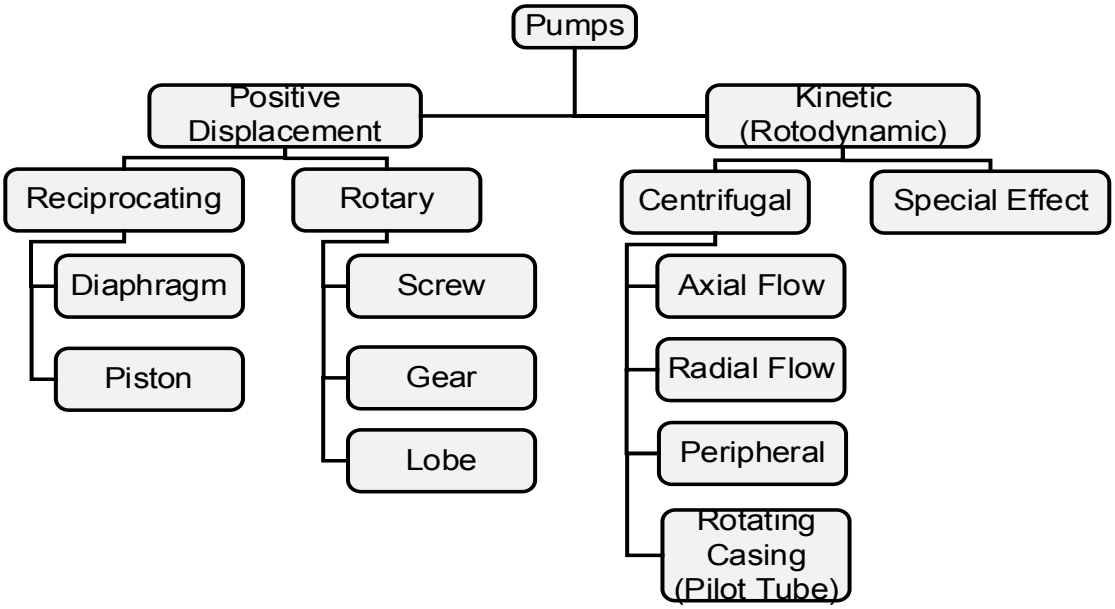

Figure 5.1 Classification of pumps.

Among the classification of pumps in Figure 5.1, the pilot tube centrifugal pump has been chosen because of its capability to give higher efficiency. For low-head applications, centrifugal pumps are employed, particularly if they are directly connected to the solar panels. The pressure difference created varies in proportion to the pump's speed as these pumps are designed for fixed-head applications. The water is thrown radially against a casing through these rotating impeller type pumps which are shaped in a manner that enough pressure is obtained for lifting water [49]. Centrifugal pumps are designed and characterized as a pump that requires smooth and continuous torque without any pulsations. The efficiency of centrifugal pumps is quite high, but it decreases at lower speeds, which might be an issue for the solar water pumping system when solar irradiance levels are low. The single-stage centrifugal pump has only one impeller, whereas other borehole pumps are multistage, with each impeller's output elapse into the centre of the next, increasing the difference in the pressure.

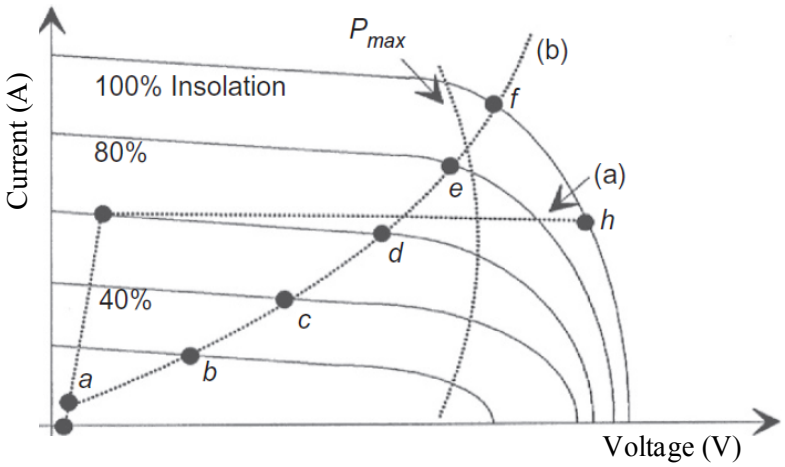

Figure 5.2 PV array I-V characteristics with two mechanical loads: (a) constant torque and (b)centrifugal pump

From Figure 5.2, the load line is clearly separated from the P_{max} line by a significant distance. The daily usage efficiency of a DC motor drive for a centrifugal pump has been found to be 87%, compared to 57% for a constant torque characteristic load. As a result, centrifugal pumps are more suitable for PV arrays [50]. The intersection of the PV array's I-V characteristics and the motor's operating point determines the system's operating point. Because the armature resistance is low, the torque-speed slope is usually steep. The speed and back emf are both zero at the start. As a result, the motor starting current is similar to that of PV array short-circuit current. The starting torque is enhanced by synchronizing the load to the PV source using MPPT.

5.1.2 Design of Centrifugal pump

The design inducement starts with the evaluation of the rating of the pump which is calculated based on the gallons of water being pumped through a particular head using following equation:

$$Pump\left(HP\right)=\frac{H\times F\times SG}{3963\times\eta} \tag{5.1}$$

where F is flow discharge in gal/min; H is head in meters; η is the efficiency of the pump; SG is specific gravity of water

In order to give load torque to the BLDC motor, the proportionality constant k_p provide the feedback to the motor. The load, i.e., water pump, is coupled to the shaft of BLDC motor. The power-speed characteristics propound the design of this pump as follows:

$$k_P\Big|_{\frac{W}{(rad/\sec)^3}}=\frac{P}{{\omega_r}^3} \tag{5.2}$$

where, where, P = required power developed by PMBLDC motor; ω_r = mechanical speed of rotor.

For a hydraulic application such as water pump rotor speed ω_r is squared up with the proportionality constant k_p, to produce desired load torque (T) to particular application. The torque-speed characteristics composes the design of the chosen water pump as follows:

$$k_P\Big|_{\frac{\text{N-m}}{(rad/\sec)^2}}=\frac{T}{{\omega_r}^2} \tag{5.3}$$

Rate of discharge (Q) of water can be expressed in liter per minute can get obtained by the expression as follows:

$$Q=\frac{T\times\omega_r}{g\times H\times 60} \tag{5.4}$$

where, g is constant of gravitational acceleration (9.8 m/s^2).

5.2 MOTOR SELECTION AND DESIGN

Pumps come in a variety of shapes and sizes, and they're employed in a variety of industrial applications. The centrifugal pump is one of the most prevalent type of pump. The sort of load that the motor will encounter is a crucial aspect in selecting motors, as it is in all applications. With regard to the pump system, factors such as speed, torque rating and power rating will be analysed. Other factors, such as vibration, ambient temperature, surroundings, ventilation and altitude, all have an impact on the motor. These criteria are relevant for all motor options, but the key considerations will be the speed, torque, and power ratings [51].

The BLDC motor design parameters is chosen for getting 230V at the input of the PMBLDC drive, as shown in table 5.1.

Table 5.1 Design parameters values of BLDC motor.

Parameters	**Design Data**
Rated Power, P	1.5kW (O.L); 1.15138 kW (C.L)
Rated Rotor Speed, N_r	2065 rpm
Rated DC voltage, V_{dc}	230 V
Total No. of poles, N	4
Moment of inertia, J	2.7 $kg.cm^2$
Stator Current, I_S	5.006 A
Voltage constant, Ke	100.0283 V/krpm
Torque constant, Kt	0.38 Nm/A
Per phase resistance, R_S	0.7 Ω
Per phase inductance, L_S	2.7 mH

The Matlab/Simulink model for BLDC motor drive is created considering the rated values of design parameters from Table 5.1, as shown in Figure B.1 of appendix B. The results obtained from this model (like stator currents, stator line and phase voltages, hall signals, stator back EMFs, electromagnetic Torque, rotor speed is further analysed.

The simulation waveform of the accelerating method for the BLDC motor from standstill to maximum speed without load and constant voltage power supply is shown in Figures 5.3 to 5.8. The drive circuit employs a DC power-supply inverter arrangement, with the inverter operating in the 120^0 conduction mode.

The phase voltage and line voltage have a degree of slope due to the trapezoidal back-EMF effect, as shown in Figure 5.4. Furthermore, the voltage waveform has narrow pulses. This is due to the voltage fluctuation generated by the freewheeling

diode's conduction during the commutation cycle. The commutation period, which is determined by the electromagnetic time constant and the motor's operating state, is equal to the width of the narrow pulse. The phase current and torque variations are comparable to those seen when a BLDC motor starts. The starting current and torque both exceed their rated values by more than ten times. However, under no load, the steady-state current and torque are small. As the simulation's damping is so substantial, the speed curve arrives at the steady state with only one overshoot. Figure 5.6 shows how the envelope of the back-EMF waveform varies in accordance with the rotor speed curve in Figure 5.8.

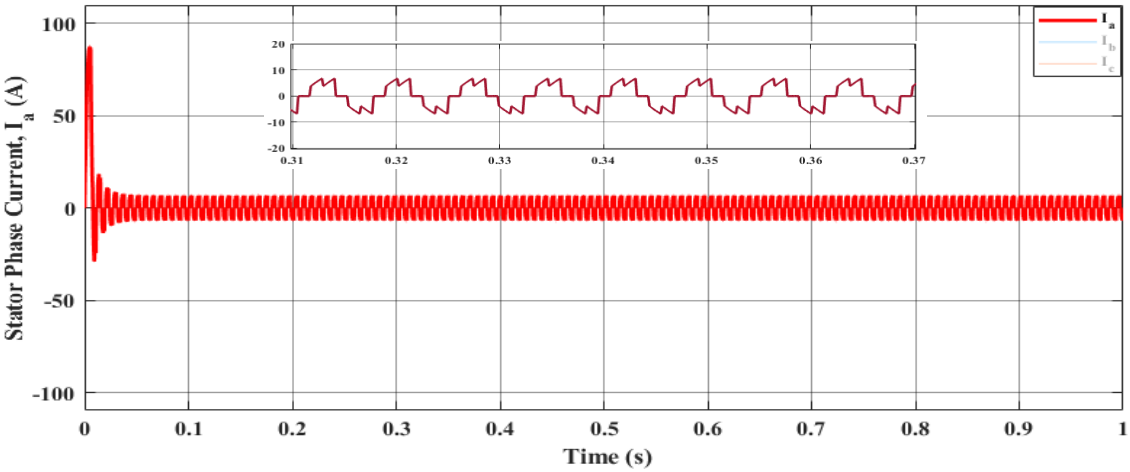

Figure 5.3 BLDC motor drive simulation results of phase 'a' stator current (I_a)

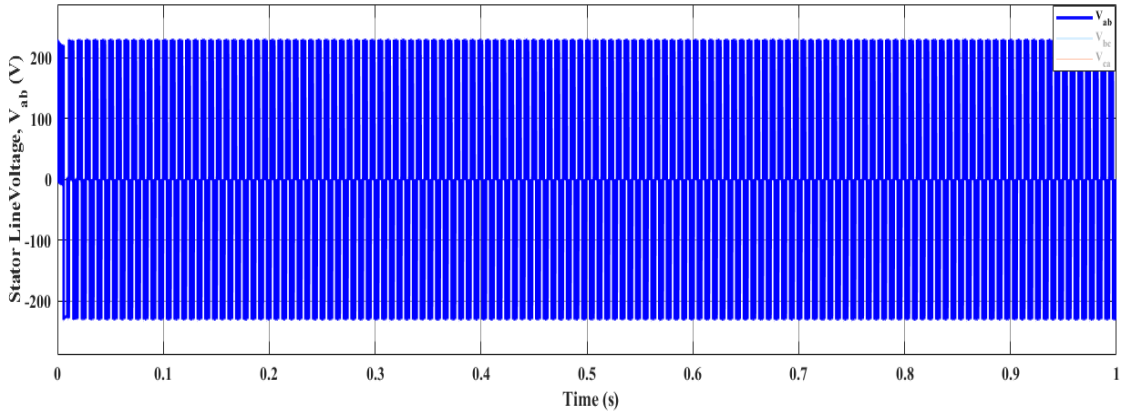

Figure 5.4 BLDC motor drive simulation results of stator line voltage (V_{ab})

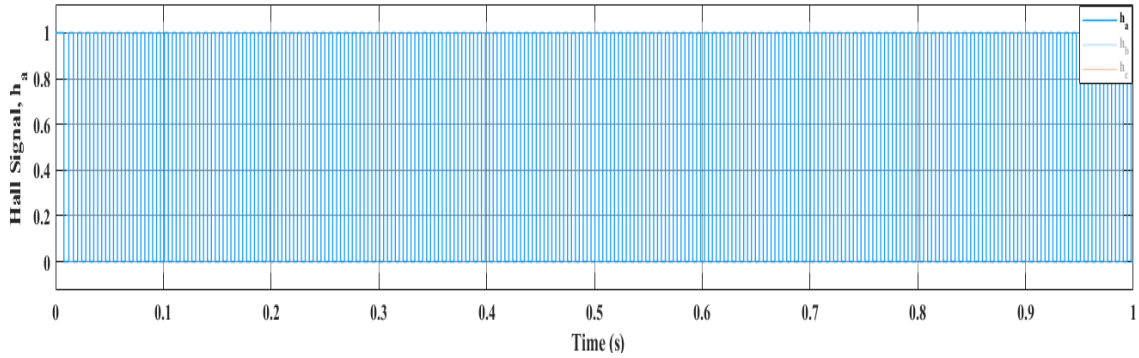

Figure 5.5 BLDC motor drive simulation results of phase 'a' hall signal (h_a)

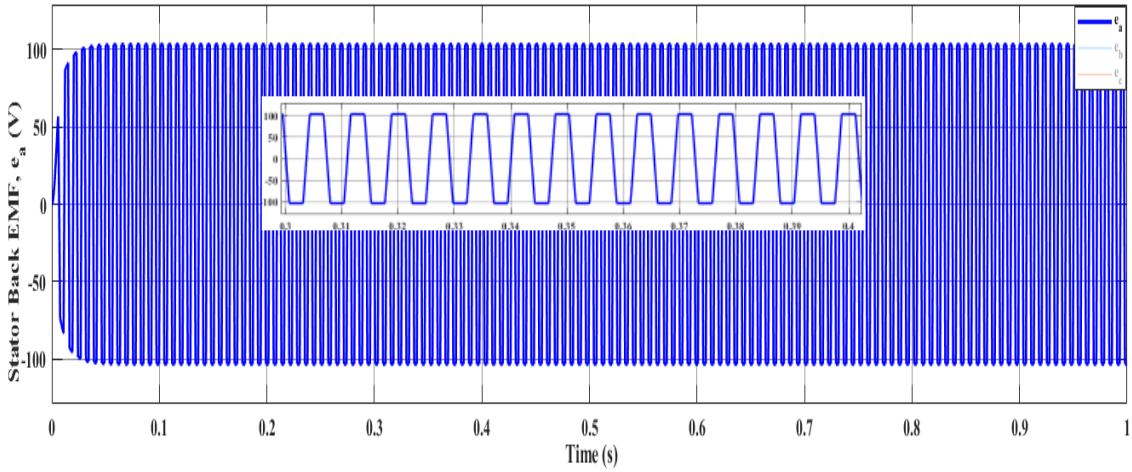

Figure 5.6 BLDC motor drive simulation results of phase 'a' stator back EMF (e_a)

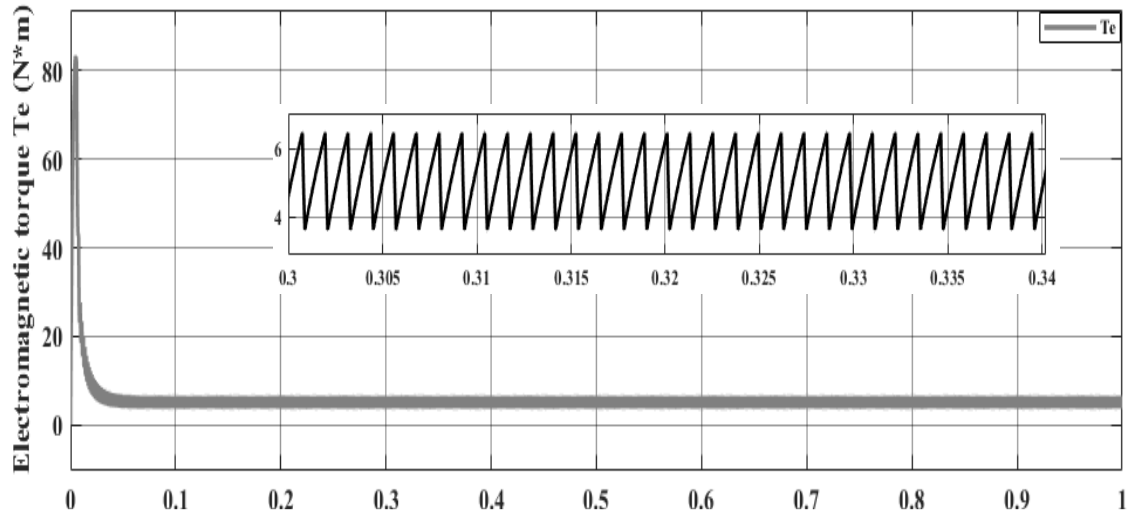

Figure 5.7 BLDC motor drive simulation results of electromagnetic torque (T_e)

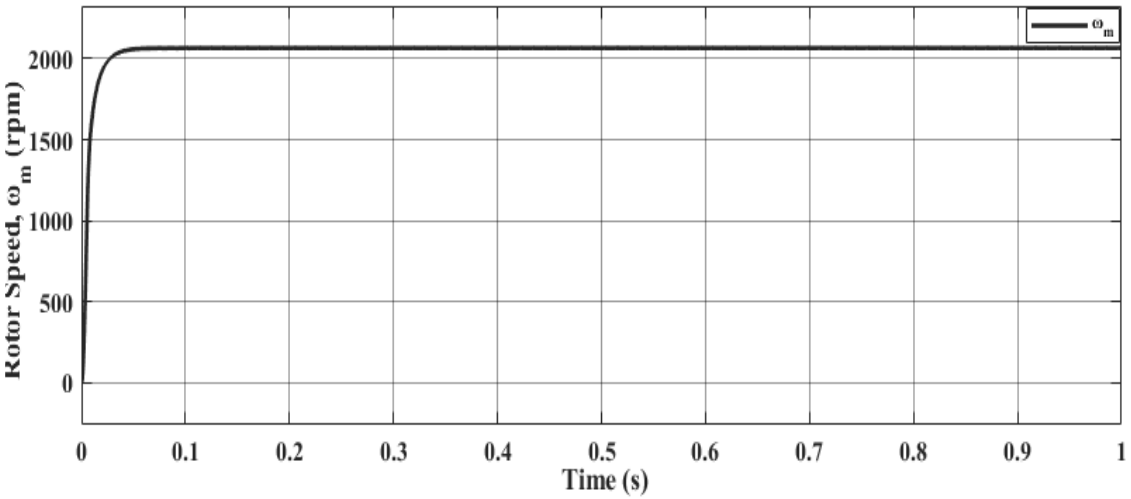

Figure 5.8 BLDC motor drive simulation results of rotor speed (ω_m)

It's worth noting that if the load increases rapidly, the motor speed will drop as the phase voltage and phase current cycle lengthens. To offset the higher load torque, an increase in current will result in an increase in torque. In addition, the current and torque ripple amplitudes have been enhanced. When the load drops abruptly, the motor speed increases as the voltage and current cycles become smaller. Furthermore, the current and torque will have a reduced amplitude and ripple, but the speed will be sufficient, i.e., the back-EMF will be significant enough. Consequently, with constant bus voltage, the current cannot immediately respond to a sudden rise in load. As a result, the rate of change of speed is quite sluggish. In this situation, DC-DC converter circuits can be utilised to boost the voltage and to accelerate the current's reaction time. Similarly, we may utilise the PWM control approach to minimize the voltage of the armature winding when the load drops unexpectedly.

In conclusion, we can observe that the dynamic process of the BLDC motor has a fast response speed. Its benefits, such as high torque output, large power density, and small size, are the major determinants of quick response speed of dynamic process. Also, the modelling results suggest that the BLDC motor's torque ripple is slightly significant. Because of this flaw, its use in high-performance drive systems has been limited. As a result, one of the BLDC motor's major problems is to reduce torque ripple.

5.3 DESIGN, MODELLING AND INTEGRATION OF SPV ARRAY-ADDC'S FED BLDC MOTOR DRIVE

The Advanced DC-to-DC converters (ADDCs) are used to match the output of a PV generator to the input to VSI for running the BLDC drive without any or very least amount of torque ripples. There are various types of advanced DC-DC converters such as the following:

- Luo converter
- SEPIC converter
- Zeta converter

The followed sections shows the simplified and applied diagrams of these three advanced types of converters. The basic components are an electronic switch (preferably IGBT or MOSFET), a toroidal core inductor to store energy, and a "flywheel" diode, which carries the current during that part of switching cycle when the switch is off. These components are designed such that the operation of ADDCs is always in Continuous Conduction Mode (CCM) resulting in the reduced stress on them. The DC-DC converters prefer the charging current to be reduced in continuous manner, in such a way that the resulting battery or DC output voltage is maintained at a specified value.

5.3.1. SPV array-LUO converter fed BLDC motor drive

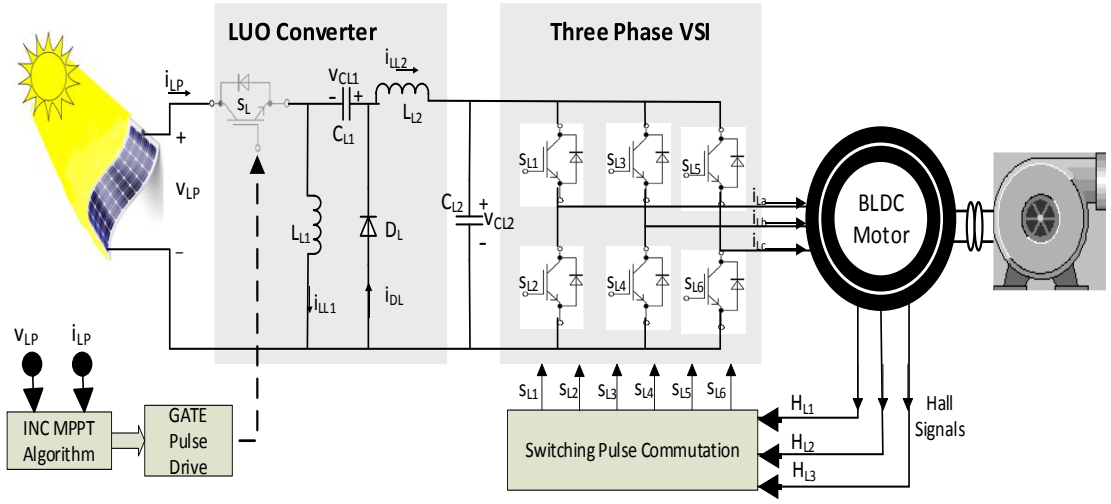

Figure 5.9 SPV array-LUO fed BLDC motor drive in open-loop system.

Luo converter contains two inductors L_{L1} and L_{L2}, two capacitors C_{L1} and C_{L2}, one diode (D_L), and an ideal switch that conducts in CCM (S_L), shown in Figures 5.9 and 5.10.

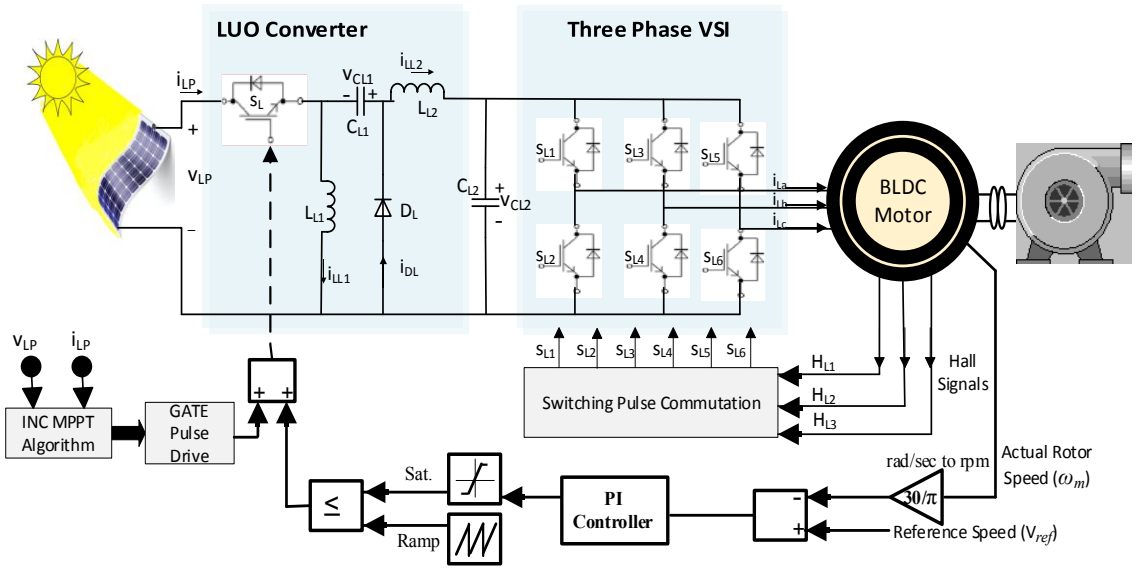

Figure 5.10 Speed control of SPV array-LUO fed BLDC motor drive (closed-loop).

The approach provided in Table 5.2 and Table 5.3, is used to design the individual elements of open-loop and closed-loop system. Luo converters combines a succession of inductors and capacitors, using small variation in duty ratio to generate large output voltage in terms of high arithmetic or geometric progression and it also provides with proper load voltage regulation and correct load current sharing.

Table 5.2 Design parameter's calculation of SPV array-LUO fed BLDC motor drive in open-loop system (without speed control)

Parameters	**Formula**	**Design Data**	**Boost Mode (D=0.25)**	**High-Boost Mode (D=0.50)**	**Super-Lift Mode (D=0.75)**
V_{LP}	$\frac{V_{CL2}}{V_{LP}} = \frac{D}{1-D}$	V_{CL2} = 230V	690V	230V	76.67V
i_{LP}	$i_{LP} = \frac{P_{mpp}}{V_{LP}}$	P_{mpp} = 2.0kW	2.899A	8.696A	26.09A
i_{LL2}	$i_{LL2} = \frac{P_{mpp}}{V_{CL2}}$	$P_{mpp} > P_{BLDC}$ (2kW>1.5kW)	8.696A	8.696A	8.696A
L_{L1}	$L_{L1} = \frac{V_{LP} * D}{f_s * \Delta i_{LL1}}$	Δi_{LL1} = 2*0.04*i_{LP} f_S = 20kHz	29.75mH	6.612mH	1.102mH
L_{L2}	$L_{L2} = \frac{V_{LP} * (1-D)}{f_S * \Delta i_{LL2}}$	Δi_{LL2} = 0.08*i_{LP}	9.92mH	6.612mH	3.306mH
C_{L1}	$C_{L1} = \frac{i_{LL2}}{6 * \omega_{min} * \Delta V_{CL1}}$	ΔV_{CL1} = 0.06*V_{CL2}	9.45µF	21.74 µF	28.36 µF
C_{L2}	$C_{L2} = \frac{i_{LL2}}{6 * \omega_{min} * \Delta V_{CL2}}$	ω_{min} = (2πNP/120) N = 2065rpm; P = 4	18.91 µF	18.91 µF	18.91 µF

Table 5.3 Design parameter's calculation of SPV array-LUO fed BLDC motor drive in closed-loop system (with speed control).

Parameters	**Formula**	**Design Data**	**Boost Mode (D=0.25)**	**High-Boost Mode (D=0.50)**	**Super-Lift Mode (D=0.75)**
V_{LP}	$\frac{V_{CL2}}{V_{LP}} = \frac{D}{1-D}$	V_{CL2} = 230V	690V	230V	76.67V

i_{LP}	$i_{LP} = \frac{P_{mpp}}{V_{LP}}$	P_{mpp} = 1.5kW	2.174A	6.522A	19.564A
i_{LL2}	$i_{LL2} = \frac{P_{mpp}}{V_{CL2}}$	$P_{mpp} > P_{BLDC}$ (1.5kW>1.2kW)	6.522A	6.522A	6.522A
L_{L1}	$L_{L1} = \frac{V_{LP} * D}{f_s * \Delta i_{LL1}}$	Δi_{LL1} = 2*0.04*i_{LP} f_S = 20kHz	39.75mH	26.46mH	13.23mH
L_{L2}	$L_{L2} = \frac{V_{LP} * (1-D)}{f_S * \Delta i_{LL2}}$	Δi_{LL2} = 0.08*i_{LP}	13.25mH	8.82mH	4.41mH
C_{L1}	$C_{L1} = \frac{i_{LL2}}{6 * \omega_{min} * \Delta V_{CL1}}$	ΔV_{CL1} = 0.06*V_{CL2}	7.07µF	14.20µF	21.26µF
C_{L2}	$C_{L2} = \frac{i_{LL2}}{6 * \omega_{min} * \Delta V_{CL2}}$	ω_{min} = (2πNP/120) N = 2065rpm; P = 4	14.15µF	14.17µF	14.17µF

5.3.2. SPV array-SEPIC converter fed BLDC motor drive

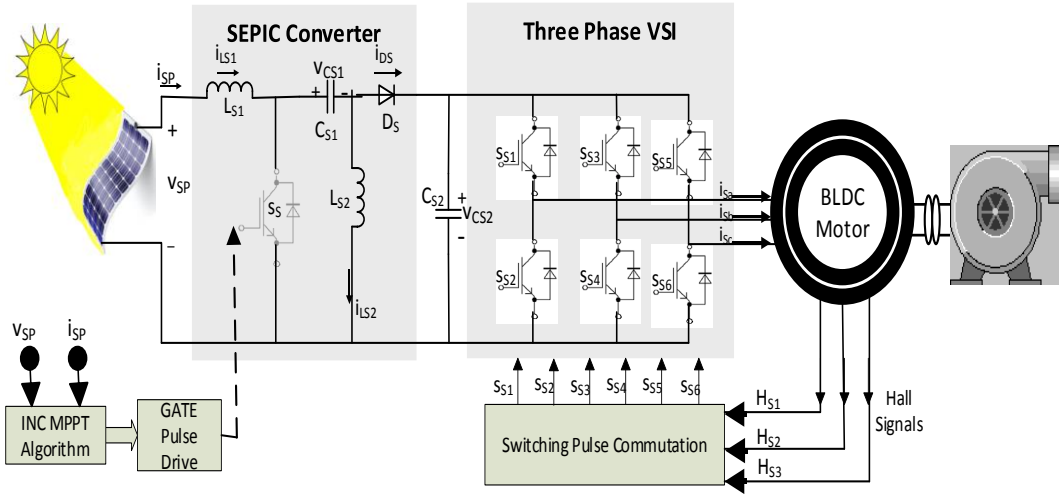

Figure 5.11 SPV array-SEPIC fed BLDC motor drive in open-loop system.

SEPIC converter contains two inductors L_{S1} and L_{S2}, two capacitors C_{S1} and C_{S2}, one diode (D_S), and an ideal switch that conducts in CCM (S_S), shown in Figures 5.11 and 5.12. The formula given in Table 5.4 and Table 5.5, is used to determine the value of individual elements of open-loop and closed-loop system. To generate a large output voltage, the ON period should be longer than the OFF duration while switching as the

inductor requires more charging time. If this is not the case, the converter will stop producing the required output due to the capacitor's inability to fully charge.

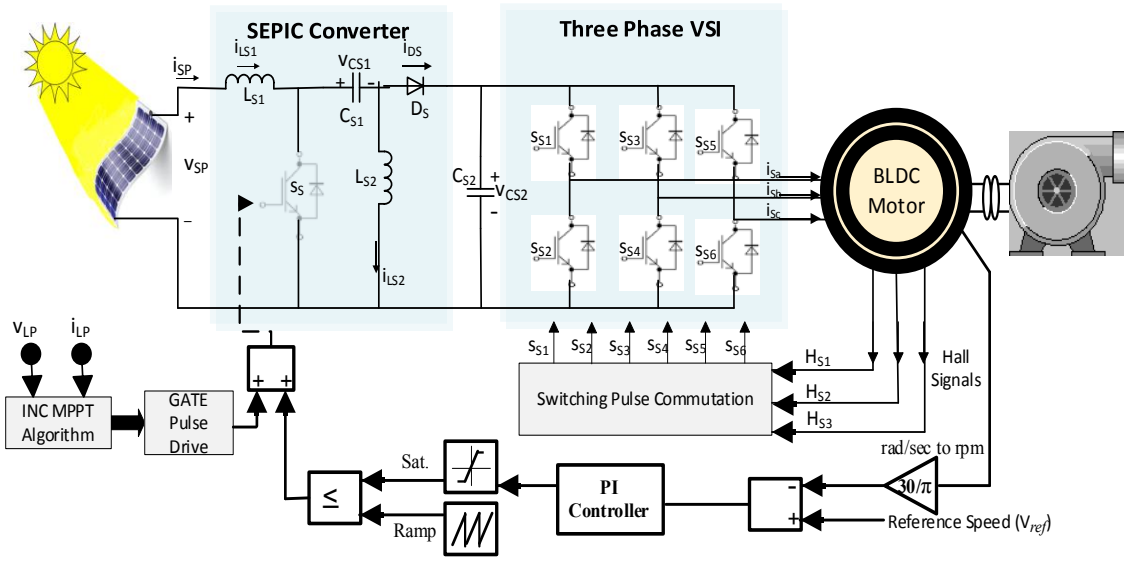

Figure 5.12 Speed control of SPV array-SEPIC fed BLDC motor drive (closed-loop).

To achieve maximum power, several control techniques such as PI control, sliding mode control, dP/dV feedback control, and fuzzy logic control are recommended. During the converter's design, the switching as well as conduction losses is diminished by using soft switching, which is further utilised to reduce the output current ripples and is implemented to regulate DC voltage flickering in solar power generation.

Table 5.4 Design parameter's calculation of SPV array-SEPIC fed BLDC motor drive in open-loop system (without speed control).

Parameters	**Formula**	**Design Data**	**Buck Mode (D=0.25)**	**Normal Mode (D=0.5)**	**Boost Mode (D=0.75)**
V_{SP}	$\frac{V_{CS2}}{V_{SP}} = \frac{D}{1-D}$	$V_{CS2} = 230V$	690V	230V	76.67V
i_{SP}	$i_{SP} = \frac{P_{mpp}}{V_{SP}}$	$P_{mpp} = 2.0kW$	2.899A	8.696A	26.09A
i_{DS}	$i_{DS} = \frac{P_{mpp}}{V_{CS2}}$	$P_{mpp} > P_{BLDC}$ (2kW>1.5kW)	8.696A	8.696A	8.696A
L_{S1}	$L_{S1} = \frac{V_{SP} * D}{f_s * \Delta i_{LS1}}$	$\Delta i_{LS1} = 0.1 * i_{SP}$ $f_S = 20kHz$	7.44mH	495.86mH	0.276mH
L_{S2}	$L_{S2} = \frac{V_{CS2} * (1-D)}{f_s * \Delta i_{LS2}}$	$\Delta i_{LS2} = 0.1 * i_{SP}$	7.44mH	495.86mH	0.276mH

C_{S1}	$C_{S1} = \frac{i_{DS} * D}{f_s * \Delta V_{CS1}}$	$\Delta V_{CL1} = 0.06 * V_{CL2}$	7.88µF	0.473µF	212.67µF
C_{S2}	$C_{S2} = \frac{i_{DS}}{6 * \omega_{min} * \Delta V_{CS2}}$	$\omega_{min} = (2\pi NP/120)$ N = 2065rpm; P = 4	0.24µF	0.473µF	70.89µF

Table 5.5 Design parameter's calculation of SPV array-LUO fed BLDC motor drive in closed-loop system (with speed control).

Parameters	**Formula**	**Design Data**	**Buck Mode (D=0.25)**	**Normal Mode (D=0.5)**	**Boost Mode (D=0.75)**
V_{SP}	$\frac{V_{CS2}}{V_{SP}} = \frac{D}{1-D}$	V_{CS2} = 230V	690V	230V	76.67V
i_{SP}	$i_{SP} = \frac{P_{mpp}}{V_{SP}}$	P_{mpp} = 1.5kW	2.174A	6.522A	19.564A
i_{DS}	$i_{DS} = \frac{P_{mpp}}{V_{CS2}}$	$P_{mpp} > P_{BLDC}$ (1.5kW>1.2kW)	6.522A	6.522A	6.522A
L_{S1}	$L_{S1} = \frac{V_{SP} * D}{f_s * \Delta i_{LS1}}$	$\Delta i_{LS1} = 0.1 * i_{SP}$ f_S = 20kHz	9.92mH	2.20mH	0.37mH
L_{S2}	$L_{S2} = \frac{V_{CS2} * (1-D)}{f_s * \Delta i_{LS2}}$	$\Delta i_{LS2} = 0.1 * i_{SP}$	9.92mH	2.20mH	0.37mH
C_{S1}	$C_{S1} = \frac{i_{DS} * D}{f_s * \Delta V_{CS1}}$	$\Delta V_{CL1} = 0.06 * V_{CL2}$	0.12µF	0.71µF	2.13µF
C_{S2}	$C_{S2} = \frac{i_{DS}}{6 * \omega_{min} * \Delta V_{CS2}}$	$\omega_{min} = (2\pi NP/120)$ N = 2065rpm; P = 4	0.35µF	0.71µF	1.06µF

5.3.3. SPV array-ZETA converter fed BLDC motor drive

Zeta converter contains two inductors L_{Z1} and L_{Z2}, two capacitors C_{Z1} and C_{Z2}, one diode (D_Z), and an ideal switch that conducts in CCM (S_Z), as shown in Figure. 5.13 and 5.14.

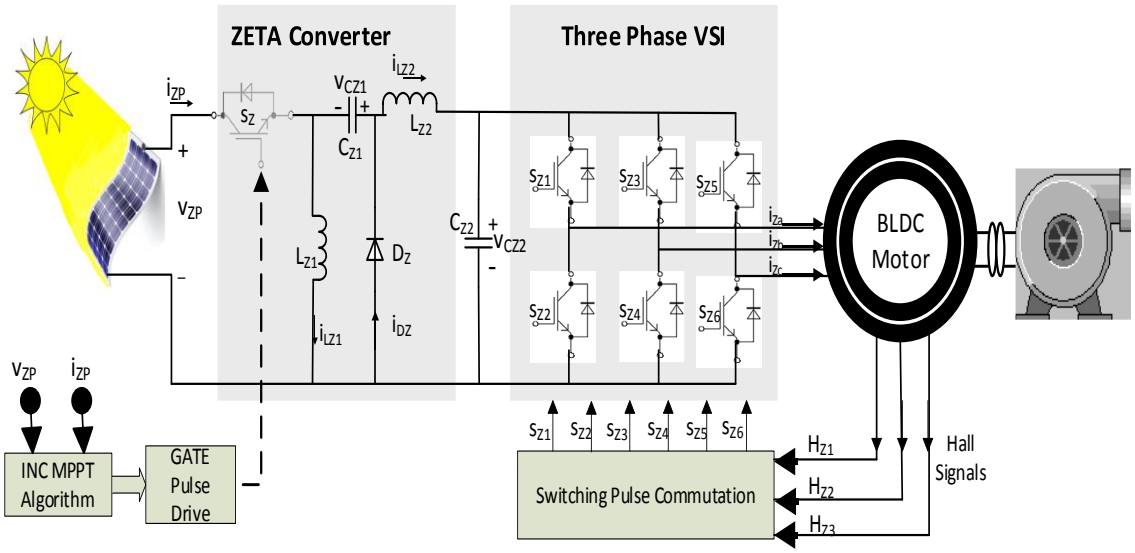

Figure 5.13 SPV array-ZETA fed BLDC motor drive for water pumping system.

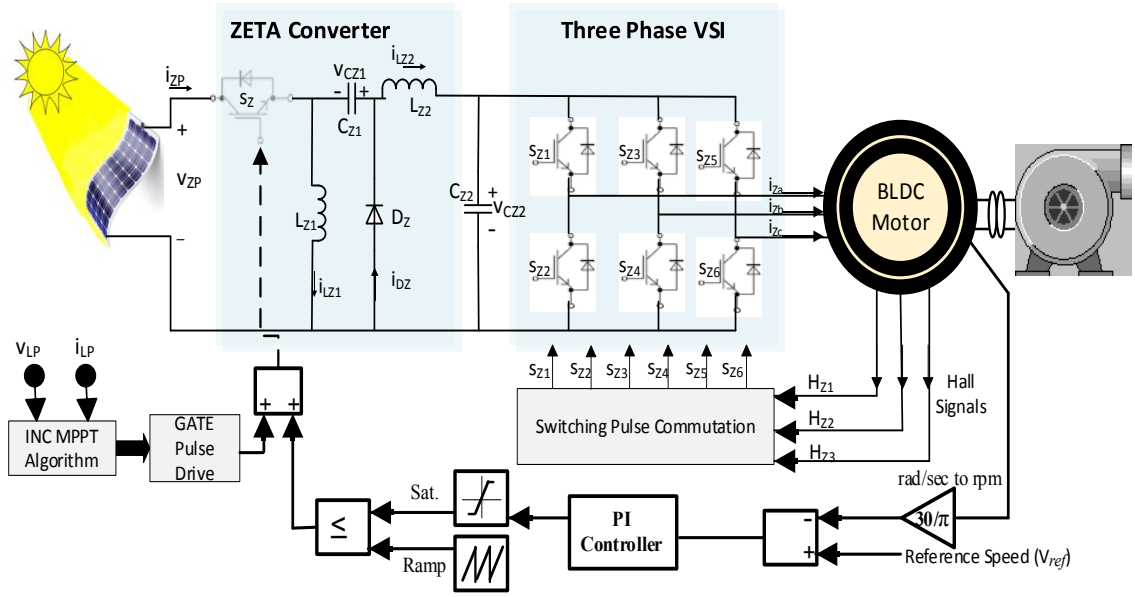

Figure 5.14 Speed control of SPV array-ZETA fed BLDC motor drive.

In one switching interval (T), the zeta converter operates in two stage. When the switch is off (first stage), the inductors L_{Z1} and L_{Z2} store energy; however, when the switch is on (second stage), the energy stored by L_{Z1} is transferred to the intermediate capacitor, C_{Z1}, and the energy stored by L_{Z2} is delivered to the load via DC link capacitor C_{Z2}, shown in Figure 5.13 and 5.14.

When compared to the input voltage, a zeta converter yields a non-inverted voltage at the output that is either increased or decreased. The ability to track MPP over the whole area of the PV curve is a key feature of the Zeta converter and it can also be used for battery storage in PV system applications. Moreover, it provides improved voltage conversion ratio, reduced input and output current ripple and can be operated in both CCM and DCM. Individual elements' values of open-loop and closed-loop system are designed using the method outlined in Table 5.6 and 5.7.

Table 5.6 Design parameter's calculation of SPV array-ZETA fed BLDC motor drive in open-loop system (without speed control).

Parameters	**Formula**	**Design Data**	**Buck Mode (D=0.25)**	**Normal Mode (D=0.50)**	**Boost Mode (D=0.75)**
V_{ZP}	$\frac{V_{CZ2}}{V_{ZP}} = \frac{D}{1-D}$	V_{CZ2} = 230V	690V	230V	76.67V
i_{ZP}	$i_{ZP} = \frac{P_{mpp}}{V_{ZP}}$	P_{mpp} = 2.0kW	2.899A	8.696A	26.09A
i_{LZ2}	$i_{LZ2} = \frac{P_{mpp}}{V_{CZ2}}$	$P_{mpp} > P_{BLDC}$ (2kW>1.5kW)	8.696A	8.696A	8.696A
L_{Z1}	$L_{Z1} = \frac{V_{ZP} * D}{f_s * \Delta i_{LZ1}}$	$\Delta i_{LZ1} = 0.06 * i_{ZP}$ f_S =20kHz	49.59mH	11.021mH	1.837mH
L_{Z2}	$L_{Z2} = \frac{V_{CZ2} * (1-D)}{f_s * \Delta i_{LZ2}}$	$\Delta i_{LZ2} = 0.06 * i_{LZ2}$	16.53mH	11.021mH	1.837mH
C_{Z1}	$C_{Z1} = \frac{i_{LZ2} * D}{f_s * \Delta V_{CZ1}}$	$\Delta V_{CZ1} = 0.1 * V_{CZ2}$	4.73µF	9.452µF	0.142µF
C_{Z2}	$C_{Z2} = \frac{i_{LZ2}}{6 * \omega_{min} * \Delta V_{CZ1}}$	$\omega_{min} = (2\pi NP/120)$ N = 2065rpm; P = 4	150.43µF	150.43µF	150.43µF

Table 5.7 Design parameter's calculation of SPV array-LUO fed BLDC motor drive in closed-loop system (with speed control).

Parameters	**Formula**	**Design Data**	**Buck Mode (D=0.25)**	**Normal Mode (D=0.50)**	**Boost Mode (D=0.75)**
V_{ZP}	$\frac{V_{CZ2}}{V_{ZP}} = \frac{D}{1-D}$	V_{CZ2} = 230V	690V	230V	76.67V
i_{ZP}	$i_{ZP} = \frac{P_{mpp}}{V_{ZP}}$	P_{mpp} =1.5kW	2.174A	6.522A	19.564A
i_{LZ2}	$i_{LZ2} = \frac{P_{mpp}}{V_{CZ2}}$	$P_{mpp} > P_{BLDC}$	6.522A	6.522A	6.522A

		(1.5kW>1.2kW)			
L_{Z1}	$L_{Z1} = \frac{V_{ZP} * D}{f_s * \Delta i_{LZ1}}$	$\Delta i_{LZ1} = 0.06 * i_{ZP}$ f_S =20kHz	66.12mH	14.70mH	2.45mH
L_{Z2}	$L_{Z2} = \frac{V_{CZ2} * (1 - D)}{f_s * \Delta i_{LZ2}}$	Δi_{LZ2} = 0.06*i_{LZ2}	66.12mH	14.70mH	2.45mH
C_{Z1}	$C_{Z1} = \frac{i_{LZ2} * D}{f_s * \Delta V_{CZ1}}$	ΔV_{CZ1} = 0.1*V_{CZ2}	3.545µF	7.089µF	10.63µF
C_{Z2}	$C_{Z2} = \frac{i_{LZ2}}{6 * \omega_{min} * \Delta V_{CZ1}}$	ω_{min} = (2πNP/120) N = 2065rpm; P = 4	107.45µF	107.45µF	107.45µF

5.4 MATLAB/SIMULINK SIMULATION RESULTS AND PERFORMANCE CALCULATIONS

5.4.1. Simulation waveforms and inferred calculation for open-loop system

The simulation results of the individual performance parameters have been obtained pertaining to Figures 5.9, 5.11 and 5.13, as illustrated below. The calculation for evaluating the performance parameters has been done using the process explained in section 4.2.3, and the results are presented in tabularized form. The combined simulation results and performance analysis visualizing. all the converters are given in section 6.1 via Table 6.1.

The Figures 5.15, 5.16 and 5.17 shows the waveforms w.r.t Figure 5.9, i.e., SPV array-LUO fed BLDC motor drive for water pumping system in open-loop system (without speed control). The calculation of performance parameters is done using these waveforms and are presented in Table 5.8.

Now, Figures 5.18, 5.19 and 5.20 shows the waveforms w.r.t Figure 5.11, i.e., SPV array-SEPIC fed BLDC motor drive for water pumping system in open-loop system (without speed control). The calculation of performance parameters is done using these waveforms and are presented in Table 5.9.

Similarly, Figures 5.21, 5.22 and 5.23 shows the waveforms w.r.t Figure 5.13, i.e., SPV array-ZETA fed BLDC motor drive for water pumping system in open-loop system (without speed control). The calculation of performance parameters is done using these waveforms and are presented in Table 5.10.

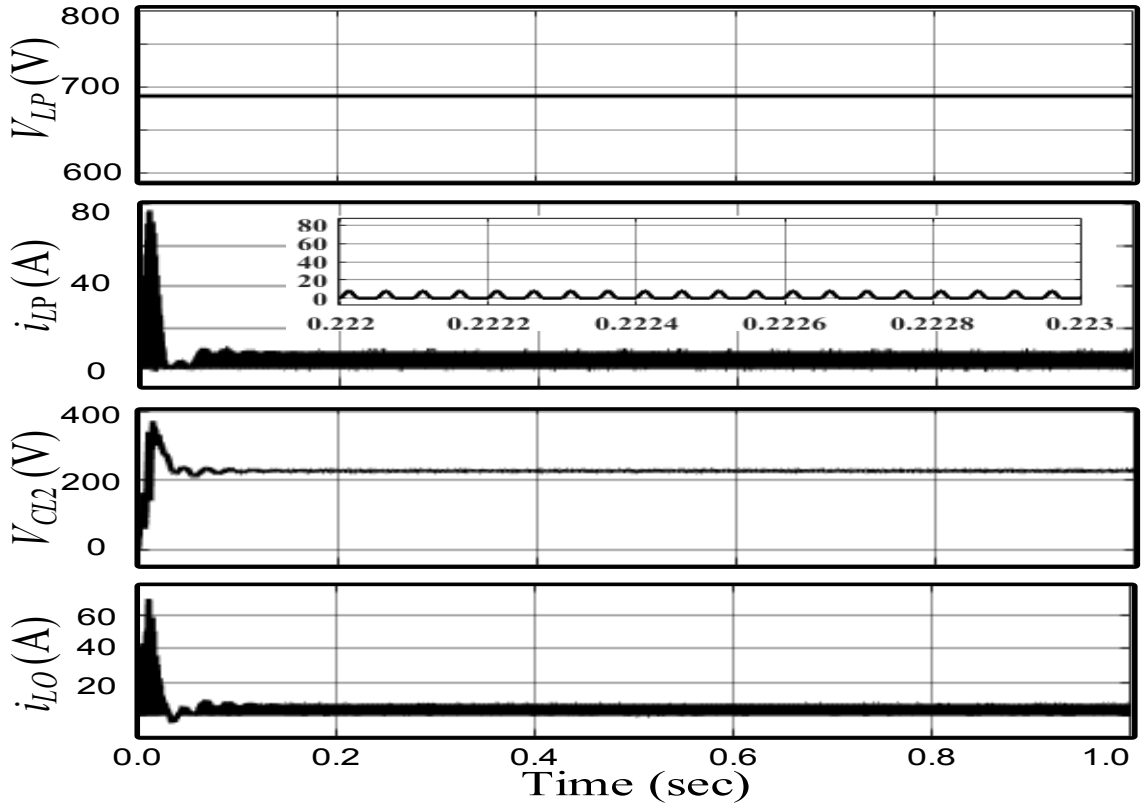

Figure 5.15 LUO converter simulation results of boost mode (D=0.25).

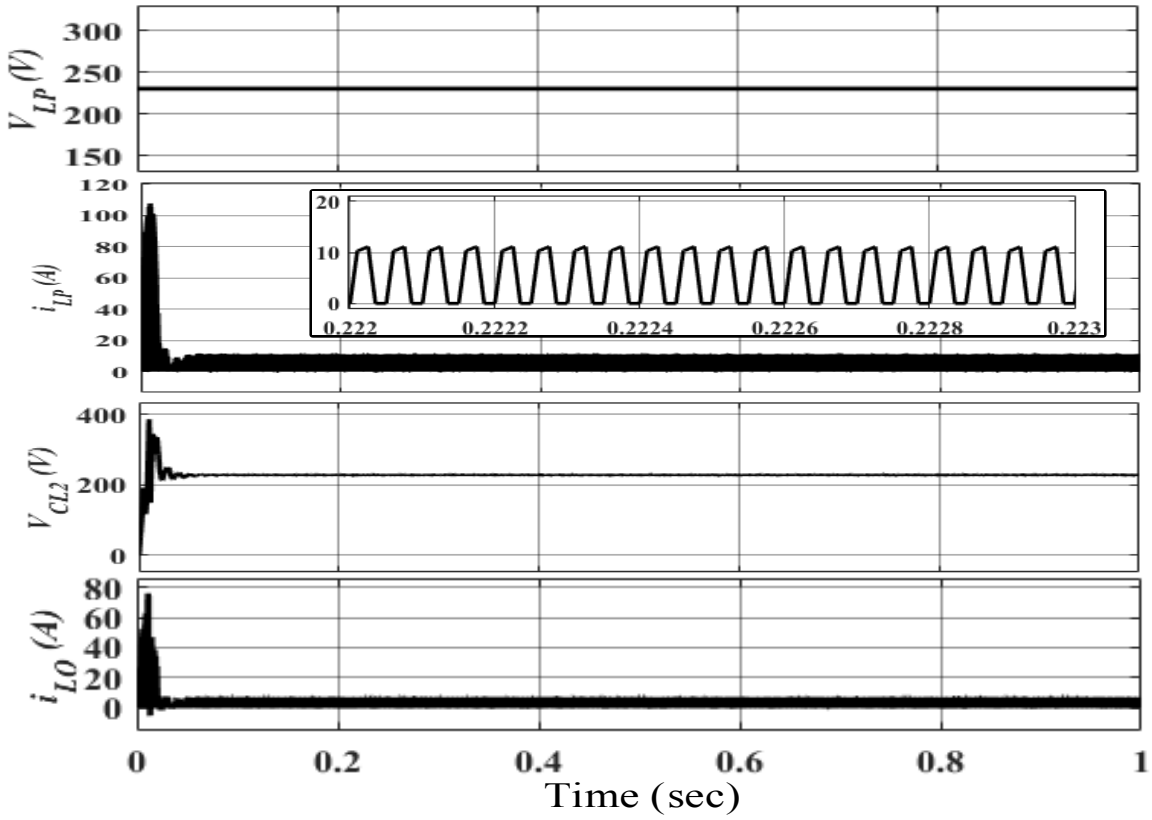

Figure 5.16 LUO converter simulation results of high-boost mode (D=0.50).

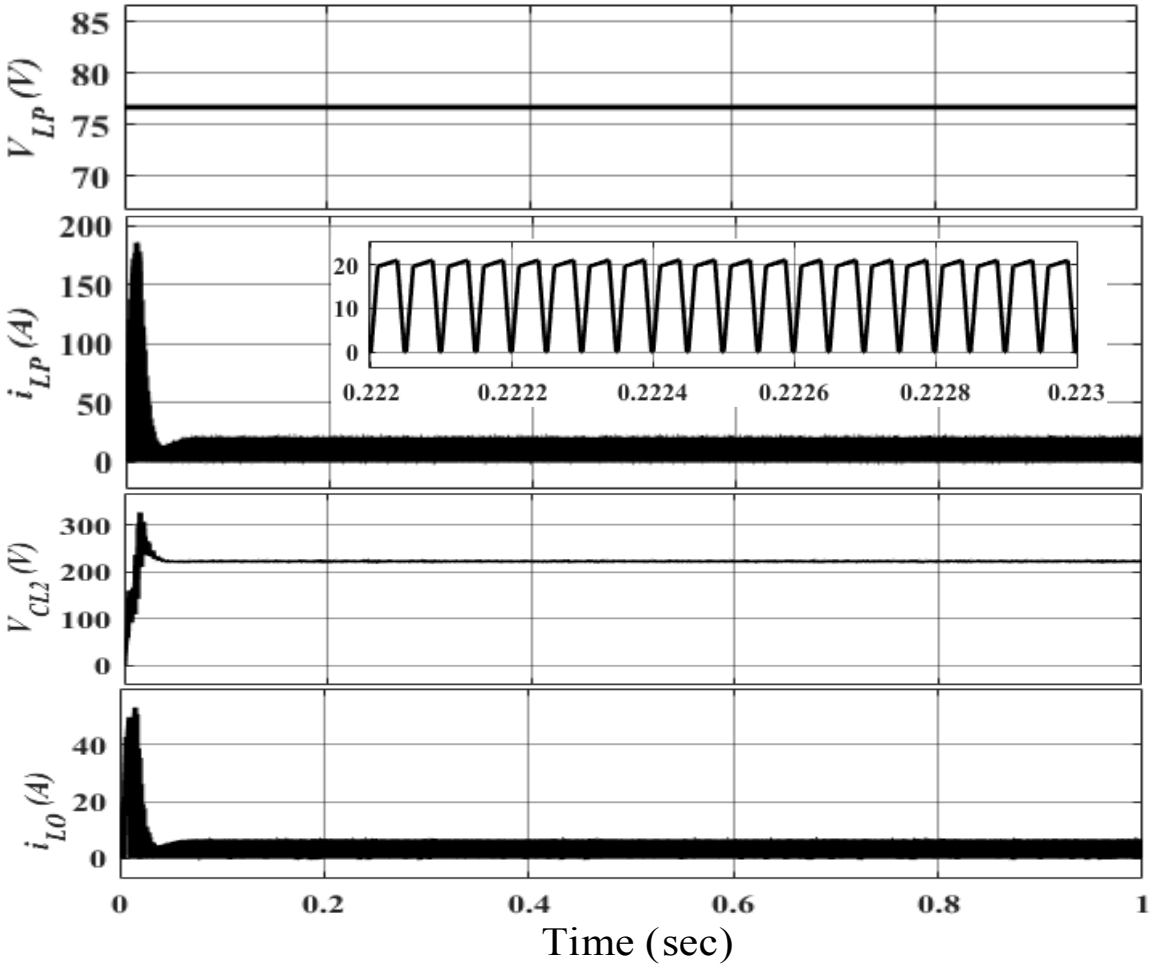

Figure 5.17 LUO converter simulation results of super-lift mode (D=0.75).

The calculation of the performance parameters from the above waveforms has been summarized in the table below.

Table 5.8 Performance parameter's calculation of SPV array-LUO fed BLDC motor drive.

Mode ▸ ▸ / Parameters ▸ ▸	Boost (D=0.25)	High-Boost (D=0.50)	Super-Lift (D=0.75)
Input Voltage [V_{LP} (V)]	690V	230V	76.67V
Input Current [i_{LP} (A)]	2.079A	5.311A	15.27A
Input Power [P_{LP} (W)]	1434.510W	1221.530W	1170.751W
Output Voltage [V_{LO} (V)]	228.9V	228.1V	223.0V
Output Current [i_{LO} (A)]	4.974A	4.972A	4.976A
Output Power [P_{LO} (W)]	1138.549W	1134.113W	1109.648W
Power Efficiency [η_{PL}(%)]	79.37%	92.84%	94.78%
Conduction Losses [P_{CL} (W)]	295.961W	87.417W	61.103W

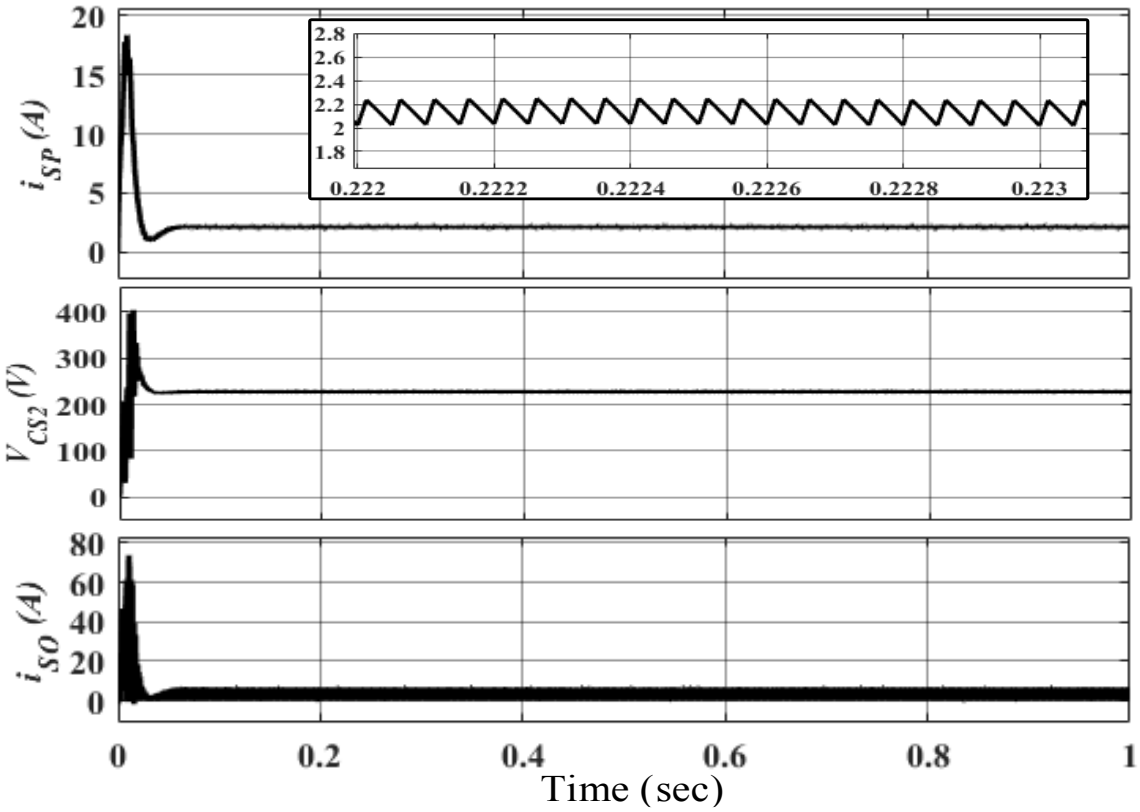

Figure 5.18 SEPIC converter simulation results of buck mode (D=0.25).

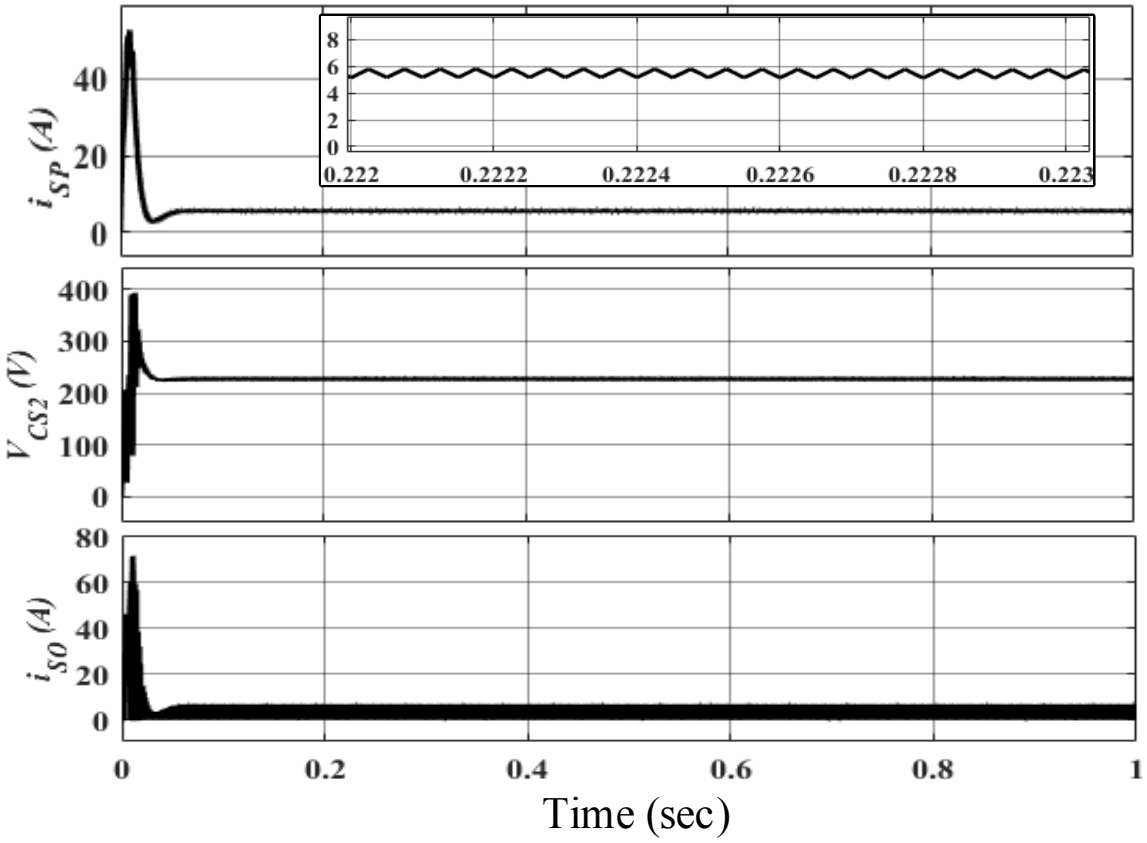

Figure 5.19 SEPIC converter simulation results of normal mode (D=0.50).

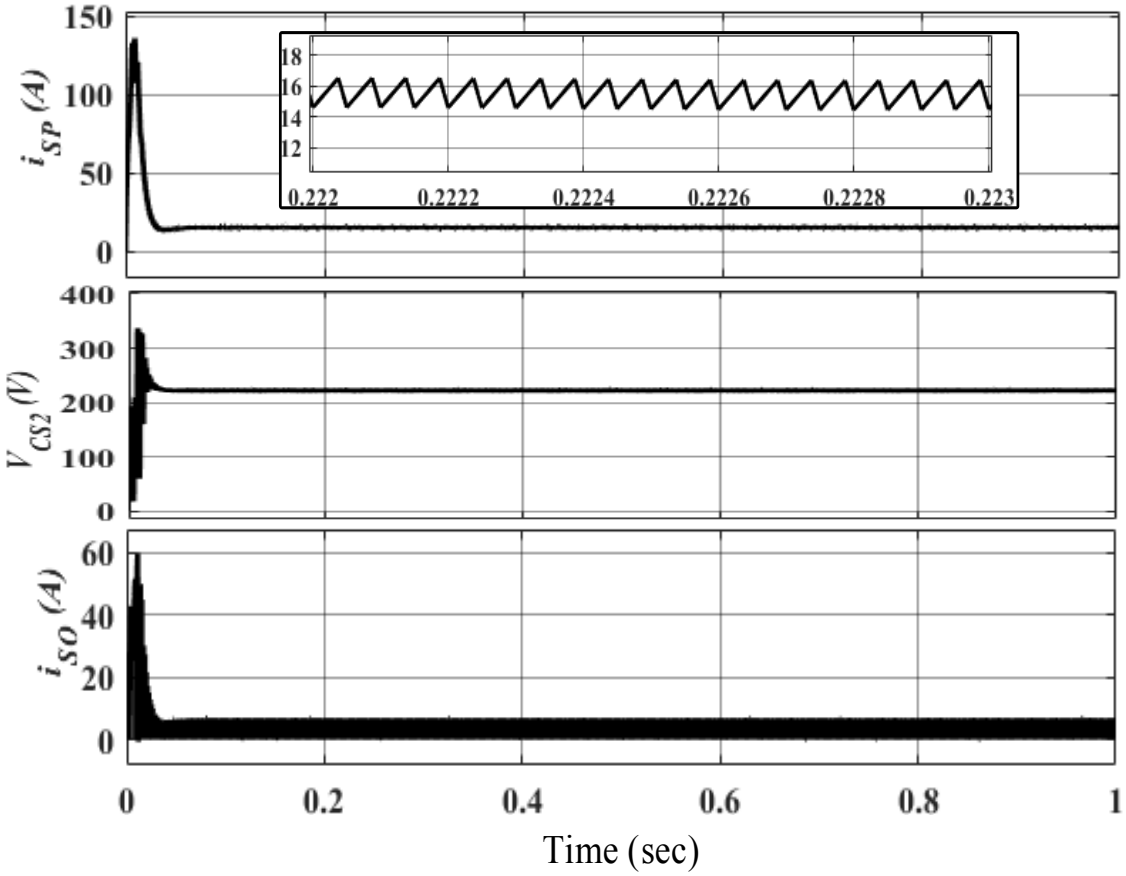

Figure 5.20 SEPIC converter simulation results of boost mode (D=0.75).

The calculation of the performance parameters from the above waveforms has been summarized in the table below.

Table 5.9 Performance parameter's calculation of SPV array-SEPIC fed BLDC motor drive.

Mode ▸ ▸ / Parameters ▸ ▸	Buck Mode (D=0.25)	Normal Mode (D=0.50)	Boost Mode (D=0.75)
Input Voltage [V_{SP} (V)]	690V	230V	76.67V
Input Current [i_{SP} (A)]	2.138A	5.473A	15.49A
Input Power [P_{SP} (W)]	1475.220W	1258.790W	1187.618W
Output Voltage [V_{SO} (V)]	228.8V	228.0V	222.9V
Output Current [i_{SO} (A)]	4.939A	4.940A	4.945A
Output Power [P_{SO} (W)]	1130.043W	1126.320W	1102.241W
Power Efficiency [η_{PS}(%)]	76.60%	89.48%	92.81%
Conduction Losses [P_{CS} (W)]	345.177W	132.470W	85.377W

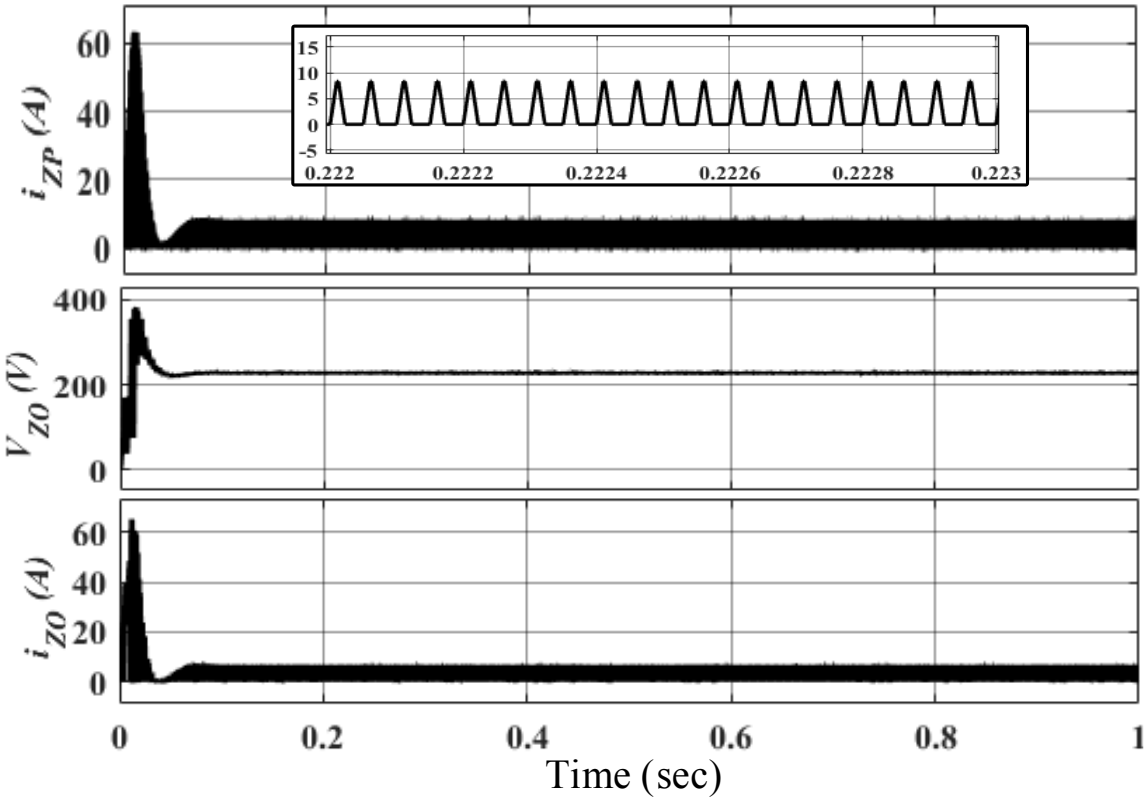

Figure 5.21 ZETA converter simulation results of buck mode (D=0.25).

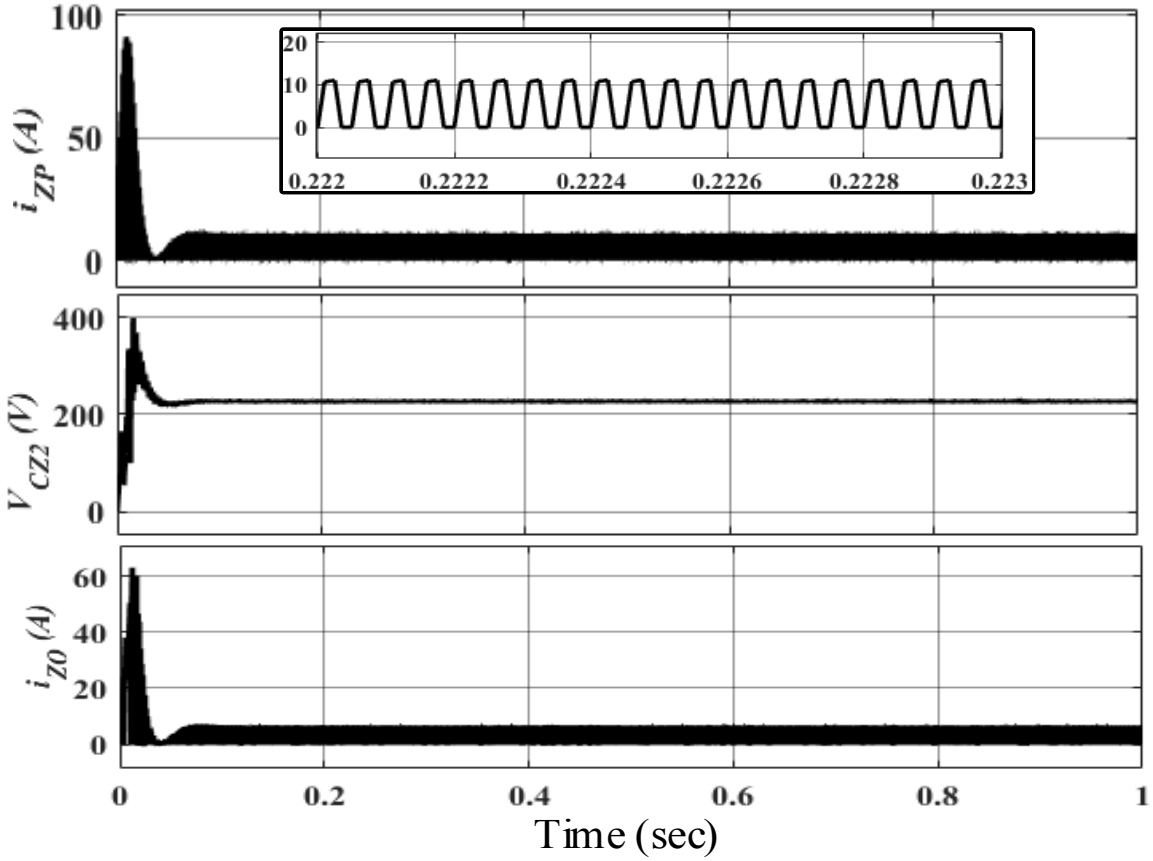

Figure 5.22 ZETA Converter simulation results of normal mode (D=0.50).

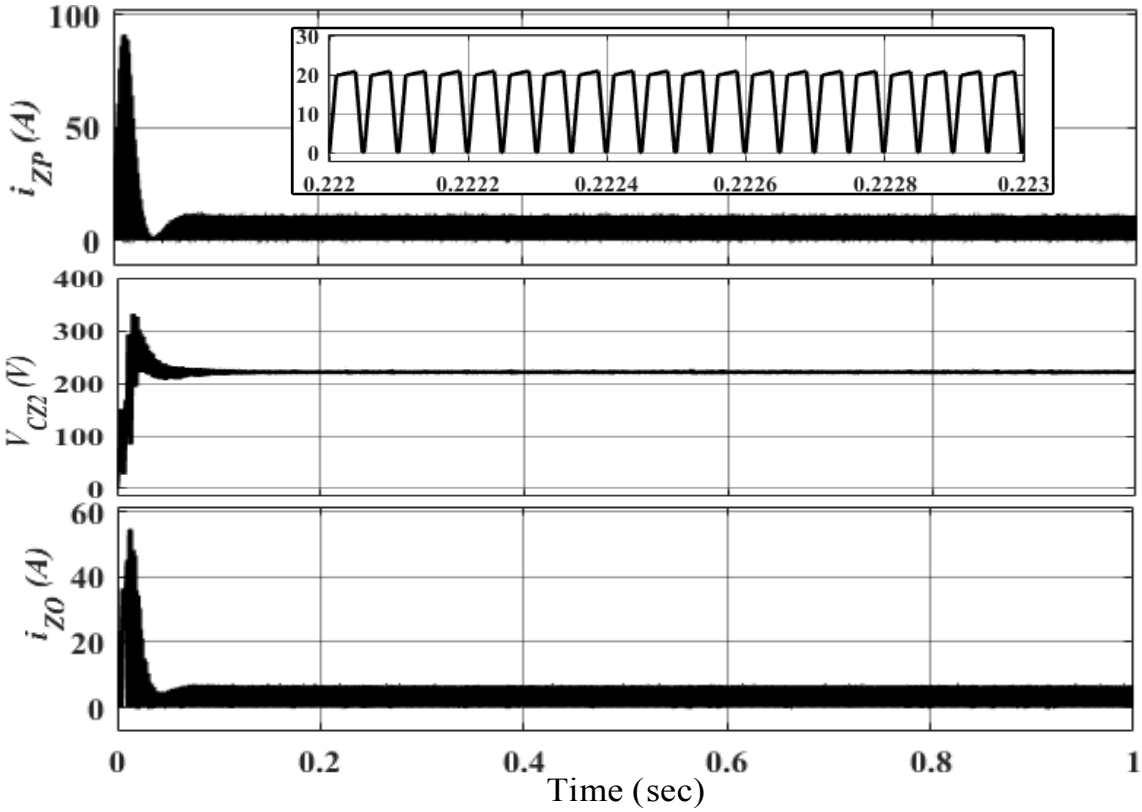

Figure 5.23 ZETA converter simulation results of boost mode (D=0.75).

The calculation of the performance parameters from the above waveforms has been summarized in the table below.

Table 5.10 Performance parameter's calculation of SPV array-ZETA fed BLDC motor drive.

Mode ▸ ▸ / Parameters ▸ ▸	Buck Mode (D=0.25)	Normal Mode (D=0.50)	Boost Mode (D=0.75)
Input Voltage [V_{ZP} (V)]	690V	230V	76.67V
Input Current [i_{ZP} (A)]	2.102A	5.401A	15.33A
Input Power [P_{ZP} (W)]	1450.380W	1242.230W	1175.351W
Output Voltage [V_{ZO} (V)]	228.9V	228.1V	222.9V
Output Current [i_{ZO} (A)]	4.975A	4.977A	4.978A
Output Power [P_{ZO} (W)]	1138.778W	1135.254W	1109.596W
Power Efficiency [η_{PZ}(%)]	78.52%	91.40%	94.41%
Conduction Losses [P_{CZ} (W)]	311.602W	106.976W	65.755W

5.4.2. Simulation waveforms and inferred calculation for closed-loop system

The simulation results of the individual performance parameters have been obtained pertaining to Figures 5.10, 5.12 and 5.14, as illustrated below. The calculation for evaluating the performance parameters has been done using the process explained in section 4.2.3, and the results are presented in tabularized form. The combined simulation results and performance analysis visualizing. all the converters are given in section 6.1 via Table 6.2.

The Figures 5.24 and 5.25 shows the input voltage and input current waveforms, and output voltage and current waveforms w.r.t Figure 5.10, 5.12 and 5.14, i.e., SPV array-ADDC fed BLDC motor drive for water pumping system in closed-loop system (with speed control), for 0.25 duty cycle (D=0.25). The calculation of performance parameters is done using these waveforms and are presented in Table 5.11.

Now, the Figures 5.26 and 5.27 shows the input voltage and input current waveforms, and output voltage and current waveforms w.r.t Figure 5.10, 5.12 and 5.14, i.e., SPV array-ADDC fed BLDC motor drive for water pumping system in closed-loop system (with speed control), for 0.50 duty cycle (D=0.50). The calculation of performance parameters is done using these waveforms and are presented in Table 5.12.

Similarly, The Figures 5.28 and 5.29 shows the input voltage and input current waveforms, and output voltage and current waveforms w.r.t Figure 5.10, 5.12 and 5.14, i.e., SPV array-ADDC fed BLDC motor drive for water pumping system in closed-loop system (with speed control), for 0.75 duty cycle (D=0.75). The calculation of performance parameters is done using these waveforms and are presented in Table 5.13.

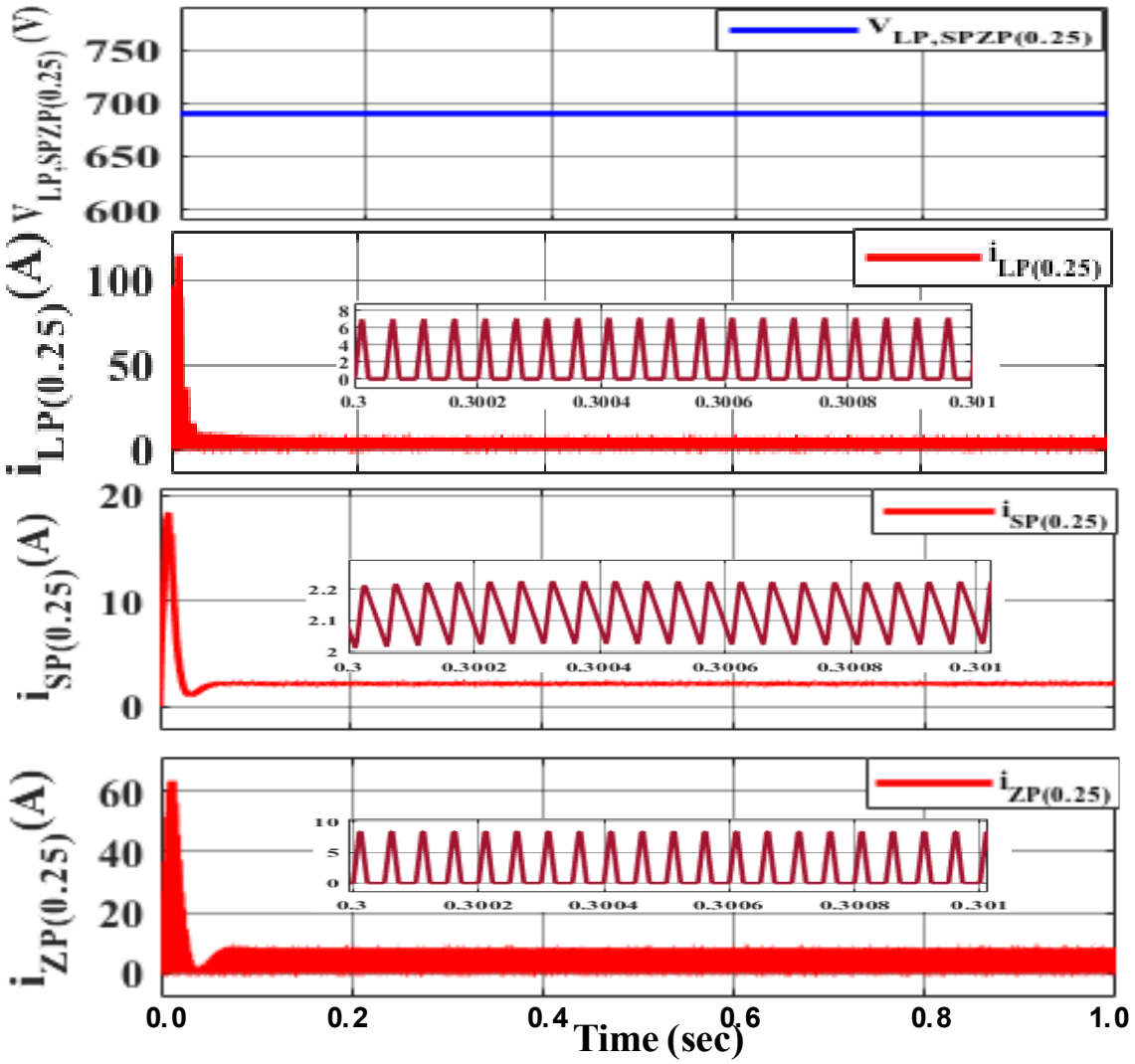

Figure 5.24 Input voltage and current waveforms for SPV array-ADDC fed BLDC motor drive system in closed-loop system (with speed control), for D=0.25.

The calculation of the performance parameters from the waveforms in Figure 5.24 and 5.25 has been summarized in the table below.

Table 5.11 Performance parameter calculations values of SPV array-ADDC fed BLDC motor drive system in closed-loop system (with speed control), for D=0.25.

Mode ▸ ▸ / Parameters ▸ ▸	LUO	SEPIC	ZETA
	Boost (D=0.25)	Buck (D=0.25)	Buck (D=0.25)
Input Voltage [V_{LP} (V)]	690V	690V	690V
Input Current [i_{LP} (A)]	1.76A	2.14A	2.10A
Input Power [P_{LP} (W)]	1214.40W	1475.22W	1450.380W
Output Voltage [V_{LO} (V)]	228.9V	228.9V	228.9V
Output Current [i_{LO} (A)]	4.975A	4.976A	4.974A
Output Power [P_{LO} (W)]	1138.78W	1139.01W	1138.55W
Power Efficiency [η_{PL}(%)]	93.77%	77.21%	78.50%
Conduction Losses [P_{CL} (W)]	75.62W	336.21W	311.83W

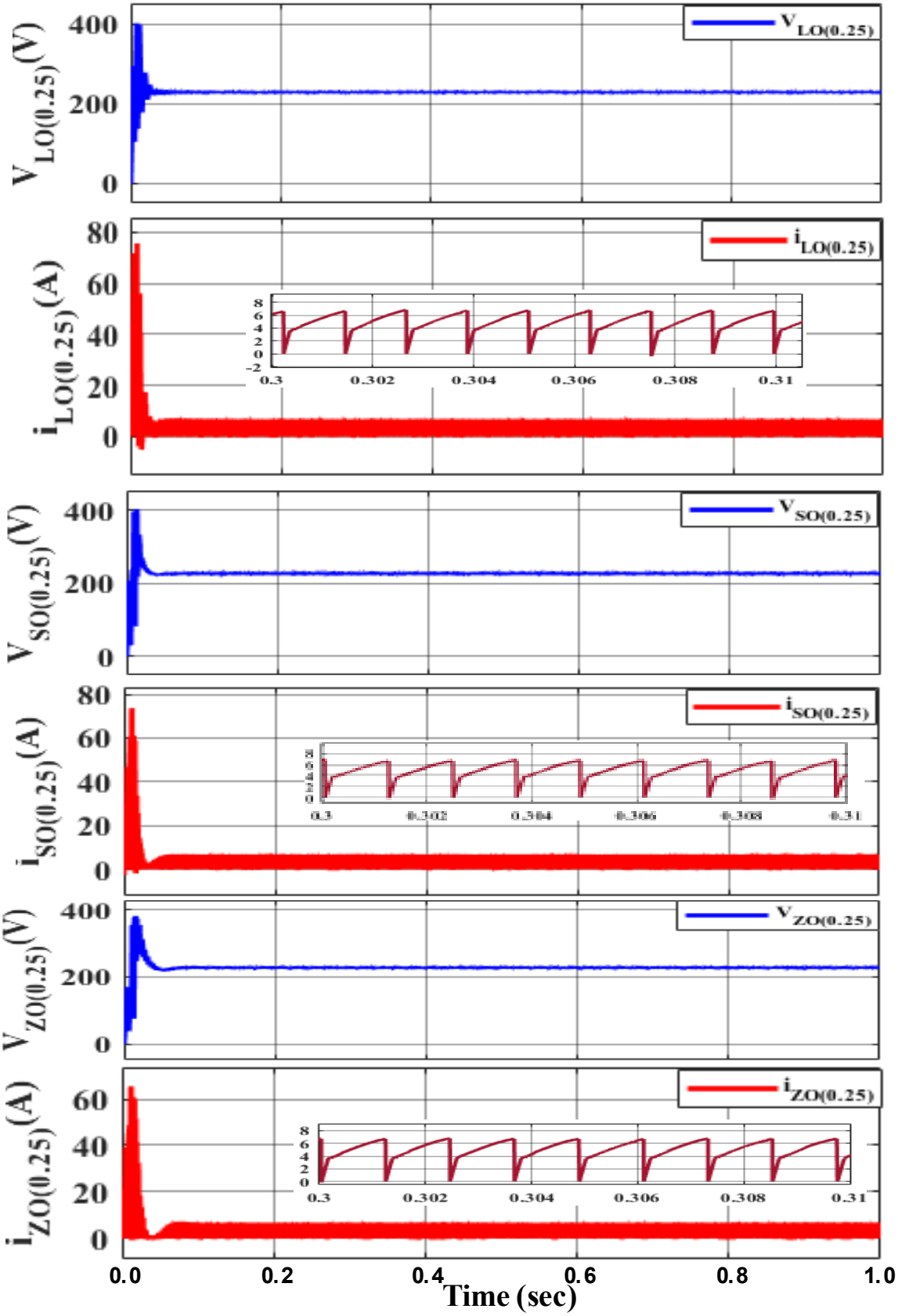

Figure 5.25 Output voltage and current waveforms for SPV array-ADDC fed BLDC motor drive system in closed-loop system (with speed control), for D=0.25.

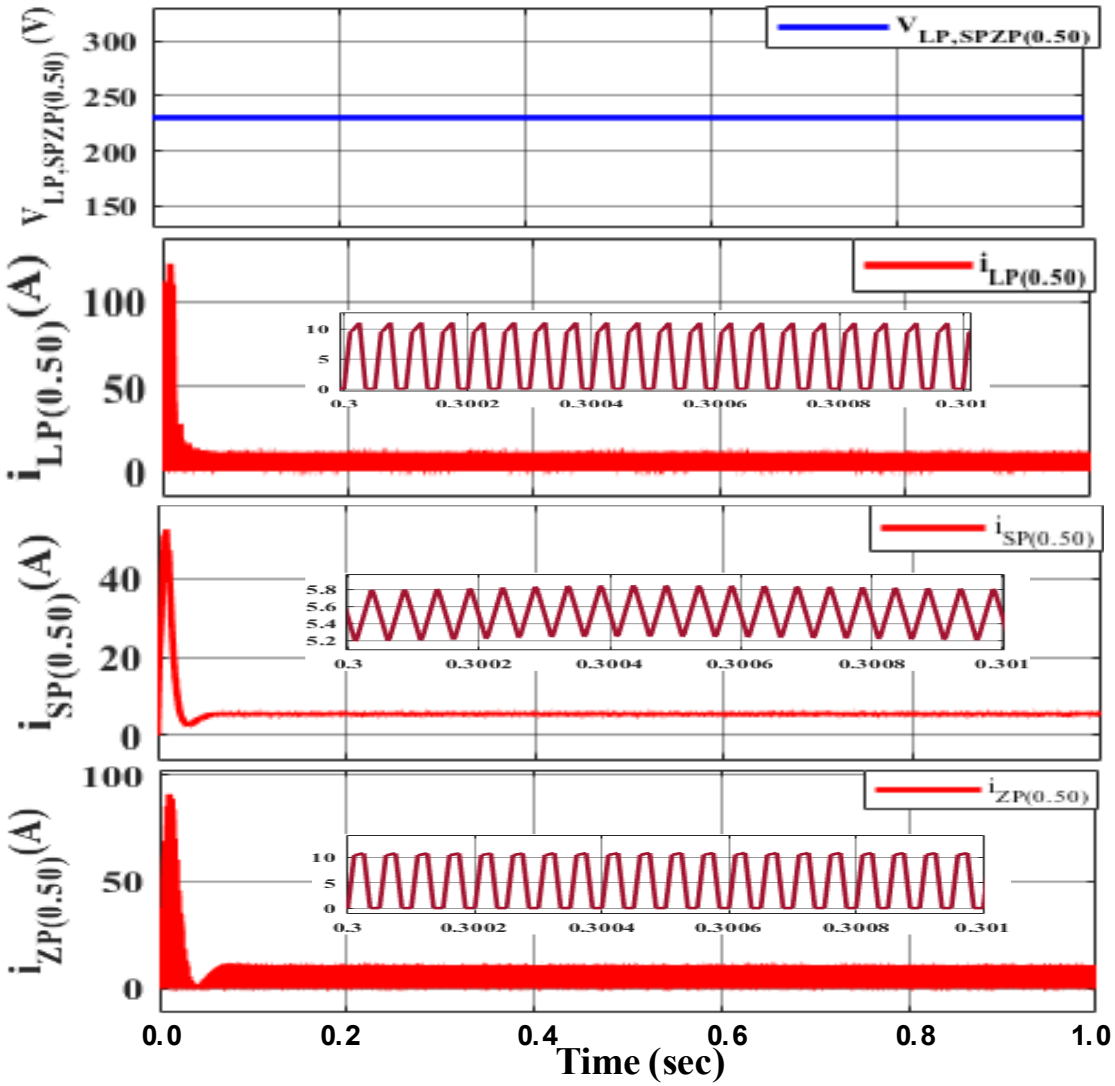

Figure 5.26 Input voltage and current waveforms for SPV array-ADDC fed BLDC motor drive system in closed-loop system (with speed control), for D=0.50.

The calculation of the performance parameters from the waveforms in Figure 5.26 and 5.27 has been summarized in the table below.

Table 5.12 Performance parameter calculations values of SPV array-ADDC fed BLDC motor drive system in closed-loop system (with speed control), for D=0.50.

Mode ▸ ▸ / Parameters ▸ ▸	LUO	SEPIC	ZETA
	High-Boost (D=0.50)	**Normal (D=0.50)**	**Normal (D=0.50)**
Input Voltage [V_{LP} (V)]	230V	230V	230V
Input Current [i_{LP} (A)]	5.16A	5.47A	5.40A
Input Power [P_{LP} (W)]	1185.65W	1258.10W	1242.46W
Output Voltage [V_{LO} (V)]	228.1V	228.1V	228.1V
Output Current [i_{LO} (A)]	4.973A	4.973A	4.976A
Output Power [P_{LO} (W)]	1134.34W	1134.34W	1135.03W
Power Efficiency [η_{PL}(%)]	95.67%	90.16%	91.35%
Conduction Losses [P_{CL} (W)]	51.31W	123.76W	107.43W

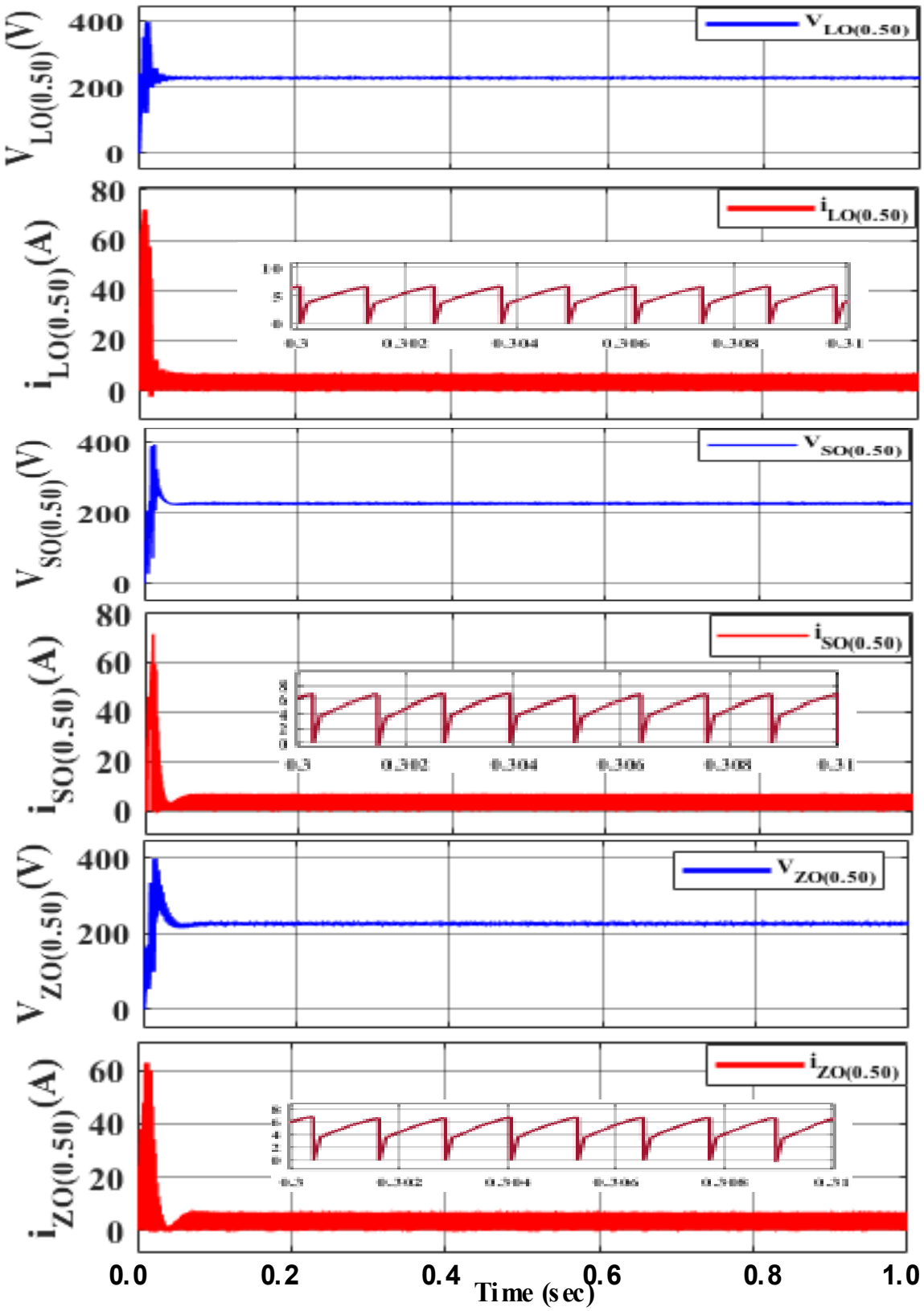

Figure 5.27 Output voltage and current waveforms for SPV array-ADDC fed BLDC motor drive system in closed-loop system (with speed control), for D=0.50.

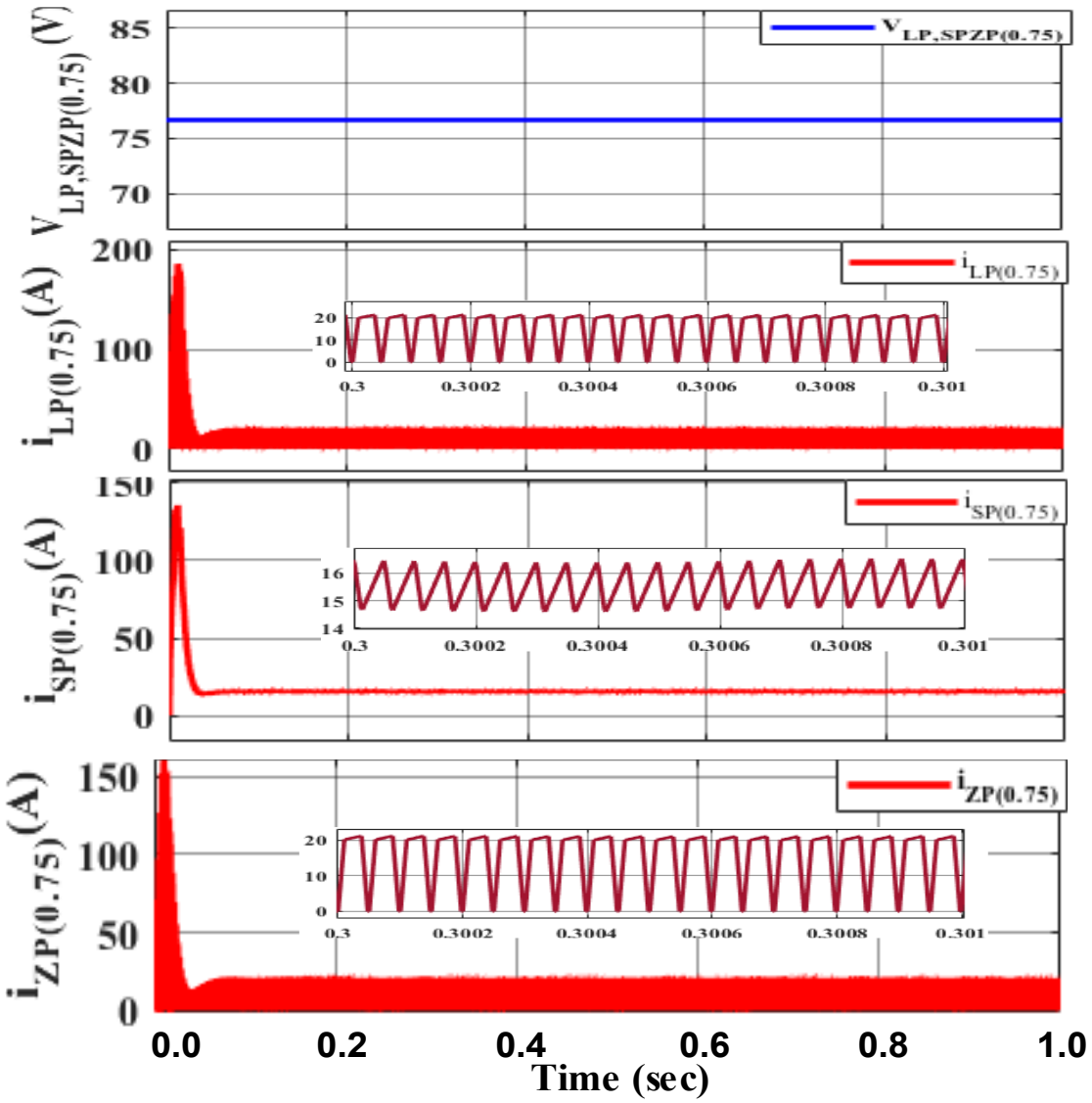

Figure 5.28 Input voltage and current waveforms for SPV array-ADDC fed BLDC motor drive system in closed-loop system (with speed control), for D=0.75.

The calculation of the performance parameters from the waveforms in Figure 5.28 and 5.29 has been summarized in the table below.

Table 5.13 Performance parameter calculations values of SPV array-ADDC fed BLDC motor drive system in closed-loop system (with speed control), for D=0.75.

Mode ▸ ▸ / Parameters ▸ ▸	LUO	SEPIC	ZETA
	Super-Lift (D=0.75)	Boost (D=0.75)	Boost (D=0.75)
Input Voltage [V_{LP} (V)]	76.67V	76.67V	76.67V
Input Current [i_{LP} (A)]	15.27A	15.48A	15.33A
Input Power [P_{LP} (W)]	1170.75W	1186.85W	1175.35W
Output Voltage [V_{LO} (V)]	223.0V	223V	222.9V
Output Current [i_{LO} (A)]	4.978A	4.978A	4.977A
Output Power [P_{LO} (W)]	1110.10W	1110.10W	1144.21W
Power Efficiency [η_{PL}(%)]	94.82%	93.53%	97.35%
Conduction Losses [P_{CL} (W)]	60.65W	76.75W	31.14W

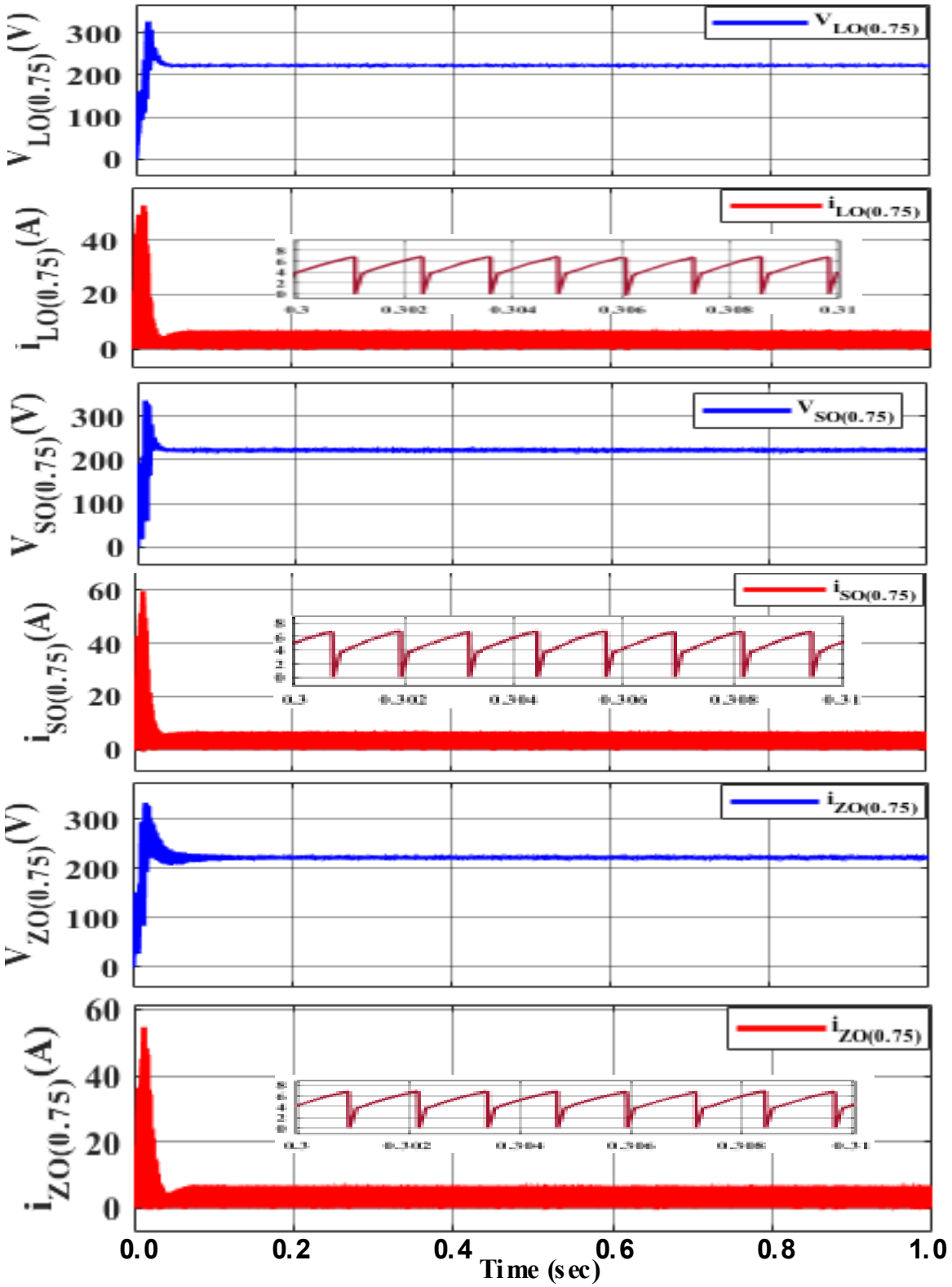

Figure 5.29 Output voltage and current waveforms for SPV array-ADDC fed BLDC motor drive system in closed-loop system (with speed control), for D=0.75.

The speed comparison between open-loop (OL) and three different modes viz. ADDC's under closed-loop (CL) speed control is analysed, as illustrated in Figure 30. As the damping in the OL system is large, the speed curve gets directly to the steady

state without overshoot. While using CL, the damping ratio is between 0 to 1, i.e., underdamped. Thus, after having some oscillations and undershoot, the speed becomes stable and stays at rated value of 2065 rpm, i.e., the dynamic balance between load torque and electromagnetic torque is achieved.

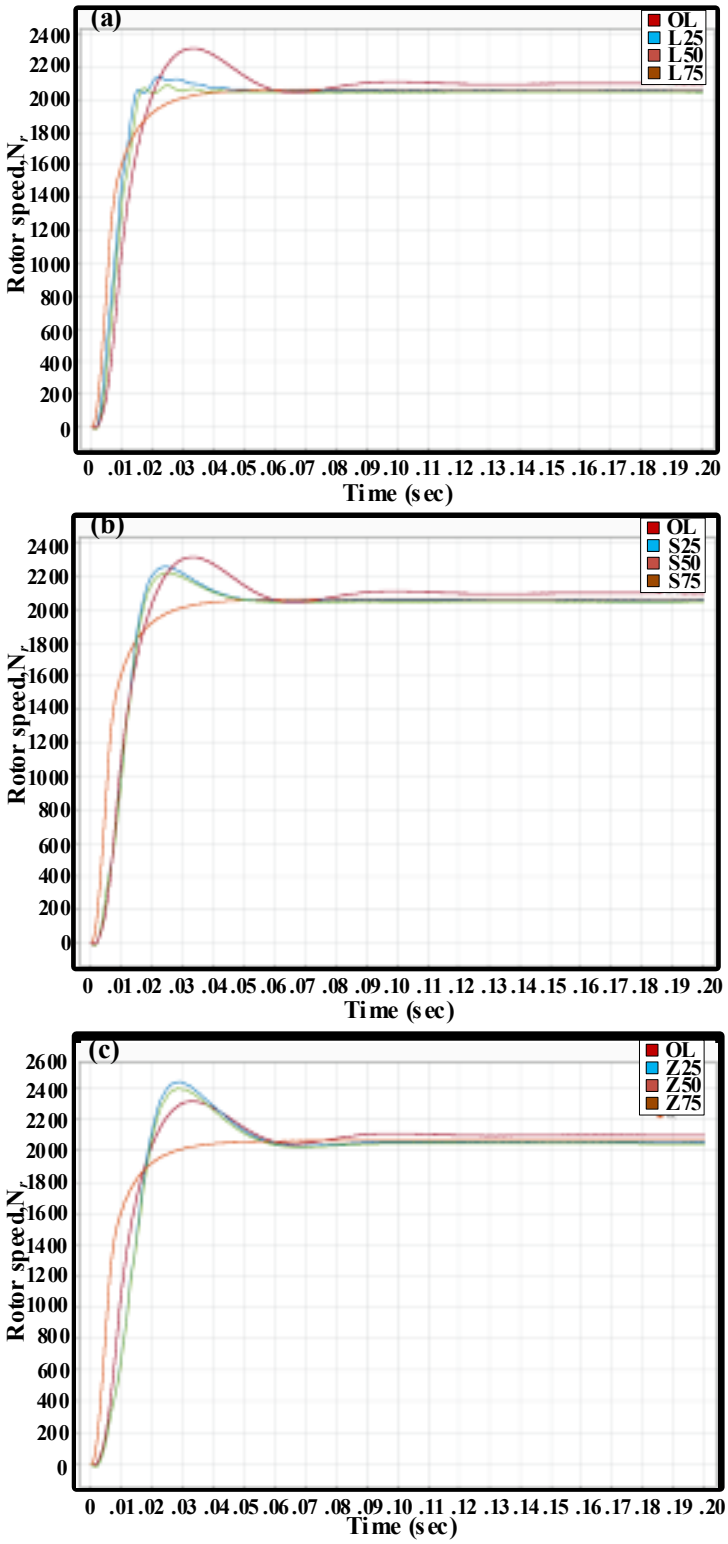

Figure 5.30 Speed comparison of closed-loop (CL), w.r.t open-loop (OL), of ADDC's: (a) Luo (D=0.25/0.50/0.75) (b) SEPIC (D=0.25/0.50/0.75) (c) Zeta (D=0.25/0.50/0.75).

Chapter 6

CONCLUSION

6.1 PERFORMANCE ANALYSIS

The input voltage from SPV array to ADDCs depends on duty cycle (D) and is constant for particular D, i.e., 690V, 230V and 76.67V for 25%, 50% and 75% of D. This results into 230V output as required by BLDC motor fed pump load. The VSI is operated in such a way as to lower the losses in the switches and to maintain the soft starting of BLDC motor with trapezoidal back-emf control. Figures. 5.15, 5.18 and 5.21 implies the waveforms of input current and voltage as well as output current and voltage for 25% duty cycle operation w.r.t the open-loop system. Similarly, Figures. 5.16, 5.19, 5.22 and Figures. 5.17, 5.20, 5.23 are the waveforms for 50% and 75% duty cycle operation w.r.t the open-loop system, respectively. Thus, from these results the input and output power, the power efficiency and the conduction losses are calculated and a conclusion table is characterized as Table 6.1.

The characterization of three different ADDCs has been carried out and their performance parameters and input-output parameters are compared, in table V, by using proper design considerations in MATLAB/Simulink software. It is found that the intended system with Luo converter in super-lift mode and Zeta converter in boost mode have higher efficiency and lower switching losses as compared to the other modes based on duty cycle alongside with inter- and intra- comparison of the ADDCs.

Table 6.1 Performance parameters analysis and evaluation results of open-loop system.

Mode / Parameters	Boost (D=0.25)	High-Boost (D=0.50)	Super-Lift (D=0.75)	Buck (D=0.25)	Normal (D=0.50)	Boost (D=0.75)	Buck (D=0.25)	Normal (D=0.50)	Boost (D=0.75)
Input Voltage [V_{LP} / V_{SP} / V_{ZP} (V)]	690V	230V	76.67V	690V	230V	76.67V	690V	230V	76.67V
Input Current [i_{LP} / i_{SP} / i_{ZP} (A)]	2.079A	5.311A	15.27A	2.138A	5.473A	15.49A	2.102A	5.401A	15.33A
Input Power [P_{LP} / P_{SP} / P_{ZP}(W)]	1434.510	1221.530	1170.751	1475.220	1258.790	1187.618	1450.380	1242.230	1175.351
Output Voltage [V_{LO} / V_{SO} / V_{ZO} (V)]	228.9V	228.1V	223.0V	228.8V	228.0V	222.9V	228.9V	228.1V	222.9V
Output Current [i_{LO} / i_{SO} / i_{ZO} (A)]	4.974A	4.972A	4.976A	4.939A	4.940A	4.945A	4.975A	4.977A	4.978A
Output Power [P_{LO} /P_{SO} / P_{ZO} (W)]	1138.549	1134.113	1109.648	1130.043	1126.320	1102.241	1138.778	1135.254	1109.596
Power Efficiency [η_{PL}/ η_{PS} / η_{PZ} (%)]	79.37%	92.84%	**94.78%**	76.60%	89.48%	92.81%	78.52%	91.40%	**94.41%**
Conduction Losses [P_{CL} / P_{CS}/ P_{CZ} (W)]	295.961	87.417	**61.103**	345.177	132.470	85.377	311.602	106.976	**65.755**

The closed-loop control of three different ADDCs has been performed and their performance is analysed, by using proper design considerations in MATLAB/Simulink software. It is found from the rotor speed curves that the high-boost mode (D=0.50) of

Luo converter, normal mode (D=0.50) of SEPIC converter and boost mode (D=0.75) of Zeta converter has better speed regulation than the other modes, as illustrated in Figure 5.30. Also, Figures. 5.24 and 5.25 implies the waveforms of input current and voltage as well as output current and voltage for 25% duty cycle operation w.r.t the closed-loop system. Similarly, Figures. 5.26, 5.27 and Figures. 5.28, 5.29 are the waveforms for 50% and 75% duty cycle operation w.r.t the closed-loop system, respectively. It has been observed that the Luo converter in high-boost and super-lift mode, and the Zeta converter in boost mode outperforms the other modes (i.e., have higher power efficiency and lower conduction losses) based on duty cycle alongside with inter- and intra- comparison of the ADDCs, as shown in Table 6.2. The strength of these high performing converters comes from the ability to generate arithmetic or geometric progression output voltage as well as high efficiency, low switching losses and high power density.

Table 6.2 Performance parameters analysis and evaluation results for closed-loop system

Mode / Parameters	Boost (D=0.25)	High-Boost (D=0.50)	Super-Lift (D=0.75)	Buck (D=0.25)	Normal (D=0.50)	Boost (D=0.75)	Buck (D=0.25)	Normal (D=0.50)	Boost (D=0.75)
Input Voltage [V_{LP}/ V_{SP} / V_{ZP} (V)]	690V	230V	76.67V	690V	230V	76.67V	690V	230V	76.67V
Input Current [i_{LP} / i_{SP} / i_{ZP} (A)]	1.76A	5.16A	15.27A	2.14A	5.47A	15.48A	2.10A	5.40A	15.33A
Input Power [P_{LP} / P_{SP} / P_{ZP} (W)]	1214.40	1185.65	1170.75	1475.22	1258.10	1186.85	1450.380	1242.46	1175.35
Output Voltage [V_{LO} / V_{SO} / V_{ZO} (V)]	228.9V	228.1V	223.0V	228.9V	228.1V	223V	228.9V	228.1V	222.9V
Output Current [i_{LO} / i_{SO} / i_{ZO} (A)]	4.975A	4.973A	4.978A	4.976A	4.973A	4.978A	4.974A	4.976A	4.977A
Output Power [P_{LO} /P_{SO} / P_{ZO} (W)]	1138.78	1134.34	1110.10	1139.01	1134.34	1110.10	1138.55	1135.03	1144.21
Power Efficiency [η_{PL}/ η_{PS} / η_{PZ} (%)]	93.77%	**95.67%**	**94.82%**	77.21%	90.16%	93.53%	78.50%	91.35%	**97.35%**
Conduction Losses [P_{CL} / P_{CS}/ P_{CZ} (W)]	75.62	**51.31**	**60.65**	336.21	123.76	76.75	311.83	107.43	**31.14**

6.2 RECOMMENDATIONS AND FUTURE WORK

The performance analysis of three different converters such as LUO, SEPIC and ZETA converters are being carried out using fuzzy logic controller, genetic algorithm-based controller, artificial neural network-based controller and other intelligent controllers. Their performance parameters and Input-Output parameters will be compared by using proper design considerations in MATLAB/Simulink software.

Also, a standalone water pumping system can be made grid connected for their applications in households and industries present in urban areas. And the possibility to integrate standalone water pumping system with battery energy storage system for industrial as well as agricultural application will be viewed in future work as an extension of this project.

REFERENCES

[1] R. N. C, P. Podgurski and D. J. Perreault, "Sub-Module Integrated Distributed Maximum Power Point Tracking for Solar Photovoltaic Applications," IEEE, pp. 2957-2967, 2013.

[2] "Climate Change 2014: Synthesis Report Summary for Policymakers," IPCC, 2014.

[3] https://mnre.gov.in/solar/current-status/

[4] J. Adam, "Global PV Demand Outlook 2015-2020: Exploring Risk in Downstream Solar Markets"," Greentech Media, 2015.

[5] R. W. Erickson, S. Mac Alpine and M. Brandemuehl, "Improved Energy Capture in Series String Photovoltaics via Smart Distributed Power Electronics," in Applied Power Electronics Conference and Exposition, Washington, DC, 2009.

[6] J. Enslin, "Renewable Energy as an Eonomic Energy Source for Remote Areas," Renewable Energy, pp. 243-248, 1991.

[7] W. H. Tang, A. J. Mahdi and Q. H. Wu, "Improvement of a MPPT Algorithm for PV Systems and Its Experimental Validation," The University of Liverpool, Liverpool, 2010.

[8] S. Nagarajan, "Understanding Photovoltaics and the Market Forces Behind Them," Texas Instruments, 2011.

[9] Manjunath Matam, Venugopal Reddy Barry, “Optimized Reconfigurable PV array based Photovoltaic water-pumping system,” Solar Energy, vol.170, pp. 1063-1073, 2018.

[10] B. Singh, U. Sharma, “Standalone Photovoltaic Water Pumping System Using Induction Motor Drive with Reduced Sensors,” IEEE Transactions on Industry Applications, vol. 54, no. 4, pp. 3645-3655, July 2018.

[11] W. Geoff, "Evaluating MPPT Converter Topologies Using A Matlab PV Model," Journal of Electrical and Electronics Engineering, pp. 1-66, 2003.

[12] Langridge, D W. Lawrance, and B. Wichert. “Development of a photovoltaic pumping system using a brushless DC motor and helical rotor pump.” Solar Energy. 56,1996, pp.151-160.

[13] Swamy, CL Putta, Bhim Singh, B. P. Singh, and Sreenivasa S. Murthy. “Experimental investigations on a permanent magnet brushless DC motor fed by PV array for water pumping system.” Proceedings of the 31st Intersociety Energy Conversion Engineering, IECEC, IEEE 3, 1996, pp.1663-1668.

[14] Hosseini S. H., F. Nejabat khah, S.A.K.H. Mozafari Niapoor and S. Danyali. “Supplying a brushless dc motor by z-source PV power inverter with FL-IC MPPT.” International Conference on Green Circuits and Systems, IEEE. 2010, pp. 485-490.

[15] Terki A., A. Moussi,A. Betka,and N. Terki. “An improved efficiency of fuzzy logic control of PMBLDC for PV pumping system.” Applied Mathematical Modelling .36, 2012, pp.934-944.

[16] Ouada, Mahdi, Mohamed Salah Meridjet, and Nabil Talbi. “Optimization photovoltaic pumping system based BLDC using fuzzy logic MPPT control.” International Renewable and Sustainable Energy Conference (IRSEC), IEEE. 2013, pp.27-31.

[17] Taghvaee, M. H., M. A. M. Radzi, S. M. Moosavain, Hashim Hizam, and M. Hamiruce Marhaban. “A current and future study on nonisolated DC–DC converters for photovoltaic applications.” Renewable and sustainable energy reviews .17, 2013, pp: 216-227.

[18] Kumar, Rajan, and Bhim Singh. “Solar photovoltaic array fed canonical switching cell converter based BLDC motor drive for water pumping system.” Annual IEEE India Conference (INDICON), IEEE.2014, pp.1-6.

[19] Kumar, Rajan, and Bhim Singh. “Solar photovoltaic array fed Luo converter based BLDC motor driven water pumping system.”9th International Conference on Industrial and Information Systems (ICIIS), IEEE. 2014, pp. 1-5.

[20] An Le, and Dylan Dah-Chuan Lu. “Design of a single-switch DC/DC converter for a PV-battery-powered pump system with PFM+ PWM control.” IEEE Transactions on Industrial Electronics. 62, 2015, pp: 910-921.

[21] Kumar, Rajan, and Bhim Singh. “BLDC motor driven water pump fed by solar photovoltaic array using boost converter.” Annual IEEE India Conference (INDICON), IEEE.2015, pp. 1-6.

[22] Singh, Bhim, and Vashist Bist. “Solar PV Array Fed Water Pumping System Using SEPIC Converter Based BLDC Motor Drive.” IEEE Transactions on Industry Application. 51, 2015.

[23] Singh, Bhim, and Rajan Kumar. “Simple brushless DC motor drive for solar photovoltaic array fed water pumping system.” IET Power Electronics. 9, 2016, pp: 1487-1495.

[24] Kumar, Rajan, and Bhim Singh. “BLDC motor-driven solar PV arrayfed water pumping system employing zeta converter.” IEEE Transactions on Industry Applications. 52, 2016, pp:2315-2322.

[25] Singh, Bhim, and Rajan Kumar. “Solar photovoltaic array fed water pump driven by brushless DC motor using Landsman converter.” IET Renewable Power Generation .10, 2016, pp: 474-484.

[26] Kumar, Rajan, and Bhim Singh. “Single stage solar PV fed brushless DC motor driven water pump.” IEEE Journal of Emerging and Selected Topics in Power Electronics, 5, 2017, pp:1377-1385.

[27] Suribabu, Ulliboina, and K. Venkata Kishore. “Photovoltaic Based Landsman Converter with Fuzzy Logic Controller Fed BLDC Motor for Water Pumping Applications.” International Journal for Modern Trends in Science and Technology.3, 2017.

[28] Kumar, Rajan, and Bhim Singh. “Solar PV powered BLDC motor drive for water pumping using Cuk converter”, IET Electric Power Applications. 11, 2017, pp: 222-232.

[29] Aparna K.S. Sarada, and C. Ganesh. “Brushless DC(BLDC) motor drive for Solar Photovoltaic (SPV) array fed water pumping system by using Fuzzy Logic Controller.” International Journal of Advanced Engineering and Science. 6, 2017, pp:26-43.

[30] Zahab, Essam E. Aboul, Aziza M. Zaki, and Mohamed M. El-sotouhy. “Design and control of a standalone PV water pumping system.” Journal of Electrical Systems and Information Technology. 4, 2017, pp:322-337.

[31] Priyadarshi, Neeraj, Sanjeevi kumar Padmanaban, Lucian Mihet-Popa, Frede Blaabjerg, and Farooque Azam. “Maximum power point tracking for brushless DC motor-driven photovoltaic pumping systems using a hybrid ANFIS-FLOWER pollination optimization algorithm.” Energies.11, 2018, pp :1067.

[32] Sashidhar S., V. Guru Prasad Reddy, and B. G. Fernandes. “A single stage sensorless control of a PV based Bore-Well submersible BLDC motor.” IEEE Journal of Emerging and Selected Topics in Power Electronics, 2018.

[33] G. Bauerlein, “A brushless DC motor with solid-state commutation”, IRE Natl. Conv. Rec. (1962) 184190.

[34] T.M. Jahns, W.L. Soong, “Pulsating torque minimization technique for permanent magnet AC motor drives—a review”, IEEE Trans. Ind. Electron. 43 (2) (Apr. 1996) 321-330.

[35] P. Pillay, R. Krishnan, “Modeling, simulation, and analysis of permanent-magnet motor drives”, Part II. The brushless DC motor drive, IEEE Trans. Ind. Appl. 25 (2) (Mar./Apr. 1989) 274-279.

[36] Z. Xiangjun. C. Boshi, “The different influences of four PWM modes on the commutation torque ripples in sensorless brushless DC motors control system”, in: Proc. the Fifth International Conference Electrical Machines and Systems, vol. 1, 2001, pp. 575-578.

[37] Luo, F. L., “Luo-converters, voltage lift technique,” In Power Electronics Specialists Conference, 1998. PESC 98 Record. 29th Annual IEEE (Vol. 2, pp. 1783-1789). IEEE, 1998, May.

[38] Luo, F. L., and Ye, H., “Advanced dc/dc converters” crc Press, 2016.

[39] R. Kumar and B. Singh, “Solar photovoltaic array fed Luo converter based BLDC motor driven water pumping system,” 9th International Conference on Industrial and Information Systems (ICIIS), pp. 1-5, 2014.

[40] Wei Gu, Dongbing Zhang, “Designing a SEPIC Converter”, National Semiconductor Application Note 1484, april 30 2008.

[41] Al-Saffar M. A., Ismail E. H., Sabzali A. J. and Fardoun A. A., “An improved topology of SEPIC converter with reduced output voltage ripple”, IEEE Trans. Power Electron. 2008; 23(5): 2377–86.

[42] Emilio Mamarelis, Petrone Giovanni and Spagnuolo Giovanni, “Design of a sliding mode controlled SEPIC for PV MPPT Applications”, 2014.1-1.

[43] Linares Flores J., Sira Ramırez H., Cuevas López E. F. and Contreras Ordaz M. A., “Sensor less passivity based control of a DC motor via a solar powered SEPIC converter full bridge combination”, J. Power Electron. 2011;11(5): 743–50.

[44] R. Kumar, B. Singh, “Solar PV array fed water pumping system using SEPIC converter based BLDC motor drive,” Eighteenth National Power Systems Conference (NPSC), pp. 1-5, 2014.

[45] Song Min Sup, Son Young Dong and Lee Kwang Hyun, “Non-isolated Bidirectional soft switching SEPIC/ZETA converter with reduced ripple currents”, J. Power Electron. 2014;14(4):649–60.

[46] R. Kumar, B. Singh, “BLDC Motor-Driven Solar PV Array-Fed Water Pumping System Employing Zeta Converter,” IEEE Transactions on Industry Applications, vol. 52, no. 3, pp. 2315-2322, May-June 2016.

[47] B. Singh and V. Bist, “A Single Sensor Based PFC Zeta Converter Fed BLDC Motor Drive for Fan Applications,” Fifth IEEE Power India Conference, pp.1-6, 19-22 Dec. 2012.

[48] V. Bist and B. Singh, “A Reduced Sensor PFC BL-Zeta Converter Based VSI Fed BLDC Motor Drive”, Electric Power Sys. Research, vol. 98, pp. 11–18, May 2013.

[49] W.V. Jones, “Motor Selection Made Easy: Choosing the Right Motor for Centrifugal Pump Applications,” IEEE Industry Applications Magazine, vol.19, no.6, pp.36-45, Nov.-Dec. 2013.

[50] Michael Volk, “Pump Characteristics and Applications,” 3rd Edition, CRC press, Taylor & Francis group, 2014.

[51] G yeong-Chan Lee, T ae-Uk lung, “Design comparisons of BLDC motors for electric water pump,” in Proc. IEEE Vehicle Power and Propulsion Conference-VPPC, pp. 48-50, 2012.

[52] W.B. Lawrance, H. Dehbonei, “A versatile PV array simulation tools”, in: Presented at ISES 2001 Solar World Congress, Adelaide, South Australia, 2001.

[53] D. Yogi Goswami, Roger Messenger, “Energy Efficiency and Renewable Energy Handbook”, Taylor & Francis Group, LLC, pp. 1413-1419, 2016.

APPENDIX A

Standard Test Conditions (STC)

The industrial standards for which solar panels are tested is known as STC which are a fixed set of conditions. This is accustomed so that the accurate comparison of SPV array-based application can be carried out easily. The three STC conditions are:

(a) **Solar cell Temperature** which is equal to 25°C. This includes temperature of only solar cell and excludes the surrounding's temperature.

(b) **Irradiance of Solar cell** which is equal to 1000 Watts per square meter. This includes the aggregate quantity of light energy incident on a given area (A) at a given time (t).

(c) **Air Mass** which is equal to 1.5. This statistic is a little confusing since it relates to the quantity of light that must pass through Earth's atmosphere before reaching the surface, and it has a lot to do with the sun's angle relative to a reference point on the planet. This value is lowest when the sun is directly overhead since the light must travel the shortest distance straight down, and it rises as the sun moves away from the reference point and must travel at an angle to reach the same position.

APPENDIX B

Matlab/Simulink Models

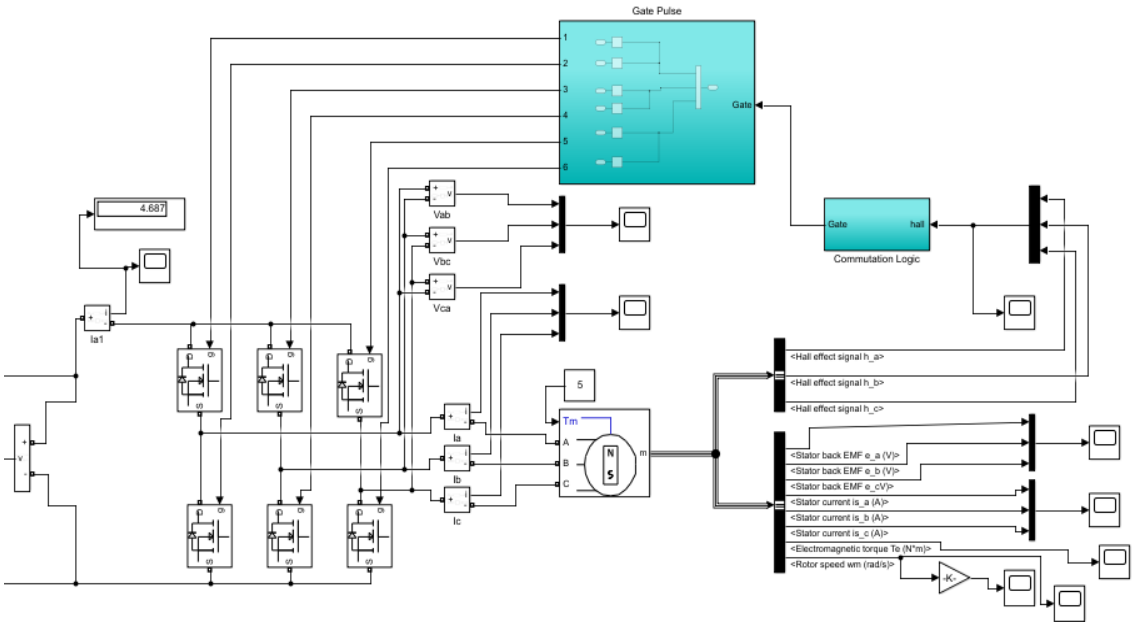

Figure B.1 BLDC motor drive simulink model using design parameters from Table 5.1, specific to the circuit diagram of Figure 3.6.

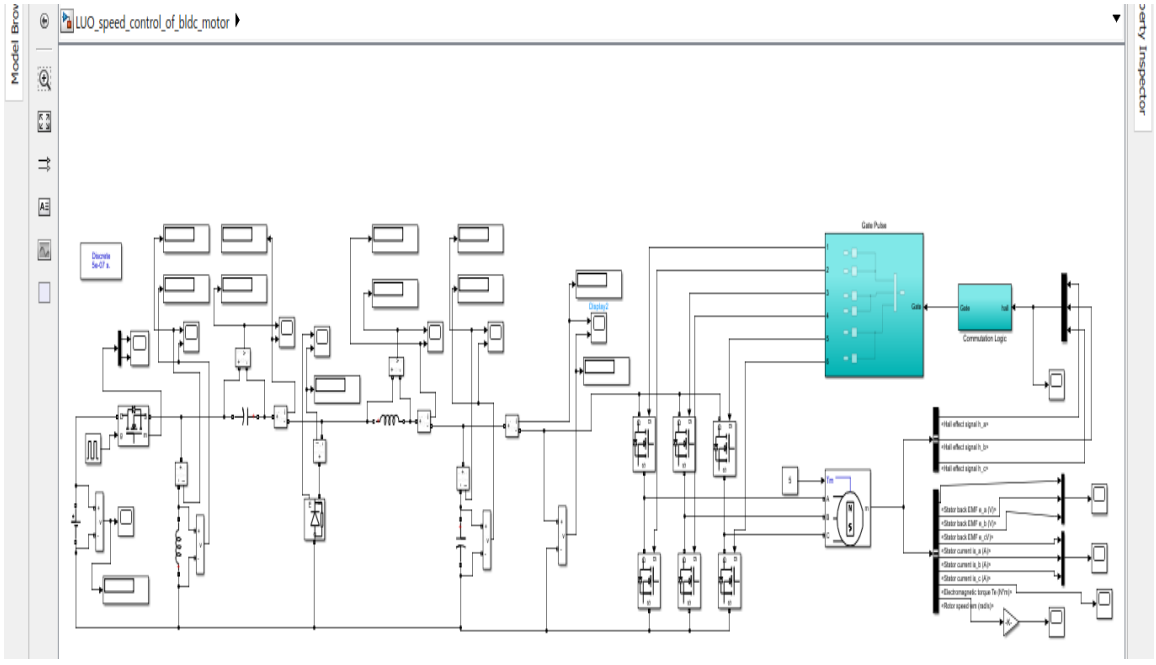

Figure B.2 MATLAB/Simulink Model of LUO Converter fed BLDC Motor Drive, specific to the circuit diagram of Figure 5.9.

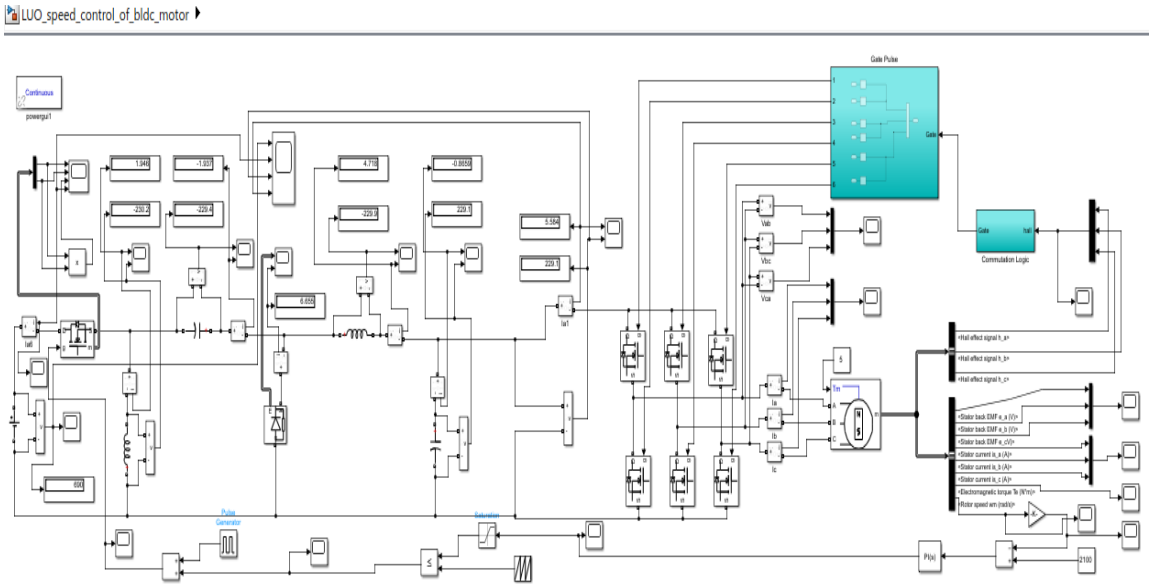

Figure B.3 MATLAB/Simulink Model of LUO Converter fed BLDC Motor Drive, specific to the circuit diagram of Figure 5.10.

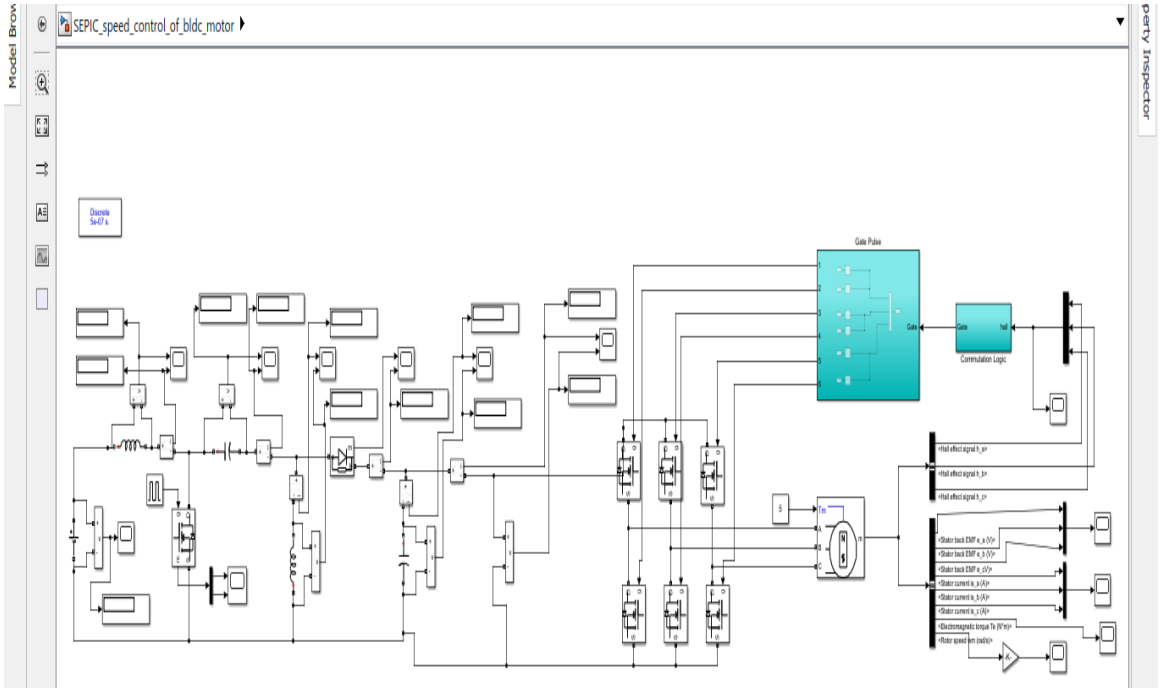

Figure B.4 MATLAB/Simulink Model of SEPIC Converter fed BLDC Motor Drive, specific to the circuit diagram of Figure 5.11.

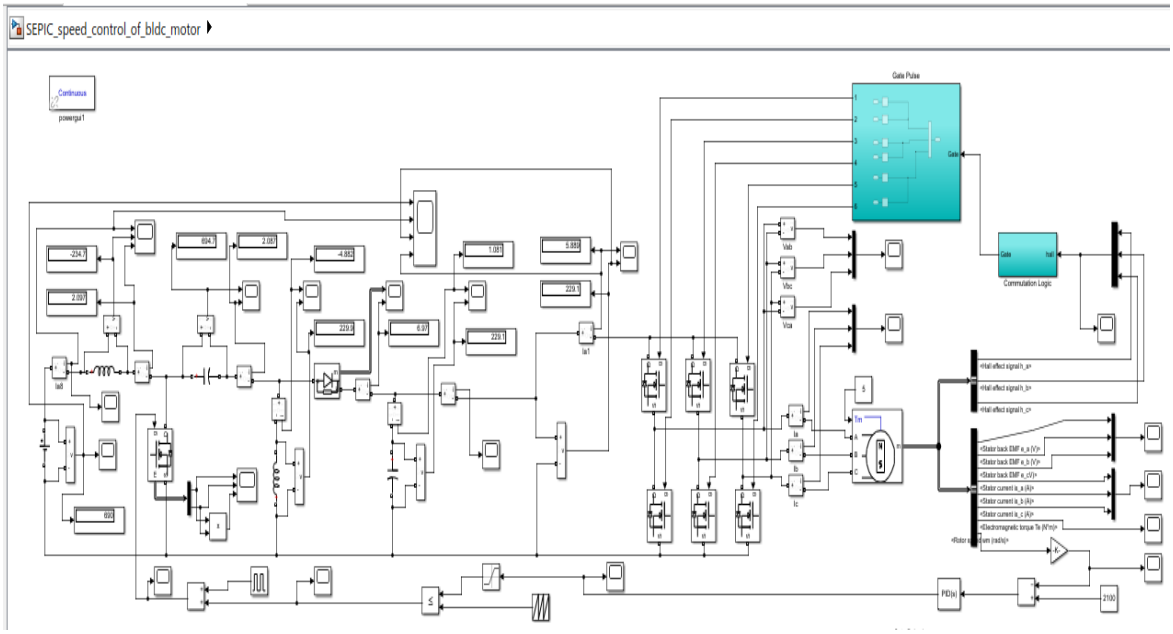

Figure B.5 MATLAB/Simulink Model of SEPIC Converter fed BLDC Motor Drive, specific to the circuit diagram of Figure 5.12.

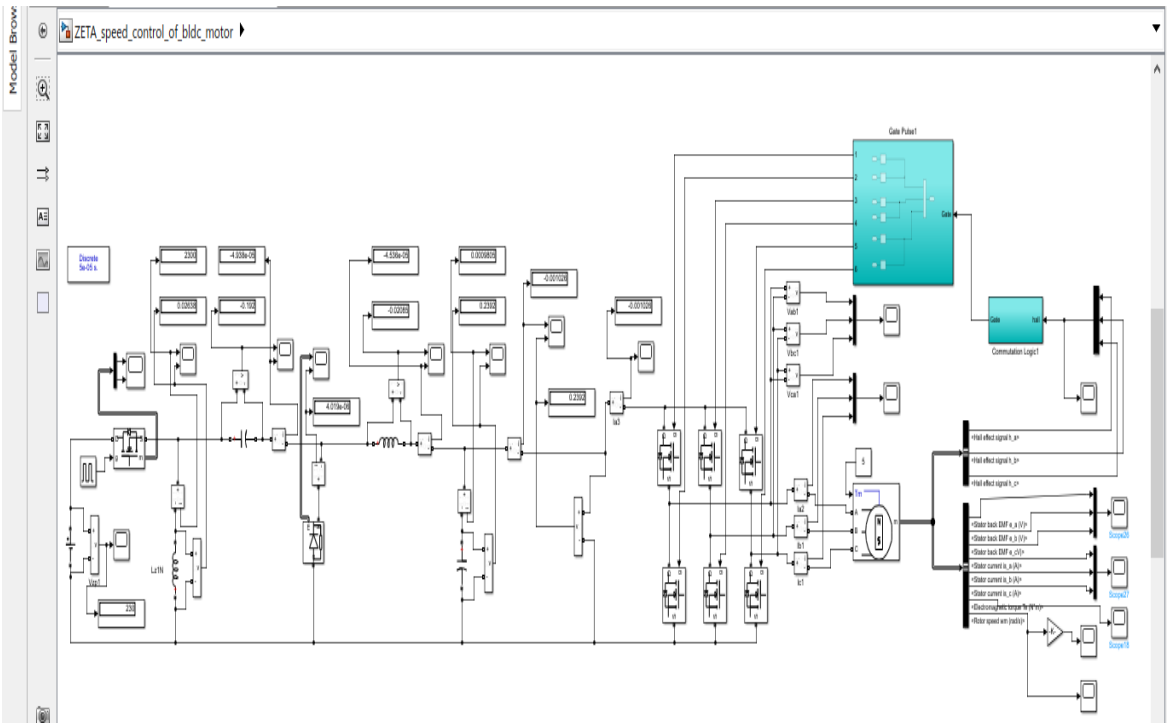

Figure B.6. MATLAB/Simulink Model of ZETA Converter fed BLDC Motor Drive, specific to the circuit diagram of Figure 5.13.

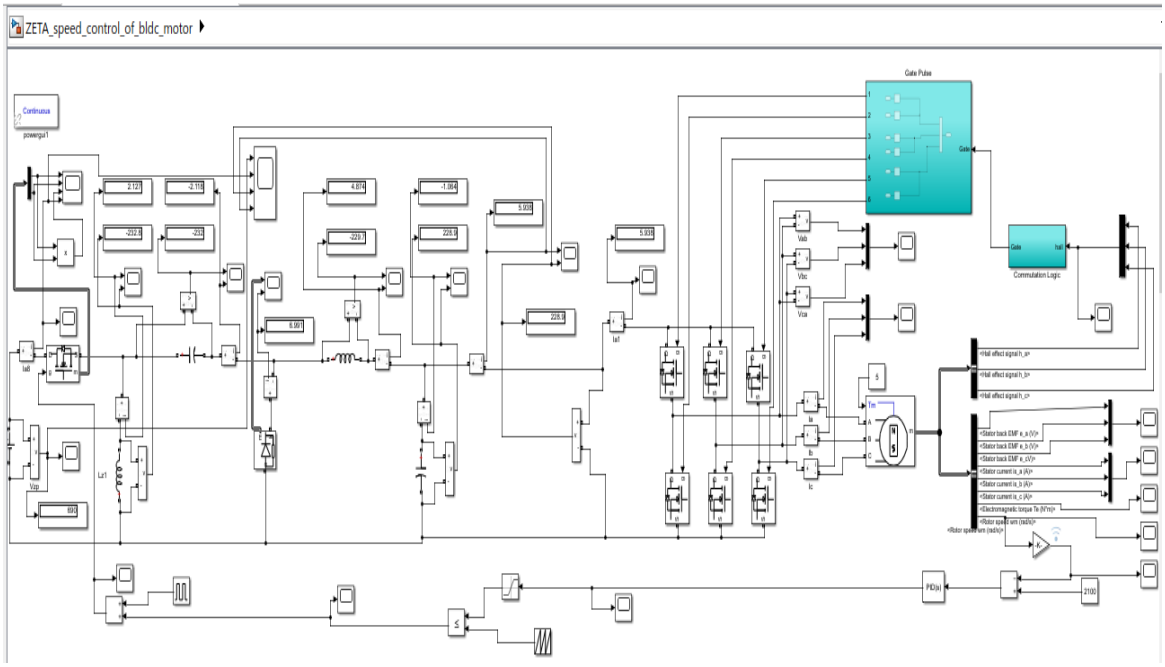

Figure B.7. MATLAB/Simulink Model of ZETA Converter fed BLDC Motor Drive, specific to the circuit diagram of Figure 5.14.

BREIF CV OF AUTHOR

Shantanu passed his B.E (Power Electronics Engineering) from Lukhdhirji Engineering College Morbi (Govt. of Gujarat) in 2017. He is currently pursuing M.Tech (2020-22) programme in Power system from the Department of Electrical Engineering of Delhi Technological University.

LIST OF PUBICATIONS

1) **"**Characterization of Advanced DC-DC Converters for BLDC Motor Driven SSWPS" is accepted in IEEE Industry Applications Society Global Conference on Emerging Technologies (IEEE IAS GlobConET-2022).

2) "Closed-Loop Control of Advance DC-DC converters for BLDC motor driven SSWPS" is accepted in 2nd IEEE International Conference on Emerging Frontiers in Electrical and Electronic Technologies (2nd ICEFEET- 2022).

The work has been accepted in peer reviewed Scopus indexed conference with the following details:

Sr. No.	Details	Information
1.	**Title of the Paper:**	Characterization of Advanced DC-DC Converters for BLDC Motor Driven SSWPS
	Author names:	Shantanu and Dr. Mayank Kumar
	Name of Conference:	IEEE Industry Applications Society Global Conference on Emerging Technologies (IEEE IAS GlobConET-2022)
	Conference Dates and Venue:	20 - 21 May 2022; Radisson Blu Greater Noida, NCR, New Delhi, Hybrid Mode
	Have you registered for the Conference?	Yes
	Status of paper:	Accepted
	Date of communication:	31st January 2022

	Date of acceptance:	19th February 2022
	Date of publication:	In proceedings of the conference (IEEE)
2.	**Title of the Paper:**	Closed-Loop Control of Advance DC-DC converters for BLDC motor driven SSWPS
	Author names:	Shantanu and Dr. Mayank Kumar
	Name of Conference:	2nd IEEE International Conference on Emerging Frontiers in Electrical and Electronic Technologies (ICEFEET- 2022)
	Conference Dates and Venue:	24 - 25 June, 2022; Online Mode
	Have you registered for the Conference?	Yes
	Status of paper:	Accepted
	Date of communication:	5th May 2022
	Date of acceptance:	31st May 2022
	Date of publication:	In proceedings of the conference (IEEE)